



*Federal University of Paraíba*

*Technology Center*

**CIVIL AND ENVIRONMENTAL ENGINEERING GRADUATE  
PROGRAM  
– MASTERS –**

**MICROSTRUCTURAL INVESTIGATION OF ALKALI SILICA AND  
GEOPOLYMER GELS**

*Fábio Mariz Maia Neto*

*Master's dissertation presented at the Federal University of Paraíba for the  
acquisition of Master's Degree*

**João Pessoa – Paraíba**

**March 2020**



*Federal University of Paraíba*

*Technology Center*

**CIVIL AND ENVIRONMENTAL ENGINEERING GRADUATE  
PROGRAM  
– MASTERS –**

**MICROSTRUCTURAL INVESTIGATION OF ALKALI SILICA AND  
GEOPOLYMER GELS**

Dissertation submitted at the Civil and Environmental Engineering Graduate Program of the Federal University of Paraíba, as partial fulfillment for the acquisition of Master's Degree.

**Fábio Mariz Maia Neto**

**Supervisor: Prof. Dr. Sandro Marden Torres**

**João Pessoa – Paraíba**

**March 2020**

M217m Maia Neto, Fábio Mariz.

Microstructural Investigation of Alkali Silica and  
Geopolymer Gels / Fábio Mariz Maia Neto. - João Pessoa,  
2020.

108 f.

Orientação: Sandro Marden Torres.  
Dissertação (Mestrado) - UFPB/CT.

1. Reação álcali sílica. 2. Gel de álcali sílica. 3.  
Geopolímero. 4. Alumínio. I. Sandro Marden Torres. II.  
Titulo.

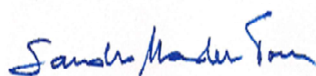
UFPB/BC

**FÁBIO MARIZ MAIA NETO**

**MICROSTRUCTURAL INVESTIGATION OF ALKALI SILICA AND  
GEOPOLYMER GELS**

Dissertation approved on 25/03/2020 as partial fulfillment for the acquisition of a Master's Degree in Civil and Environmental Engineering at the Technology Center - Federal University of Paraíba.

EXAMINING BOARD:



---

Prof. Dr. Sandro Marden Torres – UFPB

(Supervisor)



---

Prof. Dr. Hidelbrando José Farkat Diógenes – UFPB

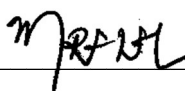
(Internal Examiner)



---

Prof. Dr. Caroline Kirk – University of Edinburgh

(External Examiner)



---

Prof. Dr. Marçal Rosas Florentino Lima Filho – UFPB

(External Examiner)



## **DEDICATION**

This piece of research is wholeheartedly dedicated to my parents, Fábio and Valéria, whose great support and continuous care enable me to conclude this work.

## ACKNOWLEDGEMENTS

First of all, I am pleased for having the opportunity to work with Professor Sandro. His invaluable contribution changed the magnitude of this work and was crucial to its final completion. In addition to that, his constant eagerness to help and persistent curiosity challenged and motivated me to seek a deeper understanding of the matter.

I would also like to express my gratitude towards Professors Marçal, Rennio, Tibério and Gardênia for their precious insights, which helped me widen my research at various perspectives.

My sincere thanks also go to the Thin Film Synthesis Laboratory team, in special Professor Kelly, Edson, Ronny and Raissa, who kindly dedicated part of their time to help me out during the FTIR and TGA experimental sections. I would also like to thank the Elizabeth Cimentos Chemical Analysis Laboratory staff, in special Degmar, Airton and Leonardo, for the assistance provided during the XRF test.

I thank my fellow labmates, Thiago, Ricardo and Marcos, for the stimulating discussions and for all the fun we have had in the last two years. Due thanks are also needed to Wiliam, who provided essential support during the Rietveld Refinement stage of this work. Additionally, I would like to thank Suellen for the help provided during part of the experimental step.

I want to acknowledge CAPES (Coordenação de Aperfeiçoamento de Pessoal de Nível Superior) and FAPESQ-PB (Fundação de Apoio à Pesquisa do Estado da Paraíba) for financial support.

Last but not least, this work would not be possible without the continuous support my family members have provided. Alongside Clara, my beloved companion throughout this work, their assistance was crucial for the completion of this work. My gratitude towards them cannot be thoroughly described with words.

## RESUMO

Durante as últimas décadas, a reação álcali sílica (RAS) tem sido considerada como uma séria preocupação para estruturas de concreto. Caracterizada pela interação química entre minerais silicatos reativos presentes no agregado e álcalis liberados pelo cimento Portland, este processo deletério resulta na formação de um produto hidrofílico conhecido como gel de álcali sílica (A-S-G). Para fins de mitigação dos efeitos nocivos desta patologia, é de conhecimento geral o efeito benéfico da incorporação de adições minerais sobre a mistura do concreto. Além disso, entende-se que as adições ricas em alumínio, como cinza volante e metacaulinita, apresentam desempenho superior àquelas constituídas apenas de sílica, entretanto, não há consenso quanto ao seu mecanismo de ação. Em paralelo à problemática, uma nova classe de materiais cimentícios conhecida como geopolímeros vem recebendo crescente interesse devido às suas excepcionais propriedades e reduzida pegada de carbono. Este material é caracterizado pela formação de um gel alcalino aluminossilicato (N-A-S-H) que é responsável por suas propriedades ligantes. Devido à semelhante composição química e ordenamento atômico destes géis, abre-se a porta para um estudo comparativo. Desta maneira, o presente trabalho tem por objetivo investigar a incorporação do alumínio sobre géis de álcali sílica cuja composição química esteja entre aquelas do A-S-G e do N-A-S-H. Para tanto, foi utilizado o método de síntese hidrotérmica, no qual soluções com quantidades apropriadas de  $\text{Al}(\text{OH})_3$ ,  $\text{Na}_2\text{SiO}_3$  e  $\text{NaOH}$  foram misturadas e reagidas à 60 °C por 30 dias. Logo após, o gel resultante foi seco à 90 °C por 15 dias e o processado em um moinho de bolas cerâmicas. O produto final foi caracterizado por meio de DRX, MEV/EDS, FTIR, FRX e TG/DSC. O DRX revelou a natureza amorfa dos géis, mas a combinação de aumento de disponibilidade de alumínio e álcalis favoreceu a formação de zeólitas. A TG e o FTIR expuseram o caráter hidrofílico dos géis e detectou que a incorporação de alumínio reduziu a capacidade de absorção da água fracamente combinada, a qual é associada à expansão da RAS. Além disso, a análise pontual do MEV/EDS observou a incorporação de alumínio em géis de sílica a uma taxa entre 0,025 e 0,05 da relação Al/Si. Estes resultados indicam que o alumínio fornecido por adições minerais pode ser incorporado na estrutura do gel de álcali sílica sem cálcio e, conseqüentemente, altera sua capacidade de absorção de água.

**PALAVRAS-CHAVE:** Reação álcali sílica, Gel de álcali sílica, Geopolímero, Alumínio.

## ABSTRACT

For the past decades, alkali silica reaction (ASR) has been a major concern to concrete structures. Typified by the chemical interaction between reactive siliceous minerals from the aggregate and alkalis commonly provided by ordinary Portland cement (OPC), this deleterious process results in the formation of a hydrophilic amorphous gel known as alkali silica gel (A-S-G). Regarding its mitigation methods, it is well-known the beneficial effect of incorporating SCM over the concrete mixture. Moreover, there seems to be a tendency that alumina-rich SCM performs better when compared to its counterparts. Despite the acknowledged positive effect, there is no consensus on how aluminum mitigates ASR. Concurrently, a promising cementitious material generally referred to as geopolymer is receiving ever-growing interest due to its remarkable properties and low carbon footprint. It is characterized by the formation of an alkaline aluminosilicate gel (N-A-S-H), which is responsible for its binding properties. Due to its similarity both in terms of chemical composition and atomic structural ordering, a comparative study between A-S-G and N-A-S-H is possible. Thus, the present study aims to investigate the aluminum incorporation into alkali silicate structures within the chemical composition in between that of A-S-G and N-A-S-H phases. To accomplish this, hydrothermal synthesis method was employed, using solutions with appropriate quantities of  $\text{Al}(\text{OH})_3$ ,  $\text{Na}_2\text{SiO}_3$  and  $\text{NaOH}$ , mixed and left reacting at 60 °C for 30 days. Afterward, the synthetic gels were dried at 90 °C for 15 days and ground in a ceramic ball mill. The resulting reaction products were characterized by means of XRD, FTIR, XRF, SEM/EDS and TGA/DSC. The XRD revealed the predominantly amorphous nature of the gels, yet a combination of increase in aluminum and alkali favored the formation of zeolite minerals. The TGA and FTIR analyses exposed the hydrophilic character of the gels and detected that the incorporation of aluminum reduced the weakly-bonded water absorption capacity, which is associated with the ASR expansion. Furthermore, the SEM/EDS spot analysis revealed the incorporation of aluminum in alkali silica gel with an Al/Si ratio of about 0,025 to 0,05. These findings indicate that aluminum species released from SCM can be incorporated into the non-calcium alkali silica gel chemical composition and, as a result, change its water absorption capacity.

**KEYWORDS:** Alkali silica gel, Alkali silica reaction, Geopolymer, Aluminum.

## TABLE OF CONTENTS

<b>1. INTRODUCTION .....</b>	<b>16</b>
1.1 MAIN OBJECTIVE.....	20
1.2 SECONDARY OBJECTIVES.....	20
1.3 ORGANIZATION OF THE CONTENTS.....	20
<b>2. LITERATURE REVIEW .....</b>	<b>22</b>
2.1 ALKALI SILICA REACTION .....	22
2.1.1 Reaction Mechanism .....	23
2.1.2 Alkali Silica Gel (A-S-G).....	26
2.1.3 SCM's Effect.....	28
2.1.4 Aluminum Effect .....	30
2.1.5 Lithium Effect .....	32
2.1.6 Calcium Effect.....	34
2.2 GEOPOLYMER.....	35
2.2.1 Geopolymeric Synthesis.....	36
2.2.2 Geopolymer Gel (N-A-S-H).....	38
2.2.3 Properties .....	39
2.2.4 Zeolite Minerals.....	42
2.3 CHARACTERIZATION TECHNIQUES .....	43
2.3.1 X-Ray Fluorescence.....	43
2.3.2 X-Ray Diffraction .....	43
2.3.3 Fourier-Transformed Infrared Spectroscopy .....	44
2.3.4 Thermal Analysis.....	44
2.3.5 Scanning Electron Microscopy.....	45
<b>3. MATERIALS AND METHODS.....</b>	<b>47</b>
3.1 PRECURSOR MATERIALS .....	47
3.2 SYNTHESIS PROCEDURE .....	49
3.3 CHARACTERIZATION TECHNIQUES .....	52
3.3.1 X-Ray Fluorescence.....	52
3.3.2 X-Ray Diffraction .....	52
3.3.3 Scanning Electron Microscopy.....	52
3.3.4 Fourier-Transformed Infrared Spectroscopy .....	53
3.3.5 Thermal Analysis.....	53

<b>4. RESULTS AND DISCUSSION.....</b>	<b>54</b>
4.1 VISUAL ASSESSMENT .....	54
4.2 X-RAY FLUORESCENCE (XRF) .....	57
4.3 X-RAY DIFFRACTION (XRD) .....	59
4.4 FOURIER-TRANSFORMED INFRARED SPECTROSCOPY (FTIR).....	65
4.5 THERMAL ANALYSIS (TGA/DTG/DSC) .....	69
4.6 SCANNING ELECTRON MICROSCOPY COUPLED WITH EDS (SEM/EDS).....	75
4.6.1 <i>Colored BSE analysis</i> .....	75
4.6.2 <i>EDS spot analysis</i> .....	76
<b>5 CONCLUSION.....</b>	<b>83</b>
5.1 IMPLICATIONS FOR CONCRETE SCIENCE AND TECHNOLOGY .....	84
5.2 RECOMMENDATION FOR FUTURE RESEARCHES.....	84
<b>REFERENCES.....</b>	<b>86</b>
<b>APPENDIX I – EDS SPOT ANALYSIS RESULT .....</b>	<b>93</b>

## LIST OF SYMBOLS

–	Simple bond
=	Double bond
≡	Triple bond
≡Si–O–Si≡	Siloxane group
≡Si–OH	Silanol group
A-S-G	Alkali silica gel
AAR	Alkali aggregate reaction
ABNT	Associação Brasileira de Normas Técnicas
Al(OH) <sub>3</sub>	Aluminum hydroxide (Bayerite)
Al <sub>2</sub> O <sub>3</sub>	Aluminum oxide (Corundum)
ASR	Alkali silica reaction
ASTM	American Society for Testing and Materials.
BFS	Blast furnace slag
BSE	Backscattering electron
C-A-S-H	Calcium aluminosilicate hydrate
C-S-H	Calcium silicate hydrate
DTA	Differential thermal analysis
DSC	Differential scanning calorimetry
EDS	Energy dispersive spectroscopy
FA	Fly ash
FTIR	Fourier-transform infrared spectroscopy
N-A-S-H	Alkaline aluminosilicate hydrate
Na <sub>2</sub> CO <sub>3</sub> .H <sub>2</sub> O	Sodium carbonate monohydrate (Thermonatrite)
Na <sub>2</sub> O <sub>eq</sub>	Equivalent sodium oxide content
Na <sub>2</sub> SiO <sub>3</sub>	Sodium silicate
NaOH	Sodium hydroxide
M <sup>+</sup>	Monovalent cation (Na <sup>+</sup> or K <sup>+</sup> )
MK	Metakaolin
NMR	Nuclear magnetic resonance
OPC	Ordinary Portland cement
SE	Secondary electron

<b>SEM</b>	Scanning electron microscopy
<b>SF</b>	Silica fume
<b>SCM</b>	Supplementary cementitious materials
<b>TGA</b>	Thermogravimetric analysis
<b>XRD</b>	X-ray diffraction
<b>XRF</b>	X-ray fluorescence



## LIST OF FIGURES

Figure 1 – Deterioration signs at Paulo Guerra Bridge, Recife-PE.....	17
Figure 2 – Silica’s solubility as a function of solution pH. ....	24
Figure 3 – Silicate minerals microstructure: a) Crystalline b) Amorphous.....	25
Figure 4 – Nanostructural modeling of alkali silica gel .....	27
Figure 5 – Ternary diagram ( $\text{SiO}_2\text{-CaO-Na}_2\text{O}$ ) of A-S-G chemical composition.....	28
Figure 6 – Ternary diagram ( $\text{SiO}_2\text{-CaO-Al}_2\text{O}_3$ ) of SCM’s chemical composition. ....	29
Figure 7 – Simplified geopolymerization model. ....	37
Figure 8 – Three-dimensional representation of N-A-S-H gel nanostructure. ....	39
Figure 9 – Compressive strength and Young’s modulus in function of Si/Al ratio. ....	40
Figure 10 – SEM micrographs of metakaolin geopolymers with different values of Si/Al ratio: a)1,15; b)1,40; c)1,65; d)1,90; e)2,15 .....	41
Figure 11 – Framework of Na-faujasite. ....	43
Figure 12 – Illustration of the diffraction phenomenon in a crystal lattice. ....	44
Figure 13 – Pear shaped region of physical-chemical interactions common in SEM.....	45
Figure 14 – Sodium silicate diffractogram.....	48
Figure 15 – Aluminum hydroxide diffractogram .....	48
Figure 16 – Synthetic gels chemical composition in the ternary diagram ( $\text{SiO}_2\text{-Al}_2\text{O}_3\text{-Na}_2\text{O}$ ).....	49
Figure 17 – Gel’s synthesis procedure summary. ....	50
Figure 18 – Zoomed-in version of the ternary diagram ( $\text{SiO}_2\text{-Al}_2\text{O}_3\text{-Na}_2\text{O}$ ) highlighting each sample location.....	51
Figure 19 – Light yellowish tone on the top surface of samples 10, 11 and 12 .....	55
Figure 20 – Visual assessment of high aluminum content gels: sample 1 resembles metakaolin geopolymer whereas samples 5 and 9 are similar to dried gypsum.....	56
Figure 21 – The explicit phase-segregated sample 10. The blue arrow indicates the likely precipitated aluminum reaction products while the red arrow points to the top surface colorless phase.....	57
Figure 23 – Chemical composition comparison between what was planned and what was achieved. ....	59
Figure 24 – XRD diffractograms of samples 1 to 4 .....	60
Figure 25 – XRD diffractograms of samples 5 to 8 .....	61
Figure 26 – XRD diffractograms of samples 9 to 12. ....	62

Figure 27 – Crystallinity degree of synthetic gels. ....	64
Figure 28 – FTIR spectra of all synthetic gels in the range of 800-400 $\text{cm}^{-1}$ . ....	66
Figure 29 – FTIR spectra of all synthetic gels in the range of 1500-800 $\text{cm}^{-1}$ . ....	67
Figure 30 – FTIR spectra of all synthetic gels in the range of 4000-1500 $\text{cm}^{-1}$ . ....	67
Figure 31 – Individual thermogravimetric and heat flow plots of samples 1-4. ....	70
Figure 32 – Individual thermogravimetric and heat flow plots of samples 5-12. ....	71
Figure 33 – Thermogravimetric result depicted in terms of loss of mass for each temperature range. ....	72
Figure 34 – Correlation between the crystallinity degree and the loss of mass at 25-100 °C and 500-750 °C. ....	72
Figure 35 – Different DTG pattern behavior on the range of 50-120 °C of samples: a) 4, 8, 11 and 12; b) 2, 3 and 7; c) 1 and 6; d) 5, 9 and 10. ....	74
Figure 36 – Colored BSE micrograph at a magnification of 25x of a) Sample 1, b) Sample 2, c) Sample 3 and d) Sample 4. The Al/Si x Na/Si scatter plot is shown in e). ....	78
Figure 37 – Colored BSE micrograph at a magnification of 25x of a) Sample 5, b) Sample 6, c) Sample 7 and d) Sample 8. The Al/Si x Na/Si scatter plot is shown in e). ....	79
Figure 38 – Colored BSE micrograph at a magnification of 25x of a) Sample 9, b) Sample 10, c) Sample 11 and d) Sample 12. The Al/Si x Na/Si scatter plot is shown in e). ...	80
Figure 39 – Relative frequency distribution of Na/Si of the synthetic gels. ....	81
Figure 40 – Relative frequency distribution of Al/Si of the synthetic gels. ....	82

## LIST OF TABLES

Table 1 – Published work involving synthetic gels (A-S-G or N-A-S-H) in the last 15 years.....	19
Table 2 – Alkali silica gel chemical composition range.....	26
Table 3 – Molar ratios used by Duxson <i>et al.</i> (2005) to synthesize geopolymers.....	40
Table 4 – Sodium silicate technical report verified by the manufacturer.....	47
Table 5 – Synthetic gels chemical composition .....	51
Table 6 – Bulk chemical composition of the synthesized gels (%wt.).....	58
Table 7 – FTIR result summary table.....	68

## 1. INTRODUCTION

Among many deleterious processes that occur in concrete structures, alkali aggregate reaction (AAR) has been receiving notorious relevance in the last decades. According to Mehta and Monteiro (2006), this pathology is characterized by chemical interaction between alkalis, usually provided by the Portland Cement, and reactive minerals that constitute the aggregate.

Depending on the type of the reactive mineral involved, AAR can be classified as alkali silica reaction (ASR), alkali silicate reaction and alkali carbonate reaction, being the former the most widely researched and widespread worldwide. This reaction produces a hygroscopic gel as a final product, known as alkali silica gel (A-S-G), in which, at the presence of humidity, is capable of expanding and exert internal pressure on the concrete, leading to cracks that will significantly reduce its mechanical performance and facilitate the intrusion of harmful external agents.

This pathology was first identified by Stanton (1940) when he studied the occurrence of expansion and cracking in concrete pavements in California in the 1930s. In this investigation, Stanton (1940) observed that the expansion only developed when certain types of mineral aggregates were present and alkali's cement content surpassed a particular threshold.

Since the second half of the twentieth century, more than 30 cases of AAR were identified in large size hydraulic structures in Brazil, including several hydropower plants, such as Furnas (MG) and Paulo Afonso IV (FAIRBAIRN, 2017). At the beginning of the twenty-first century, numerous cases were discovered in the metropolitan region of Recife. Among those, the Paulo Guerra Bridge was diagnosed with 5 mm wide cracks in its pile caps (ÁVILA; FONTE, 2002), see Figure 1, and many other commercial and residential building were identified with severe AAR damage in its foundations.

Regarding the mitigation to this deleterious process, it is well known that the employment of low alkali cement and innocuous mineral aggregates are effective ways of lowering the expansion caused by ASR (POOLE; SIMS, 2017). Moreover, the incorporation of supplementary cementitious materials (SCM), such as silica fume and fly ash, as partial replacement of cement, is another competent approach to address the ASR problem and, at the same time, recycle waste materials from other industries (DUCHESNE; BÉRUBÉ, 1994; THOMAS, 2011). Last, the application of lithium salts as SCM also proved to cause positive effects over ASR, but its low availability worldwide and the competition with other

industries made that alternative economically unfeasible (FENG et al., 2010; LEEMANN et al., 2014).

Figure 1 – Deterioration signs at Paulo Guerra Bridge, Recife-PE



Source: Helene, Carvalho, and Pacheco (2017)

Furthermore, recent studies have shown that alumina rich SCM (e.g. metakaolin and fly ash) are more effective than those composed purely by silica (e.g. silica fume) (CHAPPEX; SCRIVENER, 2012b, 2013; RAJABIPOUR et al., 2015). Nonetheless, there is no consensus on its reaction mechanism. Several studies have reported that aluminum might be incorporated in the reactive silica surface, decreasing its dissolution and thus the whole deleterious process (BICKMORE et al., 2006; CHAPPEX; SCRIVENER, 2012b; ILLER, 1973). On the other hand, aluminum might be able to effectively reduce the alkalinity of the solution since it requires the incorporation of a monovalent cation when bound in tetrahedral sites (CHAPPEX; SCRIVENER, 2012a; HONG; GLASSER, 2002). Finally, untested alternative hypotheses, such as the formation of an aluminum-containing reaction product incapable of expanding, raise the complexity of the issue.

Concurrently, a new materials class exhibiting cementitious properties has been developed since the 1970s (DAVIDOVITS, 1979). Called geopolymer or inorganic polymer, these materials are formed after the alkaline activation of aluminosilicate precursor and comprise the alkali activated materials (AAM), alongside hybrid cement, and the alkali activated slag product (GARCIA-LODEIRO; PALOMO; FERNÁNDEZ-JIMÉNEZ, 2015a). The most outstanding characteristic of these materials is the binding phase, known as N-A-S-H, which is composed by an amorphous alkaline aluminosilicate gel, with the silicon and aluminum atoms centered in tetrahedral sites linked by oxygen atoms, relatively resistant to dissolution in water (PROVIS; VAN DEVENTER, 2009).

Interestingly, N-A-S-H gel resembles in many aspects to A-S-G. First of all, the formation of both involves the dissolution of solid particles, subsequent release of ions

species in solution, coagulation of these ions and the formation of a new predominantly amorphous phase (DUXSON *et al.*, 2007a; RAJABIPOUR *et al.*, 2015). In terms of chemical composition, both are rich in silica ( $\text{SiO}_2$ ) and alkali ( $\text{Na}_2\text{O}$  or  $\text{K}_2\text{O}$ ), yet they differ in alkali silica gel might incorporate calcium ( $\text{CaO}$ ) and while geopolymers are also rich in alumina ( $\text{Al}_2\text{O}_3$ ) (DAVIDOVITS, 1994; HOU *et al.*, 2005). Moreover, similarly to C-S-H found in Portland cement hydration, both gels are known to possess short-range order, i.e. both are widely amorphous but might exhibit nanometric crystalline phases (MERAL; BENMORE; MONTEIRO, 2011).

Due to the need to investigate those materials properties, there is an increasing interest in synthesis techniques in order to produce laboratory gels that resemble those found in the field. For instance, synthetic gels facilitate the process of studying which chemical composition produces the most harmful alkali silica gel (GHOLIZADEH-VAYGHAN; RAJABIPOUR, 2017). Moreover, Hou *et al.* (2005) studied the microstructure of A-S-G found in the field, compared to synthetic ones and concluded, through XRD and NMR results, that the difference between both is minimal. Hence, it suggests that gels might be synthesized with pure reagents in order to study the properties of field gels.

Furthermore, research has been developed with similar methods in geopolymer area. García-Lodeiro *et al.* (2008), for instance, used sol-gel procedure to synthesize N-A-S-H and C-S-H gels but failed to characterize its reaction product with only FTIR. Likewise, Zheng *et al.* (2009) produced geopolymer precursors via sol-gel method and concluded through XRD and NMR that it resembles to metakaolin. Table 1 shows a list of published work in cementitious materials involving the synthesis of gels under laboratory conditions in the last 15 years.

Considering the problematic situation involving the harmful effects of ASR on concrete structures and the ever-increasing interest in a sustainable binder material, further research is needed in both ASR and geopolymer fields. Additionally, the recent trend of synthesizing gels under controlled conditions opens a myriad of opportunities to investigate materials otherwise challenging to assess, like alkali silica gel. In this work, 12 gels with intermediate chemical composition to those found of A-S-G and N-A-S-H were synthesized using pure reagents (sodium silicate, aluminum hydroxide and sodium hydroxide). In order to characterize the reaction products, XRD, FTIR, thermal analysis and SEM coupled with EDS were used.

Table 1 – Published work involving synthetic gels (A-S-G or N-A-S-H) in the last 15 years.

Authors	Title	Year
Hou, Struble and Kirkpatrick	Formation of ASR gel and the roles of C-S-H and portlandite.	2004
Hou <i>et al.</i>	Structural Investigations of Alkali Silicate Gels.	2005
Garcia Lodeiro <i>et al.</i>	FTIR study of the sol-gel synthesis of cementitious gels: C-S-H and N-A-S-H.	2008
Zheng <i>et al.</i>	Preparation of geopolymer precursors by sol-gel method and their characterization.	2009
Tsai <i>et al.</i>	Solid-state NMR study of geopolymer prepared by sol-gel chemistry.	2010
Almeida	Synthesis and characterization of alkali silica gel under accelerated condition.	2015
Walkley <i>et al.</i>	Phase evolution of Na <sub>2</sub> O-Al <sub>2</sub> O <sub>3</sub> -SiO <sub>2</sub> -H <sub>2</sub> O gels in synthetic aluminosilicate binders.	2016
Gholizadeh Vayghan, Rajabipour and Rosenberger	Composition–rheology relationships in alkali–silica reaction gels and the impact on the gel's deleterious behavior.	2016
Gholizadeh Vayghan and Rajabipour	The influence of alkali–silica reaction (ASR) gel composition on its hydrophilic properties and free swelling in contact with water vapor.	2017
Gholizadeh Vayghan and Rajabipour	Quantifying the swelling properties of alkali-silica reaction (ASR) gels as a function of their composition.	2017
Balachandran, Muñoz and Arnold	Characterization of alkali silica reaction gels using Raman spectroscopy.	2017
Shi <i>et al.</i>	Synthesis, characterization, and water uptake property of alkali-silica reaction products	2019
Geng <i>et al.</i>	Atomistic structure of alkali-silica reaction products refined from X-ray diffraction and micro X-ray absorption data	2019
Shi and Lothenbach	The combined effect of potassium, sodium and calcium on the formation of alkali-silica reaction products	2020

Source: Own authorship

## **1.1 Main Objective**

This work aims to investigate the aluminum incorporation into alkali silicate structures within the chemical composition in between that of A-S-G and N-A-S-H phases.

## **1.2 Secondary Objectives**

- Determine, through XRF, the chemical composition of the synthetic gels.
- Analyze the influence of aluminum and alkali over the formation of crystalline phases.
- Assess the hydrophilic behavior of the synthetic gels by means of thermogravimetric analysis.
- Evaluate the coordination in which aluminum and silicon atoms are incorporated in the synthetic gel's framework.
- Investigate the formation of clustered phases in the synthetic gels using SEM/EDS analysis at low magnification.
- Determine whether the synthetic gel can incorporate aluminum into its framework.

## **1.3 Organization of the Contents**

In addition to the introduction, where the scope of the research has been briefly discussed, and the objectives posed, this dissertation comprises four additional chapters, in a way to cover the entire proposed content. The chapters distribution are as follows:

Chapter 2 (Literature Review) introduces and explains the terms and theories that compose this work. This section is divided into two parts, being the first one focused on ASR, whereas the second is centered at geopolymers. Both parts emphasize topics like reaction mechanism and microstructure of reaction products. Secondary topics such as the effect of chemical elements over ASR and geopolymer properties are also discussed.

Chapter 3 (Materials and Methods) characterizes and discusses the precursor materials that were used to produce the synthetic gels and the experimental design is thoroughly detailed. Moreover, the characterization techniques and its parameters used are concisely summarized.



Chapter 4 (Results and Discussion) displays the results of the characterization of the synthetic gels by means of XRF, XRD, FTIR, Thermal analysis and SEM/EDS, and discusses its findings with the current literature in order to better understand the synthesis procedure and the reaction products itself.

Finally, Chapter 5 (Conclusion) briefly summarizes the main ideas taken from the findings. In addition to that, recommendations for future investigations about synthetic gels are given.

## 2. LITERATURE REVIEW

### 2.1 Alkali Silica Reaction

The alkali silica reaction (ASR) is a deleterious process found in concrete structures and is characterized by the chemical interaction between aggregate siliceous minerals and alkalis, generally provided by Portland Cement (MEHTA; MONTEIRO, 2006). This process results in the formation of a hygroscopic reaction product, known as alkali silica gel (A-S-G), that, in the presence of humidity, expands and exerts pressure of up to 11 MPa within concrete pore structure (STRUBLE; DIAMOND, 1981). Since concrete is considerably vulnerable to tensile stress, ASR frequently causes uniformly distributed cracks within the concrete structure.

This pathology is commonly found in concrete structures that retain excessive humidity, enough alkalis, and reactive minerals. Thus, hydraulic structures, e.g. dams, and bridge block foundations, are especially susceptible to ASR (RIVARD *et al.*, 2010). Additionally, alkali silica reaction can also occur in residential building foundations, and such was the cases found in Recife (ANDRADE; SILVA; HASPARYK, 2008).

Overall, there are three factors required for the occurrence of ASR:

- Available alkalis ( $\text{Na}_2\text{O}$  e  $\text{K}_2\text{O}$ );
- Reactive silica ( $\text{SiO}_2$ );
- Humidity ( $\text{H}_2\text{O}$ );

The alkalis are generally provided to the concrete through Portland Cement. For this reason, the equivalent alkali content ( $\text{Na}_2\text{O}_{\text{eq}}$ ), defined by Equation 1, is limited up to 0,6% in most Portland Cement standard compositions (ASTM C-150, 2007). Furthermore, the aggregate might contribute to concrete's alkali content, but its effect over concrete prism expansion is negligible even when the most alkaline aggregates were used (DROLET; DUCHESNE; FOURNIER, 2017). Even if the concrete prism expansion test might not be the most suitable technique to assess aggregate's alkali content effect over ASR, it seems that cement's alkali is far more concerning because of its reactivity. It is common knowledge that alkalis are essential to initiate the deleterious process since it maintains the high pore solution pH and maximizes silica dissolution. Additionally, alkalis are known to be incorporated into the gels chemical composition (GHOLIZADEH VAYGHAN; RAJABIPOUR; ROSENBERGER, 2016; HOU; STRUBLE; KIRKPATRICK, 2004; RAJABIPOUR *et al.*, 2015).

$$\text{Na}_2\text{O}_{\text{eq}}(\%) = \text{Na}_2\text{O}(\%) + 0,658 * \text{K}_2\text{O}(\%) \quad \text{Equation 1}$$

The reactive silica is regularly found in reactive aggregate as siliceous minerals. It is well known that the most vulnerable minerals to ASR those which contain silica in its amorphous form, e.g. opal and glass, followed by metastable crystals like tridymite and cristobalite (RAJABIPOUR *et al.*, 2015). Nonetheless, crystalline silica minerals like quartz and mica might also provoke ASR when strains or faults are present in its microstructure, which will work as an internal path by the alkali attack (TIECHER *et al.*, 2017). However, the presence of reactive minerals does not guarantee the initiation of ASR. According to Frýbort *et al.* (2018), the most likely cause of that is alkali deficiency.

Furthermore, aggregate's size seems to be of high importance when considering its effect over ASR development. Juenger e Ostertag (2004) states that silica fume, which is known for its benign effect over ASR, might generate gel's expansion when clustered on the concrete, which suggests that there might be a pessimum aggregate size responsible for maximum expansion. The results of this study seem to correlate ASR to pozzolanic reaction, as was previously reported by Urhan (1987).

Humidity is essential for ASR development since it works in two ways. Firstly, it represents the path by which alkaline ions ( $\text{Na}^+$ ,  $\text{K}^+$  e  $\text{OH}^-$ ) reach the reactive mineral surface and initiate the dissolution process. Secondly, water is absorbed by the alkali silica gel, resulting in its expansion.

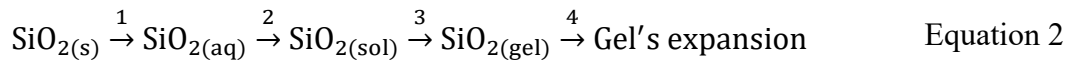
Moreover, some authors claim that the presence of calcium is fundamental to ASR expansion occur. Rajabipour *et al.* (2015) states that calcium is relevant to ASR in two ways: (a) calcium might be incorporated by alkali silica gel by substituting two monovalent alkali ions, what promotes alkali recycling and helps maintain the solution pH high, and (b) the incorporation of calcium by A-S-G change its properties, such as viscosity and water absorption capacity, what results in significant expansion prone gel.

Lastly, according to Frýbort *et al.* (2018), in case the primary requirement factors (i.e. reactive silica presence, alkaline environment, suitable temperature and humidity) are not fulfilled, ASR will not develop.

### 2.1.1 Reaction Mechanism

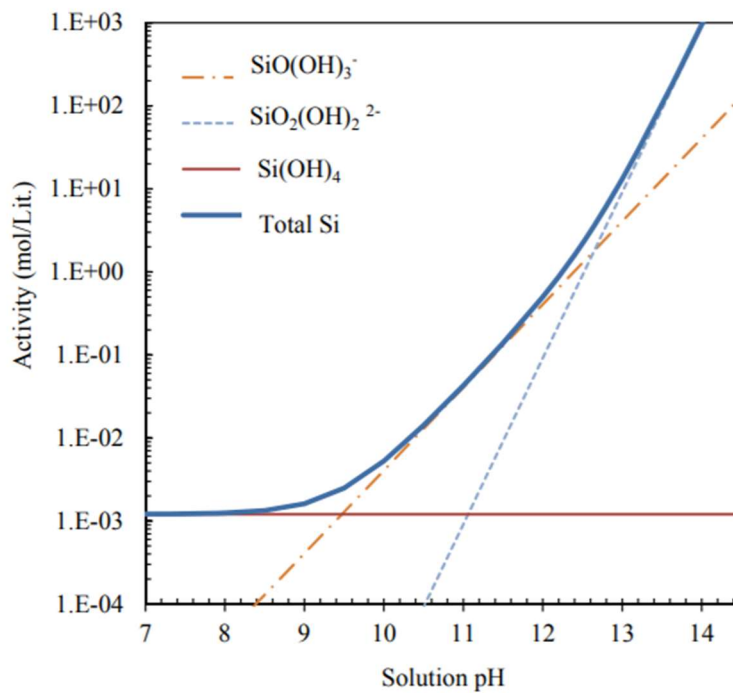
According to Rajabipour *et al.* (2015), ASR's expansion is the final result of a sequence of several chemical reactions, which includes metastable silica dissolution (1),

formation of nanocolloidal silica particles (2), formation of alkali silica gel (3) and its subsequent expansion (4). Equation 2 represents ASR's chemical steps until gel's expansion.



Among those, reaction (1) – metastable silica dissolution – is by far the slowest and, therefore, frequently controls the development of the entire deleterious process. On the other hand, temperature and alkalinity play an essential role in silica dissolution by controlling its reaction kinetics. Regarding the solution's pH, silica is almost insoluble at neutral pH, being significantly more reactive in alkaline solutions, as shown in Figure 2. That is the reason why standard tests that assess ARS expansion, i.e. mortar bar and concrete prism tests, reproduce high alkaline and temperature environment (ABNT, 2008a, 2008b).

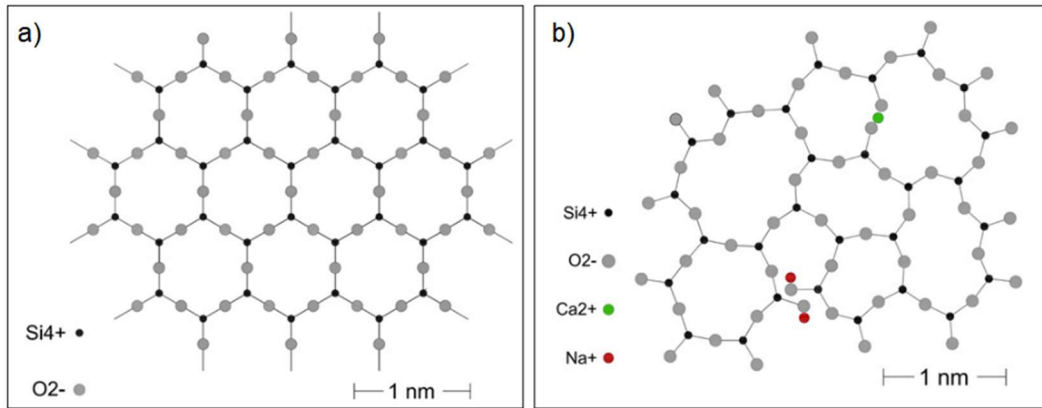
Figure 2 – Silica's solubility as a function of solution pH.



Source: Maraghechi (2014)

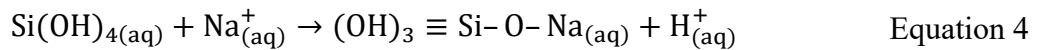
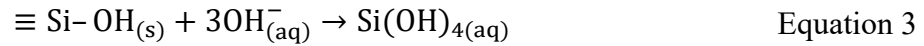
Amid the most susceptible minerals to ASR, silicate minerals, the most widespread rock group in the world, are composed by tridimensional framework of silica ( $\text{SiO}_2$ ) tetrahedra, with silicon atoms centered and linked by oxygen atoms, comprising the siloxane linkages ( $\equiv\text{Si}-\text{O}-\text{Si}\equiv$ ) that characterize this material (BLAND; ROLLS, 1998). Oxygen atoms that link two silicon atoms are called “bridging oxygens”. Moreover, at the edge of the structure, oxygen atoms might bond with hydrogen atoms and form a silanol group ( $\equiv\text{Si}-\text{OH}$ ). According to the spatial ordering of its atoms, the silicate minerals might be classified into crystalline or amorphous, as shown in Figure 3.

Figure 3 – Silicate minerals microstructure: a) Crystalline b) Amorphous

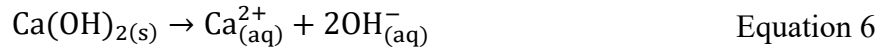
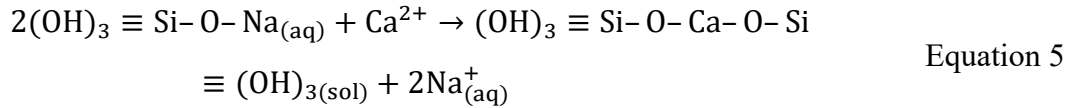


Source: Rajabipour *et al.* (2015)

The silica's dissolution is commonly found in chemical weathering processes and is initiated by the rupture of Si–O bonds inside the silicate microstructure (BLAND; ROLLS, 1998). According to Dent Glasser and Kataoka (1981), the dissolution process is commenced when hydroxyl ions (OH<sup>-</sup>) approach the silicate surface and induce the hydrolysis of Si–O bonds, releasing Si(OH)<sub>4</sub> monomers into solution, as shown by Equation 3. Thus, it is significantly relevant to consider the minerals specific surface area when assessing its potential reactivity and explains the elevated solubility rates of amorphous or poorly crystalline silicate minerals. Once released into solution, Si(OH)<sub>4</sub> monomers incorporate the available monovalent alkali (Na<sup>+</sup> and K<sup>+</sup>), as shown by Equation 4.



It can be seen through Equations 3 and 4 that there is a tendency towards pH reduction as OH<sup>-</sup> are being consumed and H<sup>+</sup> are being released. Nevertheless, calcium seems to be crucial for the maintenance of elevated pH. According to Rajabipour *et al.* (2015), Ca<sup>2+</sup> recycles the alkali ions by breaking Na–O bond and joining together two (OH)<sub>3</sub>≡Si–O<sup>-</sup> molecules. As Ca<sup>2+</sup> is being consumed, solid calcium hydroxide (Ca(OH)<sub>2</sub>), found in abundance in Portland Cement concrete as the shape of portlandite, intensifies its dissolution process. Equation 5 shows the described procedure. As a result, Na<sup>+</sup> and OH<sup>-</sup> returns to the concrete pore solution, maintaining its high pH and perpetuating the silica dissolution process. Thus, while there are portlandite crystals available near the silica dissolution site, the process tends to continue indefinitely. The formation of Equation 5 reaction product (H<sub>6</sub>CaSi<sub>2</sub>O<sub>8</sub>) marks the second step of Equation 2, called condensation (RAJABIPOUR *et al.*, 2015).



Kim and Olek (2014) also propose that ASR is a result of a series of chemical reactions occurring inside concrete. According to them, the ASR process initiates with silica dissolution caused by hydroxyl attack. The dissolved silica ions promptly react with calcium species available and produce tobermorite-like C-S-H. In this stage, silica dissolution continues at a constant rate as long as there are calcium sources accessible. Once nearby calcium reservoirs (i.e., C-S-H and  $\text{Ca}(\text{OH})_2$ ) have been depleted, Si concentration in solution starts to increase, and that leads to the formation of highly polymerized high-alkali low-calcium silica hydrates (C-(Na/K)-S-H). Further increase in silica ions concentration yields the formation of ASR gel, which readily reacts with C-S-H near the reaction site. Afterward, the gel extrudes the aggregate, reaches the cement paste, and takes up more calcium.

### 2.1.2 Alkali Silica Gel (A-S-G)

The literature demonstrates that alkali silica gel is predominantly composed of silicon, oxygen, hydrogen, monovalent alkalis (Na and K) and, in smaller proportion, bivalent alkalis (Ca and Mg) (Hou *et al.*, 2005; Hou, Struble and Kirkpatrick, 2004). These gels do not possess a fixed chemical formula. However, it is known to occasionally incorporate other elements in its structure (e.g. lithium), changing its properties and expansion capability (LEEMANN *et al.*, 2015). Regarding chemical composition, Hou, Struble and Kirkpatrick (2004) state that field gels, i.e. those found on in-service concrete structures, are known to have molar ratios presented in Table 2.

Table 2 – Alkali silica gel chemical composition range.

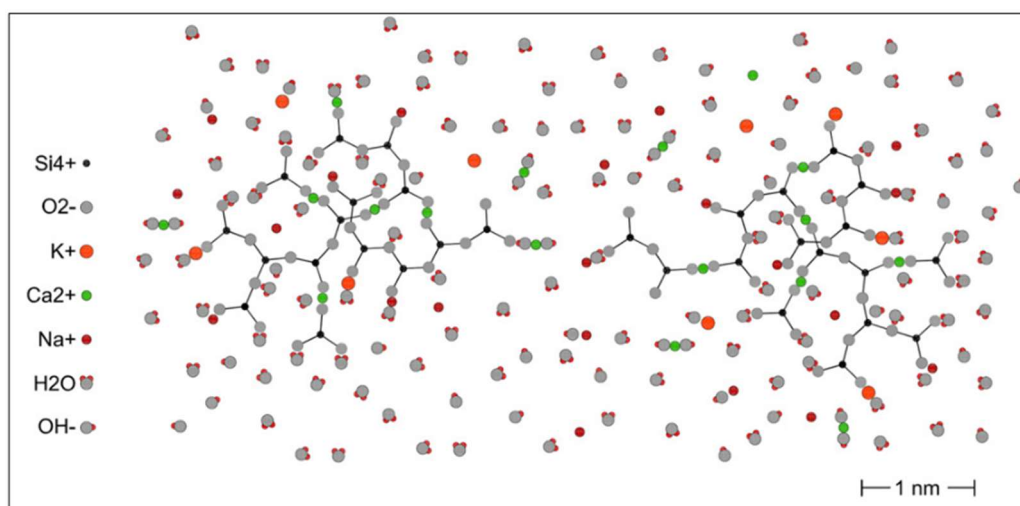
Molar Ratio	Minimum Value	Maximum Value
$\frac{\text{Na}_2\text{O} + \text{K}_2\text{O}}{\text{SiO}_2}$	0,02	0,60
$\frac{\text{CaO} + \text{MgO}}{\text{SiO}_2}$	0,00	0,20

Source: Hou, Struble and Kirkpatrick (2004)

A nanostructural representation of alkali silica gel is shown in Figure 4 (RAJABIPOUR *et al.*, 2015), where it can be seen that monovalent alkalis ( $\text{Na}^+$  e  $\text{K}^+$ ) are incorporated at the edge of the molecule, replacing hydrogen atoms in silanol group ( $\equiv\text{Si}-\text{OH}$ ). It can also be seen calcium cations ( $\text{Ca}^{2+}$ ) bonding two oxygen atoms and joining different silica clusters.

Despite the gel's variability, the literature shows that, depending on chemical composition, the gel's detrimental potential might differ widely. According to Struble and Diamond (1981), A-S-G chemical composition considerably affects its expansive behavior and particular compositions might produce innocuous gels. Likewise, Kawamura and Iwahori (2004) suggest that the formation of alkali silica gel does not imply concrete deterioration.

Figure 4 – Nanostructural modeling of alkali silica gel.



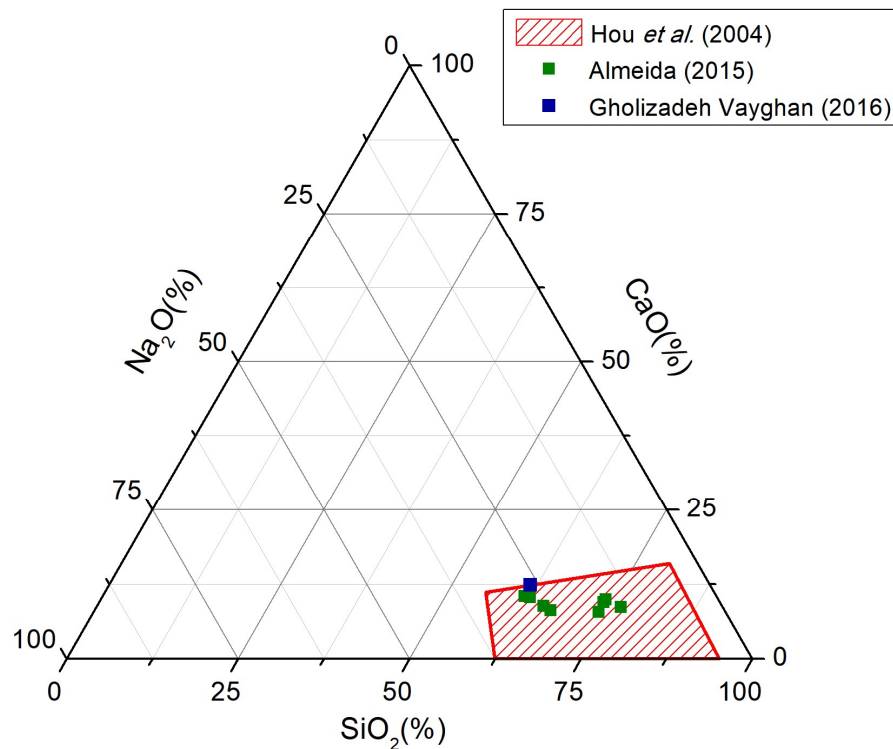
Source: Rajabipour *et al.* (2015)

Moreover, A-S-G chemical composition might undergo alterations over time (GHOLIZADEH-VAYGHAN; RAJABIPOUR, 2017). An example of this phenomenon happens when alkali silica gel forms inside of cracked mineral aggregate. In this case, the mineral crack act as a passage in which aggressive ions seize to reach the silica surface and start the dissolution process, afterward forming a low Ca/Si gel. Eventually, because of its low viscosity, the gel might be transported to the exterior of the mineral aggregate, a vicinity filled with calcium species, incorporate  $\text{Ca}^{2+}$  ions, raising its Ca/Si ratio and altering its expansive behavior.

Additionally, Gholizadeh Vayghan, Rajabipour and Rosenberger (2016) studied the relationship between A-S-G chemical composition and its rheological properties and concluded that

Lastly, the chemical composition of different alkali silica gels found in the literature is shown in Figure 5. The red quadrilateral region represents the composition of field alkali silica gels, outlined in Table 2 (HOU; STRUBLE; KIRKPATRICK, 2004). The green squares correspond to A-S-G synthesized under accelerated conditions, i.e. 28 days and up to 80°C, employing Pyrex powder and NaOH solution as precursor materials (ALMEIDA, 2015). The isolated blue square represents the chemical composition ( $\text{Ca}/\text{Si}=0,2$  and  $\text{Na}/\text{Si}=0,85$ ) of the most expansion prone alkali silica gel.

Figure 5 – Ternary diagram ( $\text{SiO}_2\text{-CaO-Na}_2\text{O}$ ) of A-S-G chemical composition



Source: Own authorship with data from Almeida (2015), Hou, Struble and Kirkpatrick (2004) and Gholizadeh Vayghan, Rajabipour and Rosenberger (2016)

### 2.1.3 SCM's Effect

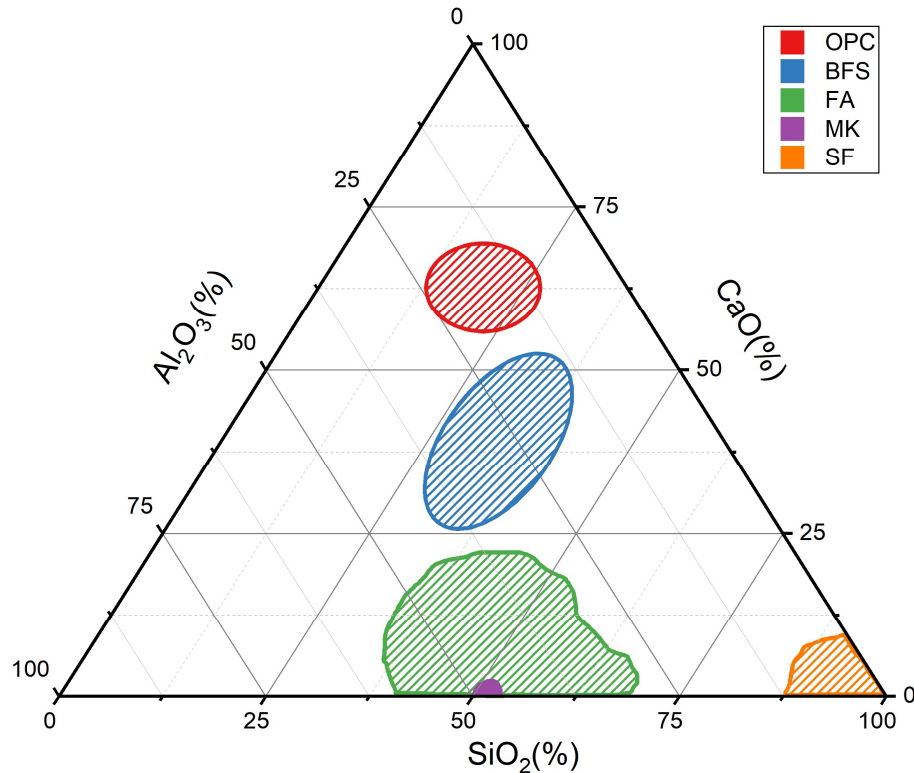
Supplementary cementitious materials (SCM) are finely divided siliceous materials incorporated into concrete mixture in order to improve its mechanical and durability properties (MEHTA; MONTEIRO, 2006). Depending on its origin source, SCM can be classified as natural, e.g., natural pozzolans, or third-party residue, e.g., fly ash and blast furnace slag.

Despite being merged as a single group, those materials might differ widely in numerous properties. For instance, silica fume and metakaolin are significantly reactive due



to their high specific area and glassy phase content, whereas limestone filler is nearly inert chemically and owns its positive effect to pure filler effect (KURDOWSKI, 2014). The difference might be significant even in the same materials group. That is the case of fly ash, a fine powder residue of coal combustion, whose chemical composition might differ considerably. Figure 6 shows the chemical composition of established supplementary cementitious materials.

Figure 6 – Ternary diagram ( $\text{SiO}_2$ - $\text{CaO}$ - $\text{Al}_2\text{O}_3$ ) of SCM's chemical composition.



Source: Adapted from Garcia-Lodeiro, Palomo and Fernández-Jiménez (2015)

Concerning its effect over ASR, it is well known that the incorporation of SCM as partial replacement of Portland Cement has a positive effect in decreasing expansion when compared to regular concrete. According to Thomas (2011), its efficiency relies on the following factors:

- Chemical composition, especially  $\text{CaO}/\text{SiO}_2$  ratio;
- The amount of concrete's alkali content;
- The amount of reactive aggregate available;

The  $\text{CaO}/\text{SiO}_2$  represents an important factor when considering whether a given SCM is effective in mitigating ASR. The lower the calcium content or the higher silica content, the greater will be the SCM efficiency (THOMAS, 2011). Therefore, it can be understood that silica fume is considerably more efficient when compared to blast furnace slag or fly ash due to its chemical composition. The hypothesis of calcium's detrimental

contribution is likely to be related to its role in A-S-G formation. On the other hand, silica's beneficial aspect is probably correlated to pozzolanic reaction, whose reaction product reduces mass transportation and increase concrete strength.

In regard to concrete's alkali content, it is known that Portland Cement is its primary source and, because of that, several standard specifications limit its alkali equivalent content ( $\text{Na}_2\text{O}_{\text{eq}}$ ) to 0,6% (ASTM C 150 - 07, 2007). Nonetheless, SCMs might also contribute to concrete's alkali content and that is an important consideration when assessing which SCM use to mitigate ASR (DUCHESNE; BÉRUBÉ, 1994). Furthermore, mineral aggregate may also release alkali to the concrete pore solution, yet its effect on ASR expansion is minimal even when the most alkaline minerals are employed (DROLET; DUCHESNE; FOURNIER, 2017). Overall, the higher concrete's alkali content, the greater is the quantity of SCM required to mitigate ASR deterioration (DUCHESNE; BÉRUBÉ, 1994; THOMAS, 2011).

Additionally, the proportion of reactive minerals is also a relevant factor when seeking mitigation alternatives to ASR expansion. Thus, the amount of SCM needed to mitigate deterioration is directly proportional to concrete's reactive aggregate content.

Numerous hypothesis has been proposed in order to explain the benign effect of SCM incorporation over ASR deleterious process. Shafaatian *et al.* (2013) investigated the mechanism in which fly ash decreases ASR expansion and observed that a reduction in concrete pore solution alkalinity was caused by the formation of low Ca/Si C-S-H gel, which has a higher alkali absorption potential, consequently decreasing silica dissolution. Likewise, Saha *et al.* (2018) also studied the influence of fly ash incorporation over ASR and concluded that the admixture modifies A-S-G chemical composition and its expansion capacity. Also, Aquino, Lange and Olek (2001) examined the effect of silica fume and metakaolin insertion and noticed that both are equally capable of mitigating ASR damaging process. Lastly, Thomas (2011) states that SCMs effectively mitigate ASR by decreasing the alkali available and that alkali binding ability is strongly related to the admixture  $\text{CaO}/\text{SiO}_2$  ratio and alkali content.

#### **2.1.4 Aluminum Effect**

Several studies have indicated the beneficial effects of aluminum incorporation on ASR and mentioned that alumina-rich SCM, e.g. metakaolin and class F fly ash, are more effective when compared to low-alumina SCM (CHAPPEX; SCRIVENER, 2012a, 2013; HAY; OSTERTAG, 2019; RAJABIPOUR *et al.*, 2015). However, the exact mechanism in

which it is obtained is still controversial. In this regard, Szeles et al. (2017) proposed five hypothetical mechanisms in which aluminum can mitigate ASR expansion: (i) Reduction of pH and alkali concentration in concrete pore solution, (ii) Consumption of  $\text{Ca(OH)}_2$ , (iii) Decrease of silica dissolution, (iv) Modification of the reaction product chemical composition and the formation of innocuous gel and (v) Increase in pore structure density and reduction in mass transport inside concrete.

Since the 1970s, studies have shown that alumina is capable of reducing silica dissolution. Iler (1973) observed that aluminum is absorbed in the colloidal silica surface when the latter is exposed to  $\text{Al(NO)}_3$  solution, creating a layer of aluminosilicates that protects the susceptible Si–O bonds from the attack of aggressive  $\text{OH}^-$  ions. Furthermore, Bickmore *et al.* (2006) report that  $\text{Al(OH)}_4^-$  ion can reduce up to 85% of quartz dissolution rate and this effect is greater at lower pH levels and higher  $\text{Al(OH)}_4^-$  concentration.

When aluminum is absorbed by the silicate mineral surface, the former replaces the latter in tetrahedral structure (HONG; GLASSER, 2002). Bear in mind that aluminum and silicon are commonly found in nature under the form of  $\text{Al}^{3+}$  and  $\text{Si}^{4+}$ , respectively, it appears clear that a monovalent cation  $\text{M}^+$  is required to charge-balance the aluminum substitution. Therefore, the hypothesis of aluminum incorporation on the surface of vulnerable reactive mineral has a welcoming secondary effect of decreasing alkali concentration in the concrete pore solution.

However, it is still debatable whether the alkali binding contribution is significant to reduce ASR or not. In this regard, some authors investigated the influence of alkali binding in C-S-H and C-A-S-H gels. Hong and Glasser (2002) state that the inclusion of aluminum on C-A-S-H gel structure tends to increase alkali binding. Conversely, Chappex and Scrivener (2012a) report that alkali binding is not sufficient to justify benign aluminum effect and that other factors are likely to contribute to it.

With the assistance of SEM image analysis, Chappex and Scrivener (2012b) noticed that aluminum species are absorbed by the reactive silica surface and significantly decrease silica dissolution, interrupting ASR development. Moreover, it was observed that a concentration of 3,9 mM of aluminum is capable of considerably decreasing aggregate degradation due to ASR (CHAPPEX; SCRIVENER, 2012b).

In a subsequent study, Chappex and Scrivener (2013) claim that the incorporation of reactive aluminosilicate might have two effects. Firstly, reactive silica present in these minerals change C-S-H chemical composition, increasing Si/Ca and alkali absorption, which reduce pH and silica dissolution. Moreover, reactive alumina might be absorbed in the

reactive mineral surface, acting as a protective barrier, and preventing further alkali attack. According to Chappex and Scrivener (2013), it is likely that a synergetic combination of these two effects might be able to explain why alumina-rich SCM feature high ASR mitigation efficiency.

Leemann *et al.* (2015) investigated the effect of aluminum provided by metakaolin and by calcium aluminate ( $C_3A$ ) over ASR and observed that aluminum is capable of reducing silica dissolution and delay ASR development, but it did not change the chemical composition of reaction products. However, it was also noted that aluminum-rich systems generated gels dominated by  $Q_2$  sites (tetrahedral chains of  $SiO_2$ ), whereas systems without aluminum produced gels abundant in  $Q_3$  sites (tetrahedral sheets of  $SiO_2$ ), commonly correlated to expansive gels (LEEMANN *et al.*, 2015).

In summary, aluminum effectively reduces reactive silica dissolution, either by alkali consumption and, consequently, pore solution pH reduction, or by the formation of a nanometric aluminosilicate layer that acts as a protective barrier, isolating vulnerable silica mineral from the aggressive environment. Nonetheless, other hypotheses such as alkali consumption due to C-A-S-H production and the formation of aluminum-containing A-S-G cannot be discarded.

### 2.1.5 Lithium Effect

The incorporation of lithium salts are known as one of the best alternatives to mitigate the ASR expansion since the 1950s, when McCoy and Caldwell (1951) investigated numerous materials that could decrease the expansion in the mortar bar accelerated test and noticed that lithium compounds featured superior performance among tested materials. Moreover, Feng *et al.* (2005) reviewed the efficacy of lithium compounds over ASR and concluded that all the studied salts ( $LiF$ ,  $LiCl$ ,  $LiBr$ ,  $LiOH$ ,  $LiOH.H_2O$ ,  $LiNO_3$ ,  $LiNO_2$ ,  $Li_2CO_3$ ,  $Li_2SO_4$ ,  $Li_2HPO_4$ , and  $Li_2SiO_3$ ) decreased ASR expansion if they were incorporated in sufficient quantity. Among these,  $LiNO_3$  seems to be the most promising since it does not increase the pore solution pH (FENG *et al.*, 2005).

Despite lithium's benign effect, it was not clear how it is achieved. In this regard, a few hypotheses can be raised: (i) Reduction in pore solution pH; (ii) Formation of Si-Li reaction product over the mineral surface, protecting it against further alkali attack; (iii) Formation of reaction product crystalline and non-expansive; (iv) Formation of amorphous

Si–Li gel significantly less expansive than conventional A-S-G; (v) Higher silica dissolution, that remains in solution and does not form A-S-G (TREMBLAY et al., 2010).

Feng et al. (2010) studied the mechanism by which  $\text{LiNO}_3$  mitigated ASR expansion and observed the formation of two lithium-containing phases, one crystalline and one amorphous, on top of the reactive mineral surface. The crystalline phase acts as a protective barrier, preventing further alkali attack (FENG et al., 2010). Furthermore, the amorphous gel phase features a low Ca/Si ratio, generating a higher density and lower mobility alkali silica gel when compared to conventional A-S-G (FENG et al., 2010). The study concluded that the combination of these two effects were responsible for  $\text{LiNO}_3$  positive effect.

Similarly, Leemann et al. (2014) investigated the effect of  $\text{LiNO}_3$  in a model system and mortar and detected that lithium is capable of changing ASR reaction product nanostructure, decreasing the amount of  $Q_3$  sites and increasing  $Q_1$  and, mainly,  $Q_2$  sites. Considering that expansive synthetic gels feature a high proportion of  $Q_3$  sites, Leemann et al. (2014) state that the reduction in these sites might be responsible for lithium's beneficial effect.

In a subsequent study, Leemann et al. (2015) highlighted that  $\text{LiNO}_3$  is effective against ASR expansion due to the formation of a high-density reaction product in the reactive aggregate surroundings. Due to lithium's preferential absorption when compared to other alkalis (Na and K) and the limited amount of lithium salt in concrete, it can be stated that lithium's efficacy in ASR mitigation is determined by the reactive mineral specific surface area (LEEMANN et al., 2015). Therefore, the higher the specific surface area of the reactive mineral, the higher will be the amount of lithium salts required to prevent ASR expansion.

Guo et al. (2019) claim that silica preferentially bound to lithium, generating a Li–Si amorphous reaction product less expansive than usual A-S-G. Additionally, it is observed the formation of Li–Si reaction products even in the presence of calcium, which suggests that lithium salts might slow down pozzolanic reaction (GUO; DAI; SI, 2019).

In summary, due to its high reactivity with silicon, lithium is capable of partially substituting sodium and potassium during the formation of alkali silica gel, altering its expansive behavior and reducing its mobility. Additionally, because of its higher density, Li–Si reaction products might be able to isolate the reactive aggregate, interrupting the silica dissolution process. Overall, it is likely that hypotheses (ii), (iii) and (iv) are the most effective ways by which lithium mitigates ASR.

### 2.1.6 Calcium Effect

Calcium is Portland Cement's main constituent element and is present in cement paste composing C-S-H, solid  $\text{Ca(OH)}_2$  (Portlandite) and dissolved in solution. Furthermore, calcium can also be incorporated in alkali silica reaction and is likely to play an essential role in its development (GHOLIZADEH-VAYGHAN; RAJABIPOUR, 2017; HOU et al., 2005; HOU; STRUBLE; KIRKPATRICK, 2004). According to Rajabipour et al. (2015), calcium is likely to influence A-S-G formation in two ways: (i) Replacing alkalis in the alkali silica gel, a process known as “alkali recycling”, and (ii) Altering A-S-G chemical composition and, consequently, its expansive behavior.

Alkali recycling is the incorporation of  $\text{Ca}^{2+}$  ions by nano-colloidal silica molecules, as described by Equation 5 (Page 26). In this process, calcium ions, which generally are abundant in concrete pore solution, replace alkali ions joining two nano-colloidal silica molecules. As a result, there is a tendency for the formation of larger silica gel molecules, the maintenance of elevated pore solution pH. As the dissolved calcium species are consumed, solid  $\text{Ca(OH)}_2$  dissolution intensifies, as shown by Equation 6 (Page 26). Therefore, as long as there are calcium reservoir and sufficient alkalis nearby reactive mineral, silica dissolution will keep going.

Regarding the effect of calcium in A-S-G chemical composition, Hou, Struble and Kirkpatrick (2004) state that alkali silica gel does not form when high Ca/Si C-S-H gel or portlandite are present. Under these conditions, dissolved silica tends to react with calcium and produces even more C-S-H, in a process similar to the pozzolanic reaction. As noted by Hou, Struble and Kirkpatrick (2004), highly polymerized A-S-G, i.e., featuring an elevated proportion of  $\text{Q}_3$  sites, will only be created when nearby calcium is thoroughly depleted. Similarly, Noguchi et al. (2018) investigated the influence of portlandite over pyrex glass dissolution and formation of A-S-G. The experimental results show that portlandite accelerated silica dissolution and the dissolution stops when portlandite is depleted (NOGUCHI et al., 2018). Furthermore, alkali silica gel is only formed when calcium concentration is lower and silica concentration is higher than usual concrete pore solution (HOU; STRUBLE; KIRKPATRICK, 2004; NOGUCHI et al., 2018).

Regarding the influence of calcium incorporation on A-S-G properties, Gholizadeh Vayghan, Rajabipour and Rosenberger (2016) investigated the effect of chemical composition on rheological properties its impact on deleterious behavior. It was shown that the pessimum combination of osmotic and rheological properties corresponds to reaction

products with intermediate calcium and high alkali content ( $\text{Ca/Si}=0,2$  e  $\text{Na/Si}=0,85$ ), which were responsible for the highest expansive pressure (GHOLIZADEH VAYGHAN; RAJABIPOUR; ROSENBERGER, 2016). Moreover, the amount of chemically bound moisture in A-S-G reaches a maximum level when  $\text{Ca/Si}$  is between 0,2 and 0,3 (LEEMANN et al., 2011). Therefore, it can be understood that calcium presence is essential for ASR development and deleterious expansion.

## 2.2 Geopolymer

Geopolymer is a term coined by Davidovits (1979) to appoint a new amorphous aluminosilicate material, produced after the alkaline activation of silica ( $\text{SiO}_2$ ) and alumina ( $\text{Al}_2\text{O}_3$ ) rich precursor material. According to Garcia-Lodeiro, Palomo and Fernández-Jiménez (2015b), these materials are also called inorganic polymers and compose the group of alkaline activated materials (AAM), alongside hybrid cement and the reaction product of high calcium content SCM alkaline activation. Additionally, Provis and Van Deventer (2009) state that the main characteristic of these materials is the binding phase composed of an alkaline aluminosilicate gel, relatively resistant to water dissolution.

Furthermore, one of the most prominent characteristics of geopolymer production is the ability to employ a wide variety of materials as its silica and alumina sources, from industrial residues (e.g., fly ash) to natural materials (e.g., kaolinitic clays). Because of its high reactivity rate and wide availability, the most commonly used precursors are metakaolin and alumina rich fly ash (DUXSON; PROVIS, 2008).

As of alkaline activators, generally are employed sodium hydroxide ( $\text{NaOH}$ ) or potassium hydroxide ( $\text{KOH}$ ) solutions, separately or combined. The use of sodium hydroxide solution is particularly more frequent due to its low cost and broad availability (PROVIS, 2009). Despite being less alkaline, sodium silicate ( $\text{Na}_2\text{SiO}_3$ ) has also been used simultaneously with hydroxide solutions and has the main advantage of providing dissolved silica to the system. Moreover, the employment of sodium silicate in the alkaline activator significantly improves its reaction product microstructure and performance (VAN DEVENTER et al., 2007).

Depending on the materials employed and curing conditions, geopolymer may exhibit a wide variety of properties and characteristics, including high compressive strength, low shrinkage, fast or slow hardening, high acidic attack resistance, fire resistance and low thermal conductivity (DUXSON *et al.*, 2007a).

Due to its exceptional binding properties, to the ability to reuse industrial waste materials and to release a significantly lower amount of CO<sub>2</sub> to the atmosphere during its production, geopolymer has been frequently studied as an eco-friendly alternative to Portland Cement (DUXSON *et al.*, 2007b). Moreover, applied as concrete (i.e., with regular aggregates in its mixture), fly ash geopolymer is reported to provide 10% to 30% lower cost when compared to conventional concrete (DUXSON *et al.*, 2007a). In addition to its building construction application, geopolymer might also be applied as refractory materials, radioactive waste immobilization, biomaterials, fiber composite and specific applications (WALKLEY *et al.*, 2016a).

### 2.2.1 Geopolymeric Synthesis

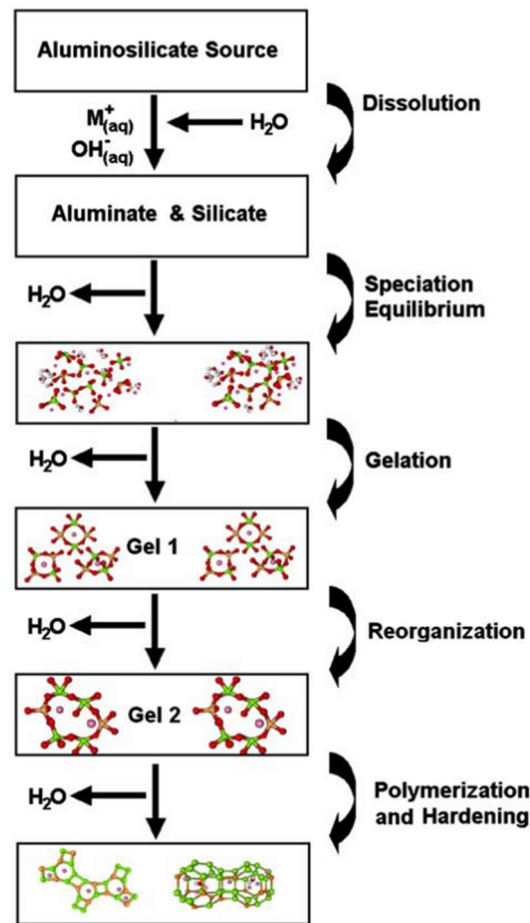
Geopolymerization is the name given to the process of geopolymer formation, since the precursor's dissolution, its amorphous binding phase development up to polymerization and hardening of the material.

Before detailing the geopolymeric synthesis, it is important to note that its process varies due to many of the precursor's properties, such as chemical composition, particle shape and size. In this sense, Khale and Chaudhary (2007) claim that mixture composition and reaction conditions, e.g., Al<sub>2</sub>O<sub>3</sub>/SiO<sub>2</sub> ratio, activator solution concentration, water/solid ratio, temperature and curing time, plays an important role in N-A-S-H development, and consequently decisively affects the material's performance. Therefore, due to its widespread and straightforward geopolymerization synthesis (VAN DEVENTER *et al.*, 2007), here will be reviewed the metakaolin geopolymerization model.

One of the pioneers in the alkaline activated materials research area, Glukhovsky (1994), proposed the following mechanism for alkaline activation of aluminosilicate precursors: a) Destruction-coagulation, b) Coagulation-condensation and c) Condensation-crystallization. Additionally, other models proposed (e.g., Davidovits (1991) and Duxson *et al.* (2007)) follow the same sequence of solid particle dissolution, coagulation of nano-molecules and the formation of a new amorphous phase. Figure 7 illustrates the simplified version of metakaolin geopolymerization model proposed by Duxson *et al.* (2007).

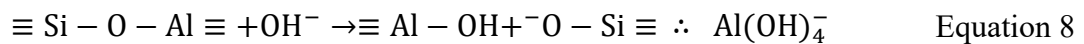
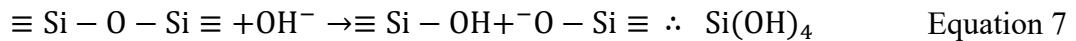


Figure 7 – Simplified geopolymerization model.



Source: Duxson *et al.* (2007)

The geopolymer formation initiates with the aluminosilicate precursor dissolution, a process that regularly occurs to rocks exposed to alkaline environment (BLAND; ROLLS, 1998). In this process, hydroxyl ions ( $\text{OH}^-$ ) attacks the surface of the solid particles, inducing the hydrolysis of  $\text{Si-O-Si}$  and  $\text{Si-O-Al}$  bonds releasing  $\text{Si}(\text{OH})_4$  and  $\text{Al}(\text{OH})_4^-$  monomers to the solution (GARCIA-LODEIRO; PALOMO; FERNÁNDEZ-JIMÉNEZ, 2015b), as indicated by Equation 7. Hence, elevated pH solution is of vital significance for AAM formation.



This step continues up to a point in which the monomer's concentration will be sufficient to cause the formation of larger molecules, creating new  $\text{Si-O-Si}$  and  $\text{Si-O-Al}$  bonds. According to Davidovits (1991), there might be formed three new bond structures: Polysialate ( $-\text{Si-O-Al-O}-$ ), Polysialate-siloxo ( $-\text{Si-O-Al-O-Si-O}-$ ) and Polysialate-disiloxo ( $-\text{Si-O-Al-O-Si-O-Si-O}-$ ). Although thermodynamically disfavoured,  $\text{Al-O-Al}$

bonds are not impossible to exist in regular geopolymer (PROVIS; YONG; DUXSON, 2009).

In addition to N-A-S-H gel, aluminosilicate alkaline activation might also generate, depending on synthesis conditions, zeolite crystalline phases, which are an alkaline aluminosilicate mineral class found in nature, including chabazite and faujasite (GARCIA-LODEIRO; PALOMO; FERNÁNDEZ-JIMÉNEZ, 2015a).

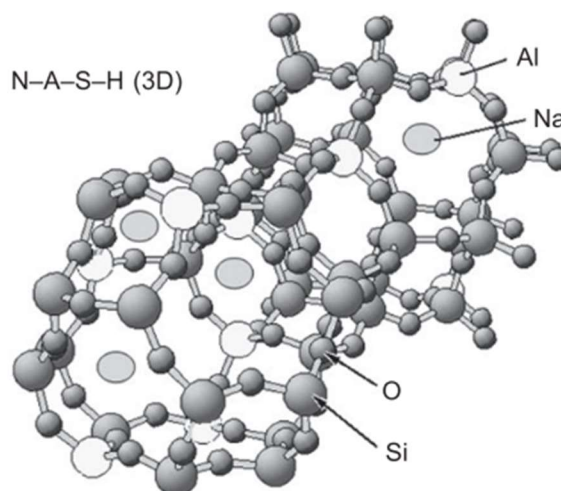
### 2.2.2 Geopolymer Gel (N-A-S-H)

The geopolymer main constituent phase is an alkaline aluminosilicate gel, known as N-A-S-H gel, in which silicon and aluminum atoms are centered in tetrahedral sites, linked by oxygen atoms. In this gel, aluminum atoms, commonly found in nature as  $Al^{3+}$ , replace silicon atoms  $Si^{4+}$  at the center of the tetrahedral structure. Therefore, the presence of monovalent cation ( $M^+$ ) is necessary in order to charge-balance the tetrahedral structure and is located near the oxygen atoms due to charge repulsion with the aluminum atom (PROVIS; YONG; DUXSON, 2009). Figure 8 represents the three-dimensional modeling of N-A-S-H gel.

As noted by Provis, Yong and Duxson (2009), the gel's nanostructure resembles in many aspects that of C-S-H, since both are predominantly amorphous, but features short-range crystallinity similar to minerals found in nature. In the C-S-H gel case, tobermorite and jennite nanocrystals are formed, whereas N-A-S-H shows zeolite minerals nanocrystals (PROVIS; YONG; DUXSON, 2009; RICHARDSON, 2008).

Moreover, according to Provis, Yong and Duxson (2009), metakaolin geopolymer properly cured and retaining  $M^+/Al$  ratio equals one, features an N-A-S-H gel well connected and with non-bridging oxygens. The absence of O-H means that water stays concentrated in pores, which vary in size (i.e., nanopores up to macropores), depending on the material's thermal history. Lastly, the study concludes that it is one of the most significant differences between N-A-S-H and C-S-H gels: geopolymer does not require chemically bounded water in its matrix.

Figure 8 – Three-dimensional representation of N-A-S-H gel nanostructure.



Source: Garcia-Lodeiro, Palomo and Fernández-Jiménez (2015b)

Due to its broadly amorphous structure, geopolymer characterization through XRD is a challenging task. Diffractograms of these materials frequently feature curvature regions peculiar to amorphous materials between  $20^\circ$  and  $40^\circ$   $2\theta$ , and, depending on the precursor employed, quartz, mullite and hematite peaks might arise as a sign of unreacted material (KHALE; CHAUDHARY, 2007). Nonetheless, with the advance of new quantitative techniques (e.g., Rietveld Refinement), studies have been developed in this area. Bhagath Singh and Subramaniam (2016), for instance, combined Rietveld Refinement with acidic dissolution to quantify the amorphous phase of fly ash and its resulting geopolymer.

### 2.2.3 Properties

As emphasized previously, since geopolymerization process varies depending on the precursor employed, it is expected that these materials will also present differences in terms of performance. For example, it is stated that fly ash geopolymer usually displays superior mechanical and durability properties when compared to their metakaolin counterparts produced under the same conditions (VAN DEVENTER *et al.*, 2007). Thus, geopolymer might be tailored for specific applications according to its properties (PROVIS, 2017).

#### 2.2.3.1 Mechanical Properties

As observed in conventional concrete, a considerable part of mechanical properties are related to the material's microstructure. Following this line, Duxson *et al.* (2005) studied the effect of Si/Al ratio over geopolymer microstructure and its mechanical properties in

metakaolin geopolymer. In this research, five samples with varying Si/Al ratios were synthesized (see Table 3) and subjected to compressive strength test, and its results are shown in Figure 9. Aiming at understanding the relationship between compressive strength and microstructure development, SEM micrographs are displayed in Figure 10.

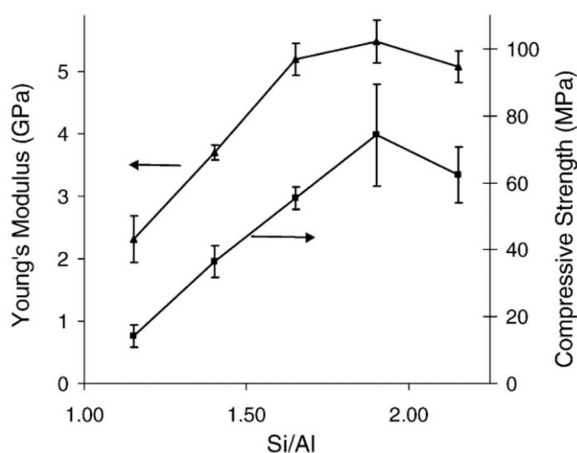
Table 3 – Molar ratios used by Duxson *et al.* (2005) to synthesize geopolymers

Molar Ratio	Si/Al	Al <sub>2</sub> O <sub>3</sub> /Na <sub>2</sub> O	H <sub>2</sub> O/Na <sub>2</sub> O
Sample A	1,15		
Sample B	1,40		
Sample C	1,65	1,00	11,00
Sample D	1,90		
Sample E	2,15		
Empirical formula: M.(SiO <sub>2</sub> ) <sub>z</sub> .AlO <sub>2</sub> .5,5H <sub>2</sub> O			

Source: Duxson *et al.* (2005)

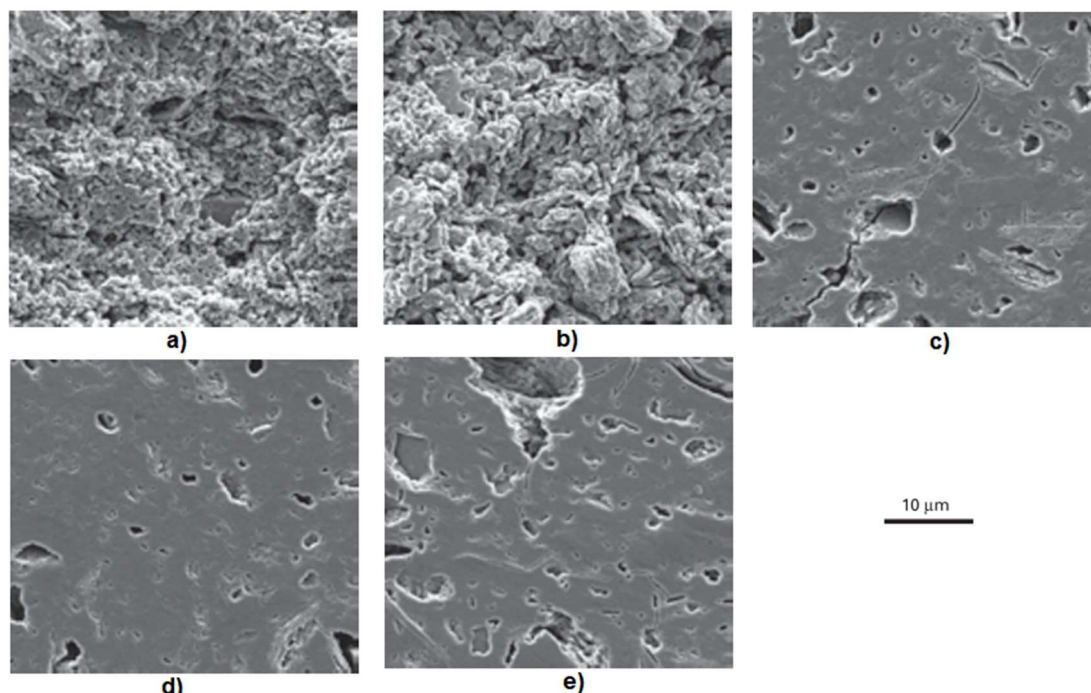
Figure 9 shows an increase in both compressive strength and Young's modulus as Si/Al increased up to 1,90 and a subsequent decrease at 2,15, which clearly shows that there is a Si/Al ratio that maximizes mechanical performance. This hypothesis is supported by SEM micrographs shown in Figure 10, which depicts samples A and B as being highly porous and samples C, D and E as being considerably more homogenous. Among these last three samples, D displays the most uniform and free of cracks, which explains its mechanical performance.

Figure 9 – Compressive strength and Young's modulus in function of Si/Al ratio.



Source: Duxson *et al.* (2005)

Figure 10 – SEM micrographs of metakaolin geopolymers with different values of Si/Al ratio: a)1,15; b)1,40; c)1,65; d)1,90; e)2,15



Source: Duxson *et al.* (2005)

Regarding synthesis conditions, it is well known that long curing times raise the formation of N-A-S-H gels rich in silicon, which favors mechanical strength development (GARCIA-LODEIRO; PALOMO; FERNÁNDEZ-JIMÉNEZ, 2015a). Khale e Chaudhary (2007) claims that extended curing times enhance polymerization process, which justifies the increase in mechanical strength, but this effect is minimal after 48h. Lastly, curing temperature also plays a crucial role in geopolymerization. It is reported that curing temperatures amid 30° to 90°C is required for the appropriate material development (KHALE; CHAUDHARY, 2007).

### 2.2.3.2 Durability

It is common knowledge that durability is highly related to the connectivity between its micropores and the chemical stability of its constituent phases. Numerous deleterious processes akin to Portland Cement concrete, such as carbonation and acidic attack, are related to the presence of susceptible calcium phases (DYER, 2014; TAYLOR, 1990). Therefore, due to the low amount of calcium in its composition, it is expected that geopolymeric concrete reacts diversely when exposed to an aggressive environment. Moreover, it was observed that geopolymer features high chemical stability, which, combined with satisfactory microporosity provided by adequate synthesis procedure,

generally yields superior durability when compared to Portland Cement concrete (FERNÁNDEZ-JIMÉNEZ; PALOMO, 2009).

Bearing in mind that AAM synthesis involves the employment of extremely alkaline solutions, it is questionable how these materials will behave regarding alkali silica reaction when applied with highly reactive aggregates. In this sense, Pouhet and Cyr (2014) investigated the effect of ASR deterioration over metakaolin geopolymeric mortar and observed that the expansion caused was significantly lower than that of conventional Portland Cement mortar. Similarly, Kupwade-Patil and Allouche (2012) studied the impact of the accelerated test, i.e., 90 days cured in 1M NaOH solution, on fly ash geopolymeric concrete and concluded that it is considerably less vulnerable to ASR when compared to Portland Cement concrete. Both studies observed the formation of an A-S-G similar phase in the aggregate-paste interface, but the absence of calcium seems to be the reason for the inferior expansion.

#### 2.2.4 Zeolite Minerals

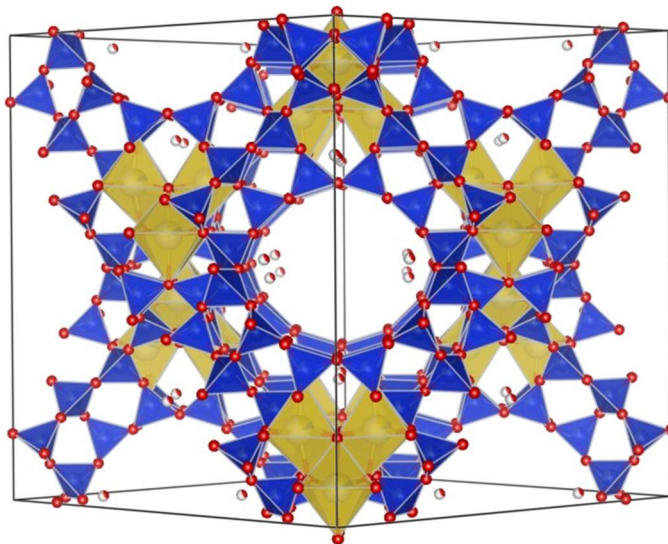
Zeolites are naturally occurring alkaline aluminosilicate minerals worldwide spread and commonly applied as absorbents and catalysts. In addition to Si, O and Al atoms, zeolites commonly feature  $\text{Na}^+$ ,  $\text{K}^+$ ,  $\text{Ca}^{2+}$ ,  $\text{Mg}^{2+}$ , and other ions, which are loosely attached to the framework and might be promptly exchanged for others when in a contact solution. It was first investigated by Swedish mineralogist Axel Cronstedt in 1756, who coined the term zeolite, which comes from the Greek *zeo* (to boil) and *lithius* (stone), for minerals that expels water when subjected to heat and thus seem to boil.

These minerals are characterized by a “honeycomb-like” framework, containing micropores of molecular dimensions, usually less than 1,3 nm in diameter (RHODES, 2007). As a consequence of this unique structure, zeolites are capable of absorbing a significant amount of liquid – possibly half of its volume, depending on the zeolite species - when immersed in solution (RHODES, 2007). The ability to soak up a considerable amount of water and exchange its ions in solution has provided zeolites with exceptional catalytic properties.

Due to its similar chemical composition, geopolymers are often compared to zeolite minerals. Nevertheless, while zeolites feature a highly organized framework, geopolymers are known for its amorphous microstructure (PROVIS; LUKEY; VAN DEVENTER, 2005). Nonetheless, several zeolite species might be formed as secondary reaction products of

geopolymerization, such as Na-chabazite, faujasite, zeolite P, zeolite Y and hydroxysodalite (DUXSON, 2006; GARCIA-LODEIRO; PALOMO; FERNÁNDEZ-JIMÉNEZ, 2015a). Figure 11 illustrates the framework of Na-faujasite, with pores of around 0,8 nm of diameter.

Figure 11 – Framework of Na-faujasite.



Source: Own authorship

## 2.3 Characterization Techniques

In this section, a brief explanation of the scientific fundamentals and importance of each characterization technique employed is given

### 2.3.1 X-Ray Fluorescence

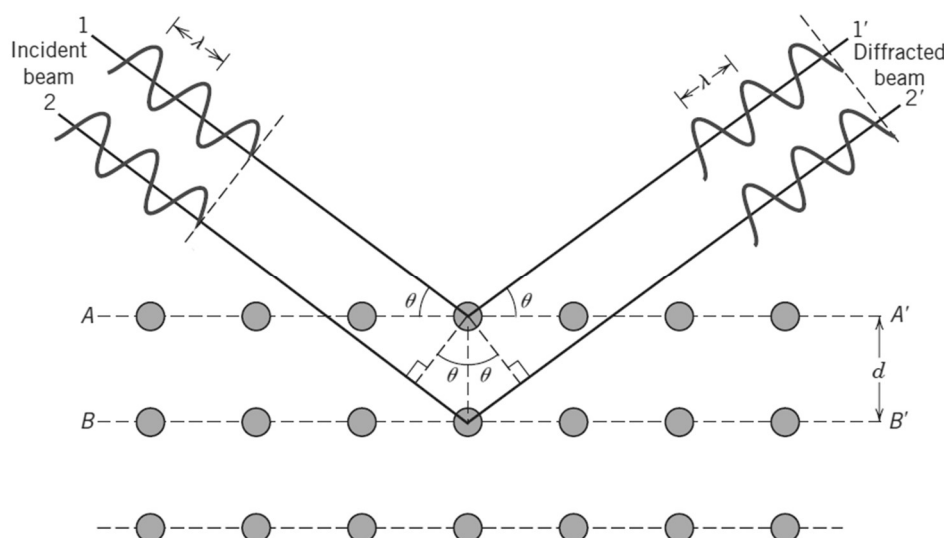
X-ray fluorescence spectroscopy (XRF) is a characterization technique designed to identify and quantify the sample's chemical elements. It operates by striking the sample with a high energy beam and detecting characteristic X-rays emitted from the irradiated atoms (YANG, 2008). This technique is not commonly applied alone, but it is especially useful when combined with other techniques (e.g. XRD) in a wide variety of applications. In this research, XRF was of great help in quantifying the chemical composition of the precursor reagents and verifying the correct composition of the reaction products.

### 2.3.2 X-Ray Diffraction

X-ray diffraction (XRD) is an analytical technique mainly used for the identification of crystalline phases. Each crystalline solid has its own XRD pattern that can be used as a “fingerprint” for its identification (WEST, 2014).

XRD is based on the phenomenon of constructive interference of monochromatic x-rays and the generation of a diagram called diffractogram. Bragg’s Law (shown in Equation 9) correlates the wavelength of the incident radiation ( $\lambda$ ) with the specimen’s interplanar spacing ( $d$ ) and the diffraction angle ( $\theta$ ).

Figure 12 – Illustration of the diffraction phenomenon in a crystal lattice.



Source: Callister and Rethwisch (2009)

$$n\lambda = 2d \sin \theta$$

Equation 9

### 2.3.3 Fourier-Transformed Infrared Spectroscopy

Fourier Transformed Infrared Spectroscopy (FTIR) is an analytical technique employed to identify functional groups in molecules or solids by examining how they interact when exposed to infrared radiation. It is well known that chemical bonds vibrate in a frequency close to that of infrared light (i.e., between  $3 \cdot 10^{12}$  to  $4,3 \cdot 10^{14}$  Hz). Therefore, chemical bonds can be excited when subjected to certain radiations in the IR spectra.

### 2.3.4 Thermal Analysis

Thermal Analysis (TA) is a group of techniques that assess materials properties according to temperature variation. Examined properties include mass, dimension, phase and mechanical behavior. Changes in materials properties caused by temperature variation are

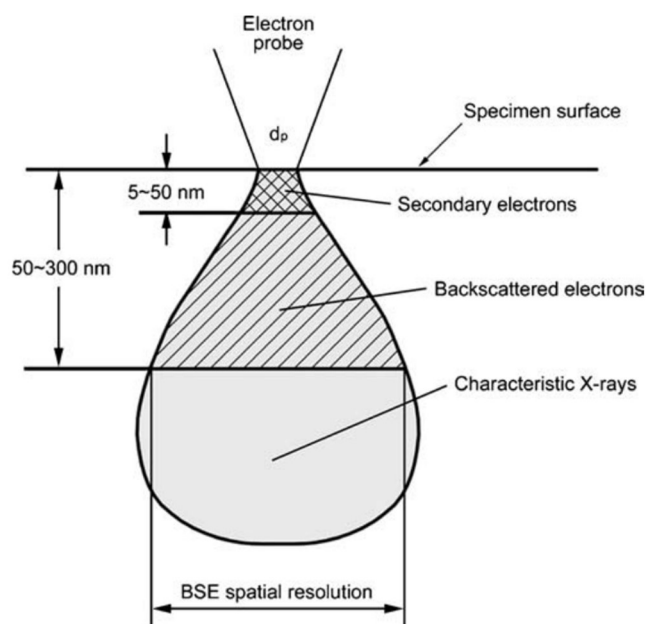


known as thermal events and include solid-phase transformation, glass transition, melting, sublimation, and thermal decomposition (YANG, 2008). Thermogravimetric (TG), Differential Thermal Analysis (DTA) and Differential Scanning Calorimetry (DSC) are among the most common TA techniques used. Thermogravimetric is generally used to quantify phase composition as a function of temperature, whereas differential thermal analysis and differential scanning calorimetry are employed to examine phase change of materials.

### 2.3.5 Scanning Electron Microscopy

Scanning Electron Microscopy (SEM) is a powerful technique capable of generating microscopic images of a specimen. An SEM image is formed by a focused electron beam that scans over the surface area of a specimen (YANG, 2008). SEM is based on the physical-chemical interactions of a high-energy electron beam with the atoms that compose the investigated specimen. When the electron beam collides with the sample, three main types of interactions are observed: formation of Secondary Electrons (SE), Backscattering Electrons (BSE) and Characteristic X-Rays, each in a particular level of the sample's depth, as shown in Figure 13.

Figure 13 – Pear shaped region of physical-chemical interactions common in SEM.



Source: Yang (2008)

SE are the products of inelastic scattering, have significantly lower energy than the incident electrons and are used to create topographic contrast of the specimen's surface area.

On the other hand, BSE are the outcome of elastic scattering, maintains around 60-80% of the incident beam's energy and are used to generate compositional contrast of the specimen. In a BSE micrograph, a dark-shaded region represents a phase composed of lighter elements (e.g., carbon), whereas a light-shaded region depicts the opposite. Alongside SE and BSE interactions, characteristic X-rays are also produced and are commonly used on chemical identification using Energy Dispersive Spectroscopy (EDS).

Likewise, XRF, EDS also identify chemical elements by detecting characteristics X-rays emitted by the specimen. Nonetheless, instead of investigating several points and calculating the average chemical composition of the specimen, EDS enables the examination of specific points while running BSE-mode SEM. Hence, it allows phase identification while examining the microstructure surface of the sample.

### 3. MATERIALS AND METHODS

This chapter presents the materials employed in the research as well as the detailed synthesis procedure. Also, the sample preparation procedure of each characterization technique are described as well as its test parameters.

#### 3.1 Precursor Materials

Throughout the research, pure reagents were used ( $\text{Na}_2\text{SiO}_3$ ,  $\text{Al}(\text{OH})_3$  and  $\text{NaOH}$ ) to synthesize A-S-G and N-A-S-H under laboratory conditions. The decision for these materials owns to its system purity. Whereas the use of Portland Cement and metakaolin would imply in the formation of similar A-S-G and N-A-S-H found in service structures, they would also provide inseparable calcium and sulfur-based subproduct that turn future analysis needlessly troublesome.

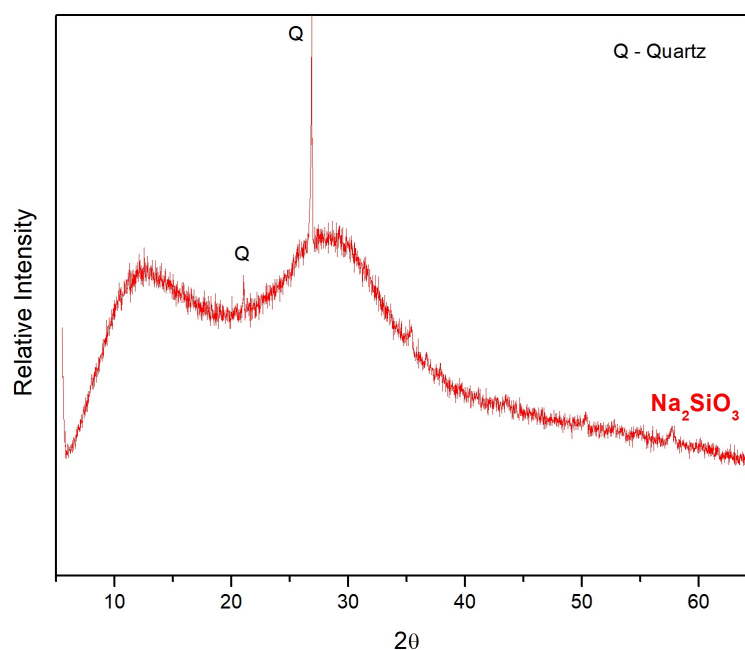
Sodium silicate used was provided by Diatom Mineração Ltda, model FR3342. It is a viscous translucent liquid and its chemical composition resembles that of commercial glass. The supplier verified the technical report displayed in Table 4. For characterization purposes, the material was dried at  $100^\circ\text{C}$ , milled, and sieved to a particle size less than  $75\ \mu\text{m}$ . The resulting powder was subjected to XRD, and the outcome is shown in Figure 14, which depicts a widely amorphous material retaining few quartz peaks.

Table 4 – Sodium silicate technical report verified by the manufacturer.

Attribute	Variation	Observed
$\text{Na}_2\text{O}$ (%)	8,20 - 8,90	8,89
$\text{SiO}_2$ (%)	27,50 - 30,00	29,37
$\text{SiO}_2 / \text{Na}_2\text{O}$	3,24 - 3,45	3,30
Solid fraction (%)	35,70 - 38,90	38,26
Moisture (%)	61,10 - 64,30	61,74
Density (g/l)	1,37 - 1,40	1,397
$^\circ\text{Be}$	39,00 - 41,20	41,00
Viscosity (cP)	70,00 - 200,00	165,00

Source: Diatom

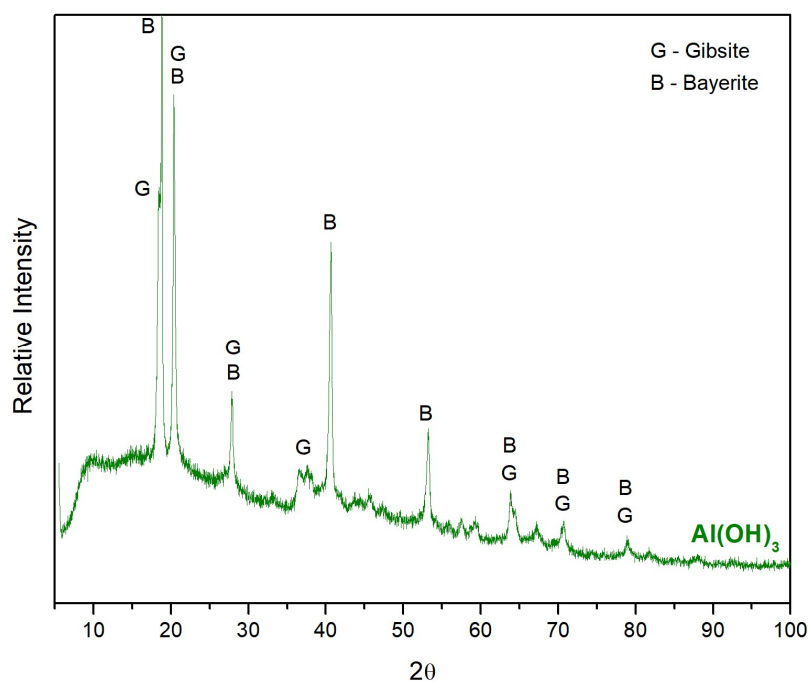
Figure 14 – Sodium silicate diffractogram



Source: Own authorship

The aluminum hydroxide used was produced by Proquímios Comércio e Indústria Ltda. It consists of a finely divided white powder. The XRF certified its purity: Al<sub>2</sub>O<sub>3</sub> (95,51%), Na<sub>2</sub>O (1,70%), SiO<sub>2</sub> (0,55%) and 2,24% of impurities. Its diffractogram (see Figure 15) displays a material predominantly dominated by bayerite and gibbsite peaks, polymorphic forms of Al(OH)<sub>3</sub>.

Figure 15 – Aluminum hydroxide diffractogram



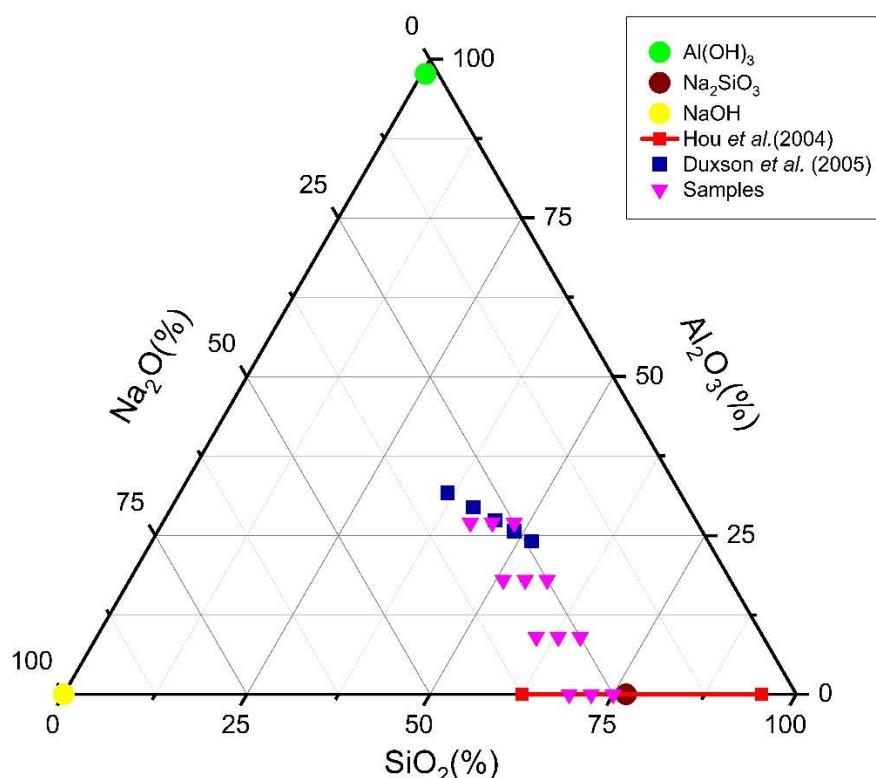
Source: Own authorship

The sodium hydroxide employed was produced by Neon Comercial Ltda, in the form of pellets and showing a high degree of purity (at least 98,20% Na<sub>2</sub>O). The water used was previously distilled and supplied by New Materials Technology Laboratory (TECNOMAT).

### 3.2 Synthesis Procedure

Before start producing synthetic gels, it was necessary to delineate the geopolymer and alkali silica gel composition. For the case of geopolymer, were considered the molar ratios provided by Duxson *et al.* (2005) and previously mentioned in Table 3. Concerning A-S-G composition, were taken into account the values reported by Hou, Struble and Kirkpatrick (2004), representative of alkali silica gels found in concrete structures, and aforementioned in Table 2. In order to simplify the chemical system, calcium-containing alkali silica gels were excluded from synthetic gels, setting CaO/SiO<sub>2</sub> to 0 and maintaining the original range of Na<sub>2</sub>O/SiO<sub>2</sub> (i.e., 0,05 to 0,6). As a result, the entirety of synthetic gel samples could be described in terms of SiO<sub>2</sub>, Al<sub>2</sub>O<sub>3</sub> and Na<sub>2</sub>O mass percentage.

Figure 16 – Synthetic gels chemical composition in the ternary diagram (SiO<sub>2</sub>-Al<sub>2</sub>O<sub>3</sub>-Na<sub>2</sub>O)

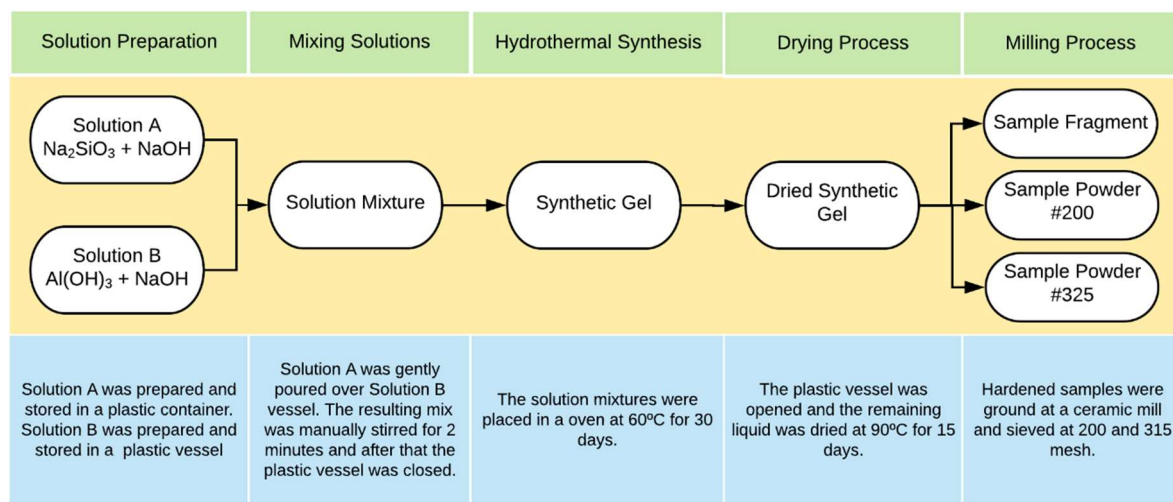


Source: Own authorship with data from Duxson *et al.* (2005) e Hou, Struble and Kirkpatrick (2004)

Since geopolymer composition is described in a diverse way to A-S-G composition (i.e., geopolymers are described as a function of Si/Al and Al<sub>2</sub>O<sub>3</sub>/Na<sub>2</sub>O ratios whereas A-S-

G is described in terms of  $\text{Na}_2\text{O}/\text{SiO}_2$  and  $\text{CaO}/\text{SiO}_2$  ratios), a new composition system was needed to cover all of these materials and its intermediate samples. For that purpose, a ternary diagram as a function of  $\text{SiO}_2$ ,  $\text{Al}_2\text{O}_3$  e  $\text{Na}_2\text{O}$  mass percentage was chosen since it was fully capable of showing the geopolymer and A-S-G as well as its intermediate gels.

Figure 17 – Gel's synthesis procedure summary.



Source: Own authorship.

Subsequently, 12 intermediate compositions to those of A-S-G and geopolymer were chosen to be synthesized. Figure 16 illustrates the location of Duxson's geopolymer composition (in blue), Hou's alkali silica gel range composition (in red) and the 12 arbitrary intermediate gels composition (in pink). Last, Table 4 shows the chosen chemical composition for the 12 synthetic gels, and Figure 18 displays the location of each sample in the ternary diagram ( $\text{SiO}_2$ - $\text{Al}_2\text{O}_3$ - $\text{Na}_2\text{O}$ ).

Once the synthetic gels chemical composition was established, the next step was to quantify the exact amount of each reagent needed to achieve that composition. For that purpose, two solutions were considered: Solution A, comprised of sodium silicate and sodium hydroxide, and Solution B, formed by aluminum and sodium hydroxide and distilled water. With the assistance of Microsoft Excel's Solver add-in, the precise quantity and concentration of solutions A and B for each sample were determined.

Firstly, solution A was produced by weighting sodium silicate in a plastic container and then adding the adequate quantity of sodium hydroxide. Thereafter, solution B was conceived by including an appropriate amount of aluminum and sodium hydroxide to a different plastic vessel containing water. Lastly, when all the solutions were prepared, each solution A was inserted in its corresponding solution B's vessel. The resulting solution was manually mixed for two minutes, closed, and stored in a 60°C oven for 30 days. Afterward, the vessels were opened and dried at 90 °C for two weeks. The residual dried samples were

crushed in a ceramic ball mill and sieved in a 75  $\mu\text{m}$  mesh. The resulting powder was submitted to several characterization tests in order to study its microstructure.

Table 5 – Synthetic gels chemical composition

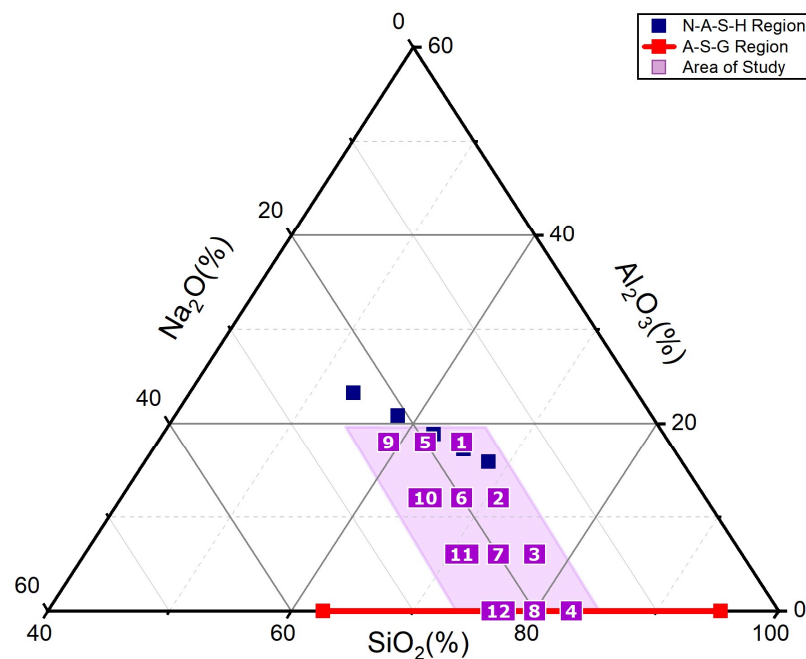
Samples	SiO <sub>2</sub>	Al <sub>2</sub> O <sub>3</sub>	Na <sub>2</sub> O	
1	48%	27%	25%	Low Alkali
2	57%	18%	25%	
3	66%	9%	25%	
4	75%	0%	25%	
5	45%	27%	28%	Intermediate Alkali
6	54%	18%	28%	
7	63%	9%	28%	
8	72%	0%	28%	
9	42%	27%	31%	High Alkali
10	51%	18%	31%	
11	60%	9%	31%	
12	69%	0%	31%	

<span style="display:inline-block; width:10px; height:10px; background-color:lightblue; border:1px solid black;"></span> High Aluminum
<span style="display:inline-block; width:10px; height:10px; background-color:lightpurple; border:1px solid black;"></span> Intermediate Aluminum
<span style="display:inline-block; width:10px; height:10px; background-color:lightpink; border:1px solid black;"></span> Low Aluminum
<span style="display:inline-block; width:10px; height:10px; background-color:lightcoral; border:1px solid black;"></span> No Aluminum

Source: Own authorship

Figure 18 – Zoomed-in version of the ternary diagram (SiO<sub>2</sub>-Al<sub>2</sub>O<sub>3</sub>-Na<sub>2</sub>O) highlighting each sample location



Source: Own authorship with data from Duxson *et al.* (2005) and Hou, Struble and Kirkpatrick (2004)

### **3.3 Characterization Techniques**

In this section, a brief explanation of the sample preparation of each experimental section is given. Moreover, detailed test parameters are also discussed.

#### **3.3.1 X-Ray Fluorescence**

XRF analysis was done in a PANalytical Axios Max spectrometer at Elizabeth Cimentos Chemical Analysis Laboratory, and the results are shown in terms of mass oxide (%). The samples were prepared according to the fused bead method, in which 1,5 g of synthetic gel were mixed with 6,0 g of lithium metaborate and 0,02 g of ammonium iodite. The resulting mixture was placed in a platinum crucible and subjected to 1000 °C for 15 minutes and cast into a flat mold, where it is rapidly cooled, forming a glassy, translucent disc.

#### **3.3.2 X-Ray Diffraction**

XRD analysis was carried out in a Bruker D2 Phaser diffractometer using CuK $\alpha$  radiation with a scanning rate of 0,01°/s, in the range of 5° to 100° 2 $\theta$  and with a measurement time of 3s per step. An acceleration voltage of 30 kV and a current of 10 mA were used. The analysis was done in a zero-background sample holder, and acetone was used as a solvent to pour the powder over the sample holder surface.

#### **3.3.3 Scanning Electron Microscopy**

For this analysis, fragments of approximately 2 cm of diameter were selected and slashed in a cut-off machine. The cut was done as a cross-section done, that is, to represent both top and bottom regions of the sample. The exception of this were samples 5 and 9, whose fragile nature inhibited an incisive cut. For these samples, a mid-section cut was performed. Afterward, the samples were impregnated with an epoxy resin in a 3 cm diameter polyvinyl chloride cylindrical mold. Subsequently, the samples were dried polished with silicon carbide paper with progressing grades of 400 to 2000, cleaned with isopropyl alcohol in an ultrasonic bath and gold coated to improve conductivity.



The SEM/EDS analysis was carried out in two sections. First, a colored BSE micrograph at 25x magnification was taken to depict a broader perspective of the sample. Afterward, a spot analysis consisting of around 100-150 points were selected at 2000x magnification and measured in terms of C, O, Na, Si and Al atomic concentration. In both sections, a FEI Quanta 450 scanning electron microscope coupled with a XFlash Detector 630M was used. The analysis was carried out in high-vacuum mode (around  $10^{-3}$  Pa), filament voltage of 20 kV, a spot of 6 nm and working distance of 10 mm.

### **3.3.4 Fourier-Transformed Infrared Spectroscopy**

FTIR was done in an IRTracer-100 Shimadzu spectrophotometer at the Thin Film Synthesis Laboratory – UFPB. The samples were prepared following the KBr pellet method, in which 1 mg of the synthetic gel was mixed with 100 mg of KBr. The resulting mixture was placed in a flat mold and pressure was applied, producing a thin translucent pellet that was submitted to the experiment.

### **3.3.5 Thermal Analysis**

Thermal analysis was run in an SDT 650 thermal analyzer at the Thin Film Synthesis Laboratory – UFPB. Around 7 mg of corresponding samples were placed in an alumina crucible and exposed to thermal treatment starting at 25 °C up to 1350 °C, at a constant heating rate of 20 °C/min. Inert atmosphere (Argon) was used to prevent any possible reactions with the released gases.

## 4. RESULTS AND DISCUSSION

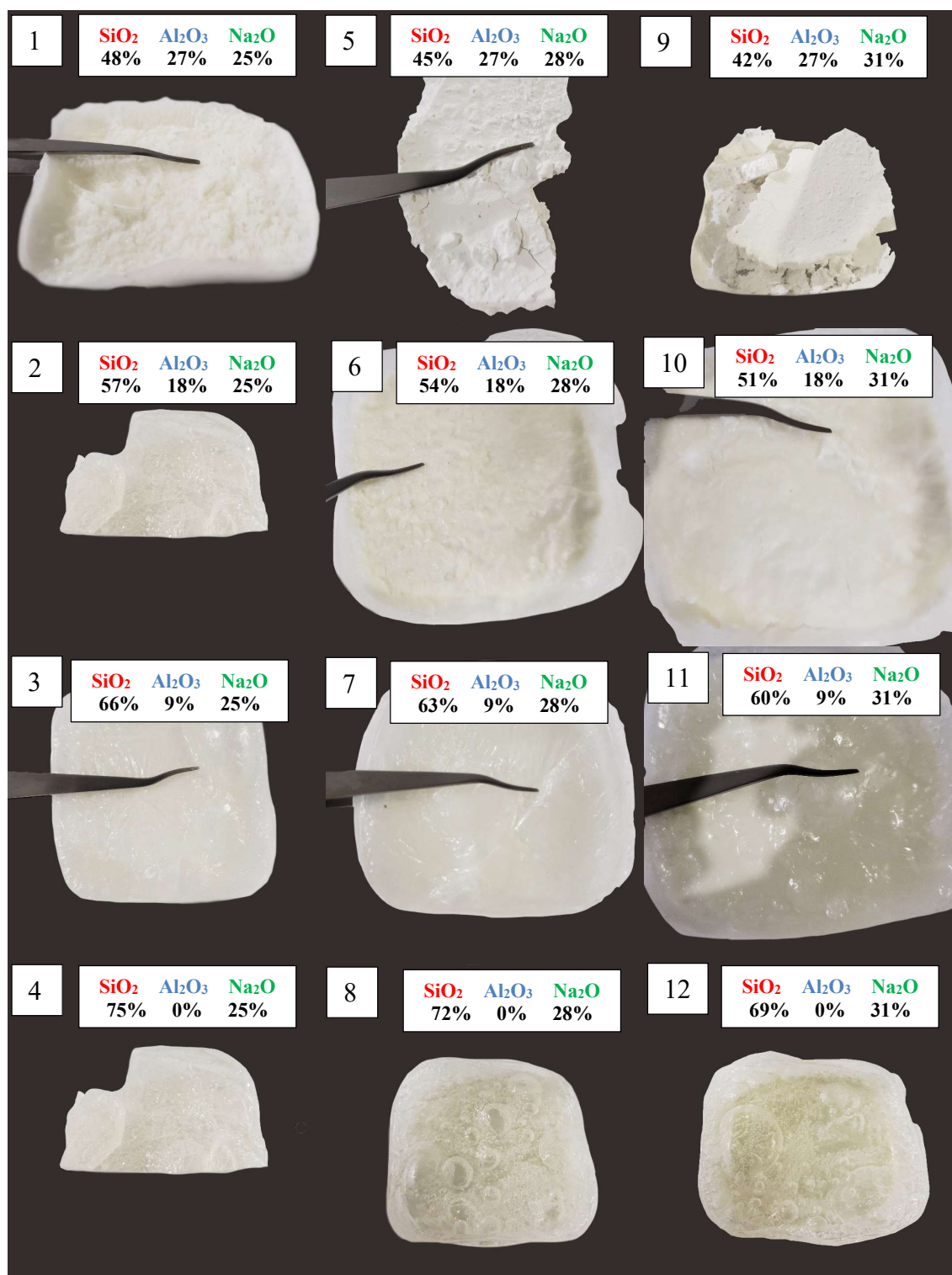
### 4.1 Visual Assessment

The visual assessment of the samples was done before the grinding, i.e., right after they spent 15 days drying at the oven at 90 °C and the results are shown in Figure 19. In this image, the samples are represented as follows: each row corresponds to a particular amount of aluminum and each column is associated with a certain quantity of alkalis. For example, in the first row are depicted samples 1, 5 and 9, which features a high amount of aluminum and the second row are displayed samples 2, 6, and 10, which possesses an intermediate amount of aluminum. In terms of alkalis, samples with low, intermediate, and high quantity of alkalis are shown in the first, second and third columns, respectively.

It was seen that the specimens showed similar color patterns when compared to the proportion of its precursors, that is, samples with a high quantity of aluminum are mainly white due to the aluminum hydroxide, whereas samples with no aluminum (samples 4, 8 and 12) are predominantly colorless. Contradicting this tendency, samples 10, 11 and 12 features a light yellowish tone on its top surface, as can be seen in Figure 19. Since these were the gels with the highest amount of alkali availability – alongside sample 9 – it is hypothesized that this yellowish tone is related to an alkali-bearing phase that was precipitated during the drying process.

Regarding the high aluminum content specimens (1, 5 and 9), sample 1 resembles the most to metakaolin geopolymers, presenting a smooth bottom surface and a white and rigid body, shown in Figure 20. On the other hand, samples 5 and 9 are incredibly porous, crumbly, easily disintegrated when tried to grind and look similar to dried gypsum. These samples likely went on different thermodynamic paths, forming distinct phases. This hypothesis is corroborated by x-ray diffractograms discussed in section 4.2. As mentioned in section 3.3 (Characterization Techniques), a fragment of around 2 centimeters of diameter was collected from each sample to produce a SEM specimen. In all samples, these fragments represent a cross-section cut, i.e., depicts both the top and bottom surface of the gel. The exception to this were samples 5 and 9, since its crumbly nature prevented a vertical cut.

Figure 19 – Light yellowish tone on the top surface of samples 10, 11 and 12

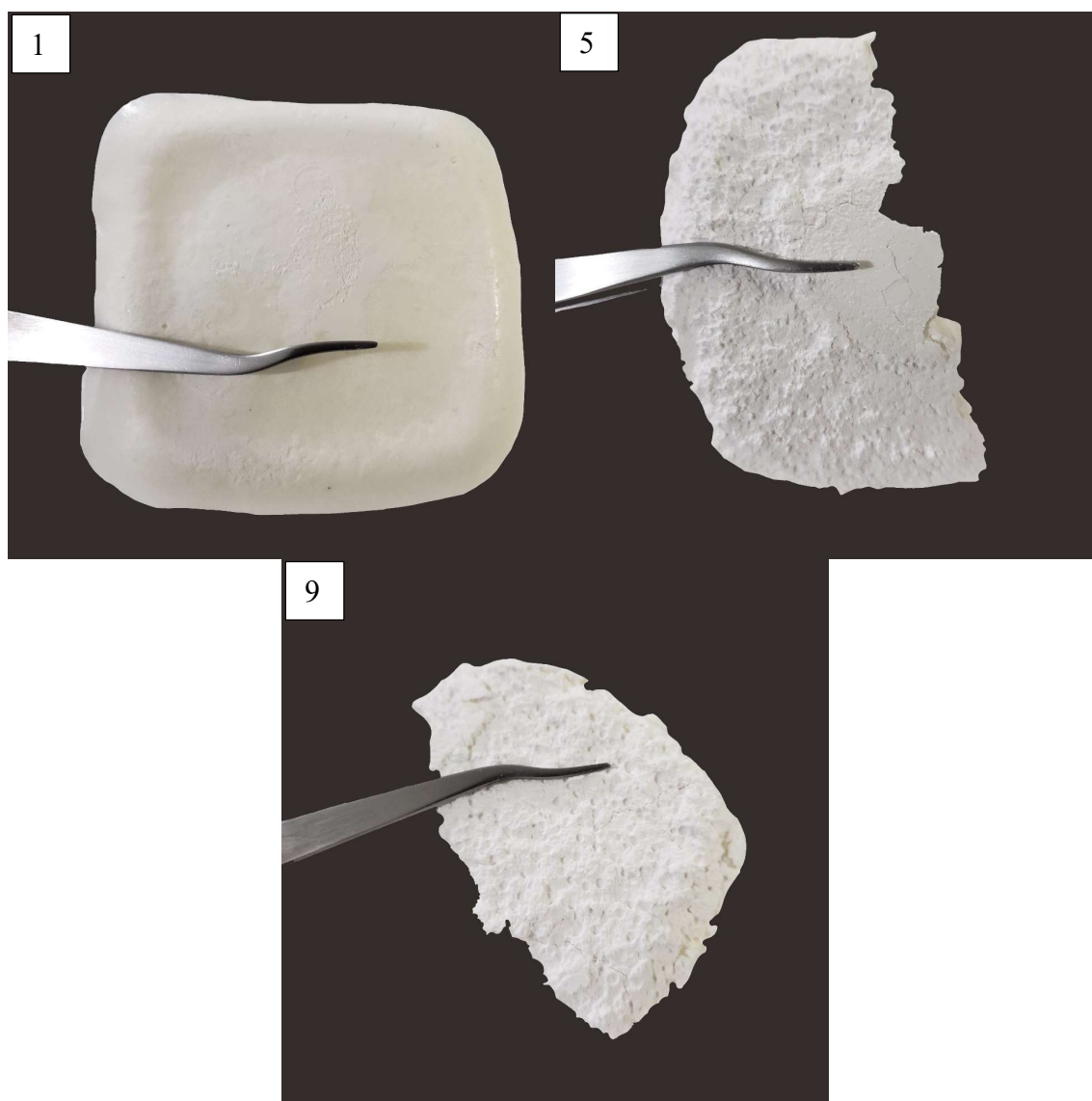


Source: Own authorship

Moreover, two distinguished phases were seen in sample 10, one grayish-white layer at the bottom and another transparent at the top surface. The same phenomenon was seen in a lower degree in intermediate samples (1, 2, 3, 6, 7, 11). It is suspected that aluminum reaction products precipitate, leaving the alkali silica gel at the top. Sample 10 shows the

highest degree of phase segregation, up to the point of being completely hollow in its interior, as is depicted in Figure 21. Interestingly, alongside samples 5 and 9, sample 10 also proved to be extremely easy to grind. The crumbly structure of these samples explains the easiness to grind and is associated with its microstructure. The weakest specimens are the same that features the highest proportion of crystallinity degree, as seen in Figure 26.

Figure 20 – Visual assessment of high aluminum content gels: sample 1 resembles metakaolin geopolimer whereas samples 5 and 9 are similar to dried gypsum.

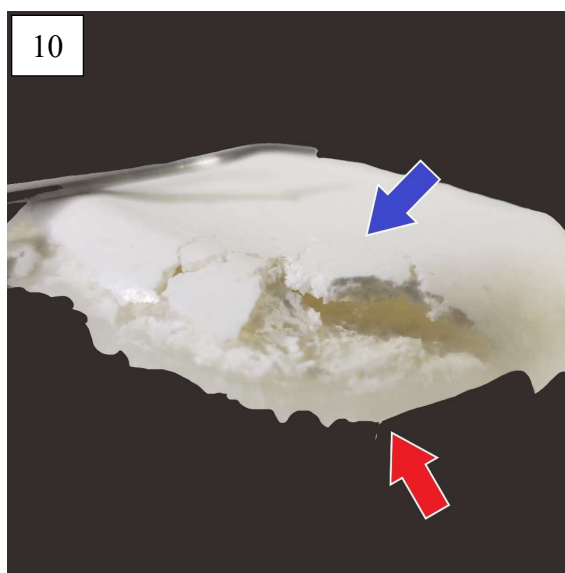


Source: Own authorship

Due to its translucent aspect, samples with no aluminum (4, 8 and 12) resemble considerably to commercial glass. Regarding the gel's color, sample 4 is clearly colorless, while sample 12 features a light yellowish tone. Sample 8 coloration seems to be less transparent than sample 4, yet not so colorful as sample 12. This color shifting is correlated with an increase in the alkali availability and was possibly caused by the precipitation of an

alkali-bearing during the drying process. Also, these samples are the only ones that display large diameter pores (i.e., more than 2 cm). Despite that, these samples prove to be the hardest to grind, requiring several sections of 50 minutes to provide few grams of particles with less than 74  $\mu\text{m}$  of diameter.

Figure 21 – The explicit phase-segregated sample 10. The blue arrow indicates the likely precipitated aluminum reaction products while the red arrow points to the top surface colorless phase.



Source: Own authorship

The visual assessment section was especially useful because the samples showed interesting characteristics that are correlated with other investigation techniques. For example, samples with crumbly structure were the ones that showed the highest proportion of zeolite minerals, as detected by the XRD analysis. Additionally, the SEM/EDS analysis corroborated the hypothesis of samples with a clear phase separation, in which an aluminosilicate phase lays at the bottom while the remaining alkali silica gel stays on top.

## 4.2 X-Ray Fluorescence (XRF)

Table 6 shows the bulk chemical composition of the synthetic gels in terms of mass oxide (%). Minor impurities observed include  $\text{Fe}_2\text{O}_3$ ,  $\text{CaO}$ ,  $\text{MgO}$ ,  $\text{SO}_3$  and  $\text{K}_2\text{O}$  and its sums vary between 1,81% in the purest gel (sample 6) and 2,22% in the most impure gel (sample 2). As expected, the gels are primarily composed of  $\text{SiO}_2$ ,  $\text{Al}_2\text{O}_3$  and  $\text{Na}_2\text{O}$  and, since only minor impurities were found, it can be represented in a ternary diagram.

Table 6 – Bulk chemical composition of the synthesized gels (%wt.).

<i>Sample</i>	SiO <sub>2</sub>	Al <sub>2</sub> O <sub>3</sub>	Na <sub>2</sub> O	Fe <sub>2</sub> O <sub>3</sub>	CaO	MgO	SO <sub>3</sub>	K <sub>2</sub> O
<i>1</i>	64,55%	22,34%	10,85%	0,60%	0,72%	0,32%	0,26%	0,31%
<i>2</i>	72,36%	14,17%	11,19%	0,66%	0,64%	0,30%	0,21%	0,41%
<i>3</i>	76,27%	10,39%	11,33%	0,46%	0,62%	0,30%	0,21%	0,37%
<i>4</i>	82,39%	4,19%	11,56%	0,46%	0,51%	0,27%	0,20%	0,39%
<i>5</i>	62,66%	23,69%	11,71%	0,50%	0,61%	0,28%	0,28%	0,23%
<i>6</i>	70,45%	14,73%	12,96%	0,46%	0,58%	0,26%	0,24%	0,27%
<i>7</i>	76,89%	8,28%	13,02%	0,44%	0,52%	0,25%	0,21%	0,31%
<i>8</i>	79,74%	6,17%	12,11%	0,49%	0,58%	0,30%	0,19%	0,36%
<i>9</i>	60,94%	24,67%	12,46%	0,50%	0,63%	0,29%	0,28%	0,24%
<i>10</i>	68,05%	16,42%	13,69%	0,45%	0,59%	0,24%	0,26%	0,23%
<i>11</i>	73,85%	10,97%	13,22%	0,49%	0,60%	0,30%	0,21%	0,33%
<i>12</i>	79,57%	5,28%	13,25%	0,47%	0,55%	0,28%	0,18%	0,37%

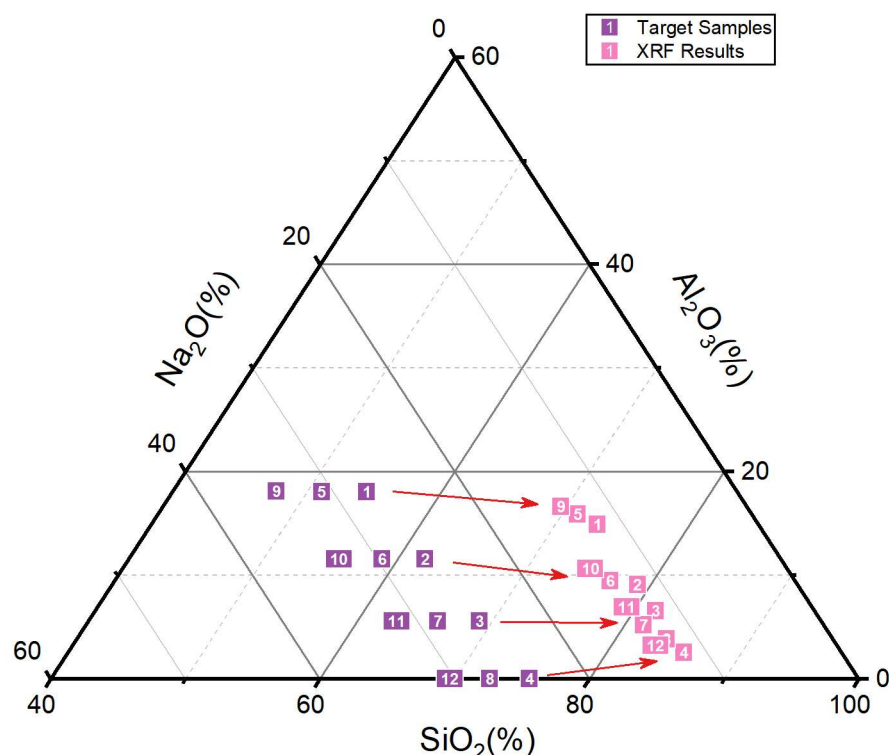
Source: Own authorship

Figure 22 compares the chemical composition of the reaction products (in pink) to what was previously targeted (in purple). The sample's chemical composition shifted to the right, a region with lower alkali and higher silica content when compared to the samples before reacting. As it seems, the alkali was only partially absorbed by the gel, leaving the remaining alkali in solution. Furthermore, the amount of incorporated Na<sub>2</sub>O is alike among all samples, varying between 10,85% (sample 1) to 13,69% (sample 10).

Unfortunately, the liquid phase of these gels was lost during the drying process, thus compromising a future assessment of this hypothesis. Also, a pH evaluation during the early and late stages of the gel formation could have been useful to clarify the absorption of the Na<sup>+</sup> ions.

Regarding the aluminum absorption, the XRF showed reasonably similar results to what was expected, except for the samples 4, 8 and 12, in which no aluminum content was predicted. In these samples, Al<sub>2</sub>O<sub>3</sub> content varies between 4% and 6% of the total weight. This might be due to minor Al<sub>2</sub>O<sub>3</sub> impurities presented in either the sodium silicate or sodium hydroxide used for the synthesis.

Figure 22 – Chemical composition comparison between what was targeted and the XRF result,



Source: Own authorship

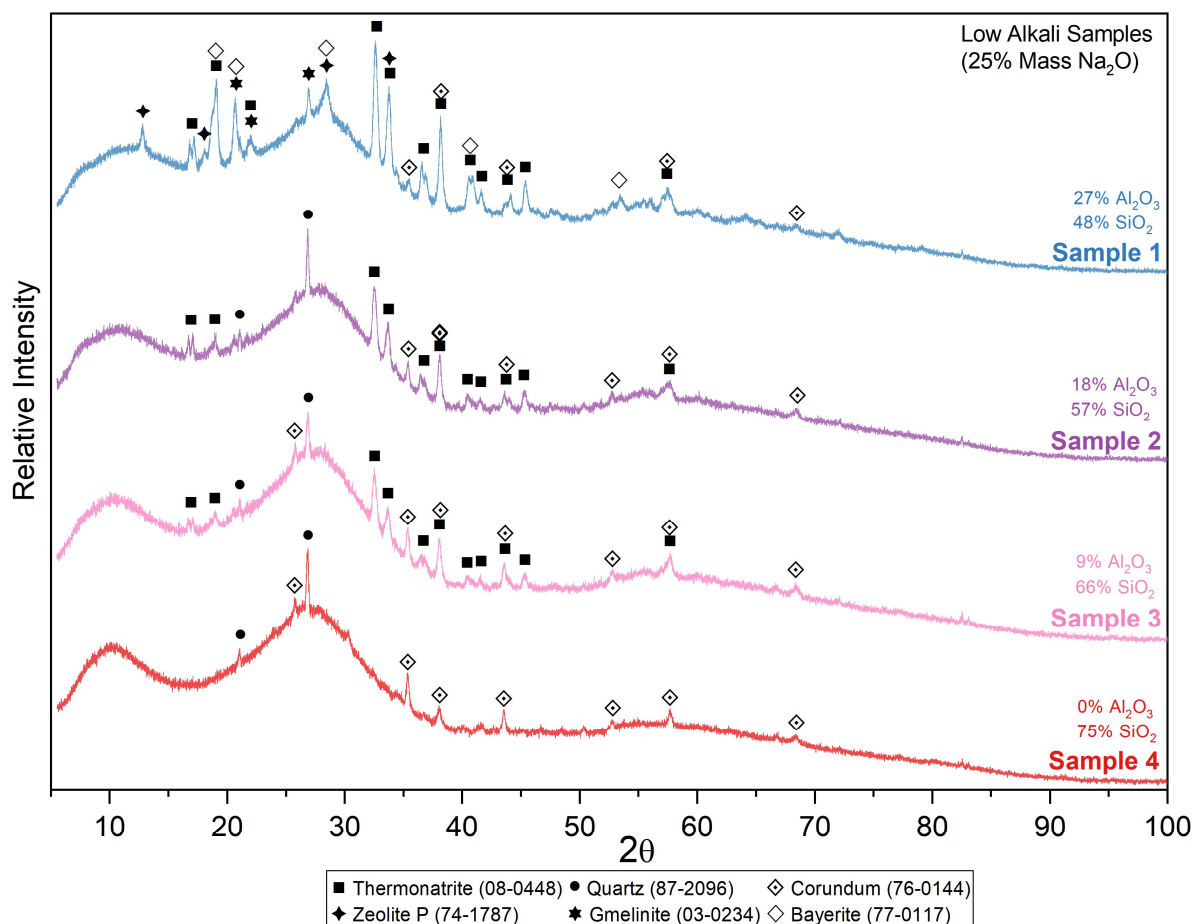
Considering the gels with high and intermediate aluminum content (samples 1, 5, 9, 2, 6, 10), an increase in the amount of incorporated  $\text{Al}_2\text{O}_3$  was always accompanied by an increase in the amount of absorbed  $\text{Na}_2\text{O}$ . The same trend is also observed in gels with less alumina, although it is not as pronounced as in high alumina content samples. This phenomenon is strongly correlated to the absorption of monovalent cations due to the incorporation of aluminum atoms into tetrahedral sites. Hence, it indicates that the aluminum atoms incorporated by the gel are found in tetrahedral coordination and, as a result, requires the absorption of an alkali cation to charge balance the tetrahedral site.

### 4.3 X-Ray Diffraction (XRD)

Figure 23 to 25 show the XRD diffractograms of the synthesized gels and are organized as follow: samples with low alkali content (25% mass  $\text{Na}_2\text{O}$ ) are shown in Figure 23 while intermediate (28% mass  $\text{Na}_2\text{O}$ ) and high alkali content (31% mass  $\text{Na}_2\text{O}$ ) are shown in Figure 24 and Figure 25, respectively. Additionally, samples with high aluminum proportion (27% mass  $\text{Al}_2\text{O}_3$ ) are displayed in blue, whereas no aluminum samples (0% mass

$\text{Al}_2\text{O}_3$ ) are shown in red. Intermediate (18% mass  $\text{Al}_2\text{O}_3$ ) and low aluminum content (9% mass  $\text{Al}_2\text{O}_3$ ) samples are displayed in violet and pink, respectively.

Figure 23 – XRD diffractograms of samples 1 to 4



Source: Own authorship

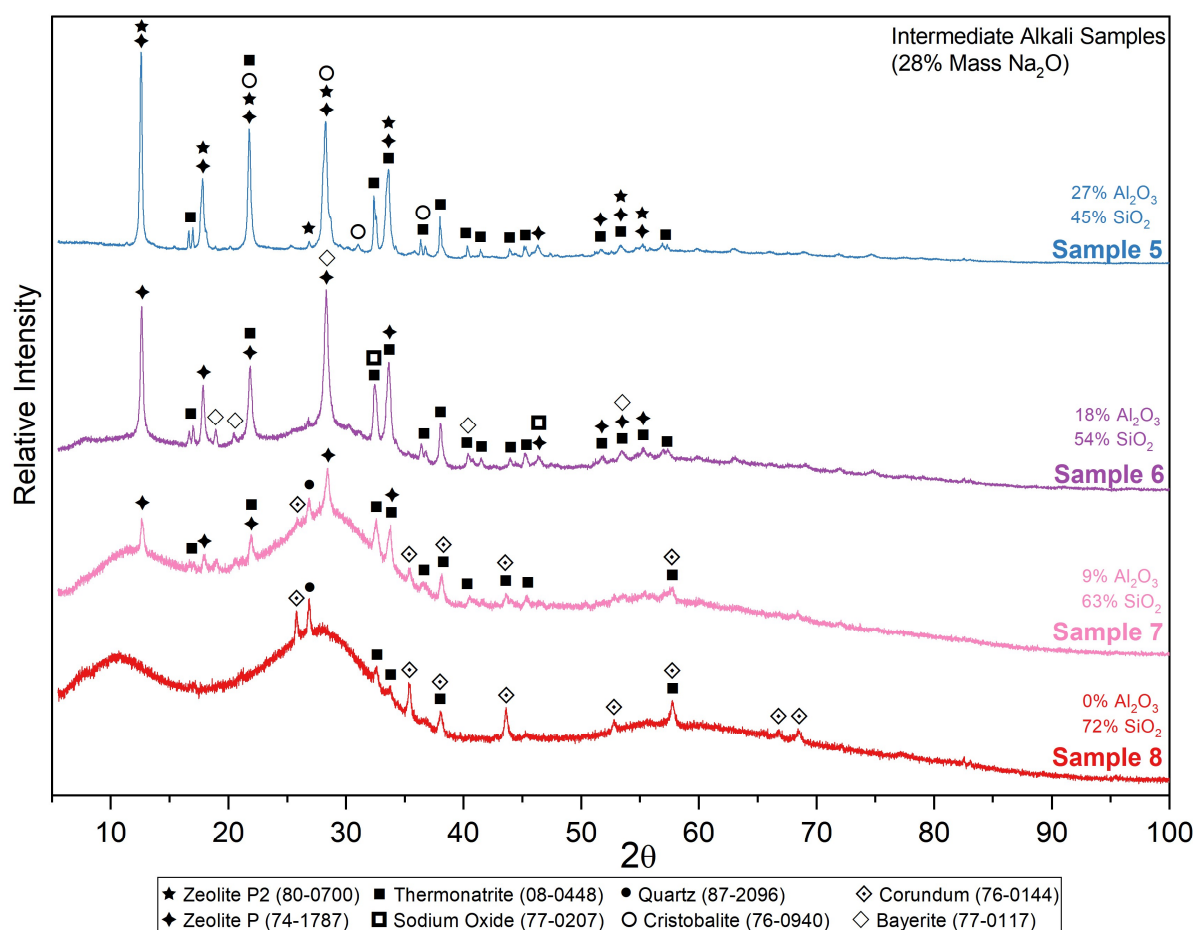
Quickly glancing through all diffractograms, it can be noticed that all samples feature a semi-crystalline nature and that the crystallinity degree is directly proportional to the amount of aluminum absorbed. For instance, samples 4, 8 and 12 are predominantly amorphous, whereas samples 5 and 9 are significantly more crystalline. The remaining samples are somewhat an intermediate stage of both extremes. In terms of alkali availability, the difference was minimum. Samples with higher alkali content showed a slightly superior crystallinity degree when compared to its less alkaline counterparts.

Regarding the identified phases, these may be arranged into four categories: zeolite minerals, aluminum-bearing phases, sodium-bearing phases, and silica polymorphs. The emergence of zeolitic crystals only occurred when enough aluminum and alkalis were available. It can be seen by comparing the intensity of zeolitic peaks within samples with the same aluminum content. For example, sample 1 showed zeolitic peaks that are not seen in



samples 2 and 3 (see Figure 23), but these are considerably lower when compared to the peaks found in samples 5 and 9.

Figure 24 – XRD diffractograms of samples 5 to 8



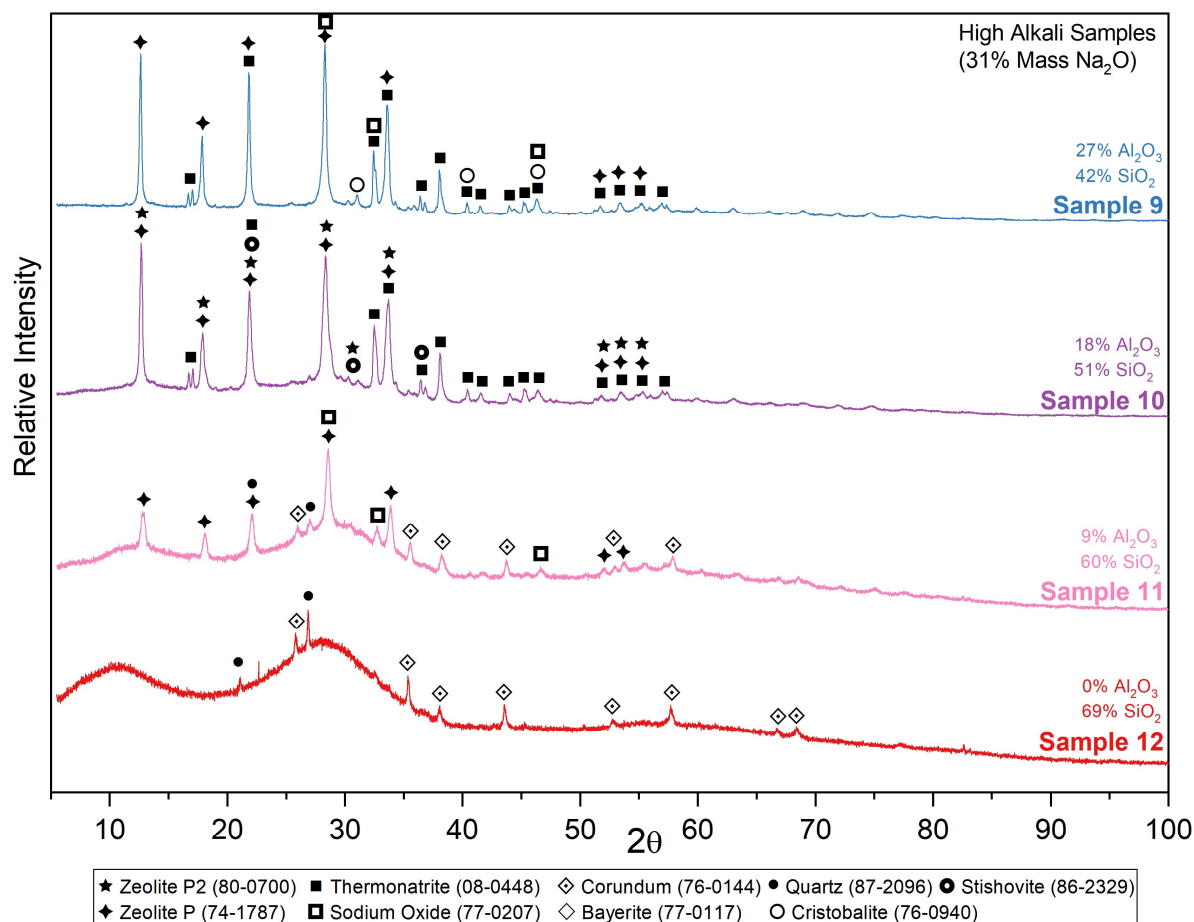
Source: Own authorship

Among the zeolite minerals found, zeolite P ( $\text{Na}_{3,6}\text{Al}_{3,6}\text{Si}_{12,4}\text{O}_{32} \cdot 10,6\text{H}_2\text{O}$ ) was by far the most common, featuring in samples 1, 5, 6, 7, 9, 10 and 11. Different zeolite minerals identified include zeolite P2 ( $\text{Na}_4\text{Al}_4\text{Si}_{12}\text{O}_{32} \cdot 14\text{H}_2\text{O}$ ) and gmelinite ( $\text{NaAl}(\text{SiO}_3)_2 \cdot 3\text{H}_2\text{O}$ ), which were found in samples 1 and samples 5 and 9, respectively. Under the synthesis conditions employed, that is, hydrothermal synthesis at 60 °C throughout 30 days, zeolite P seems to be the most stable zeolite phase, and that is likely the reason it was found in the samples mentioned above.

In previous studies, zeolite P had been encountered as a secondary reaction product of the geopolymer synthesis alongside other zeolite minerals, like faujasite and Na-chabazite (GARCIA-LODEIRO; PALOMO; FERNÁNDEZ-JIMÉNEZ, 2015a). This might indicate that the extended synthesis time, that is, 30-days synthesis period instead of the usual 1-2 days needed to produce metakaolin geopolymer, provided enough heat to crystallize the

available aluminosilicate gel and, as a result, produced the zeolite minerals that were detected by the XRD.

Figure 25 – XRD diffractograms of samples 9 to 12.



Source: Own authorship

Additionally, zeolite P has been previously synthesized in hydrothermal conditions using perlite, rice husk ash, kaolin waste as well as aluminosilicate glasses in the temperature varying from 60 to 250 °C (HÅKANSSON; FÄLTH; HANSEN, 1990; HILDEBRANDO et al., 2014; KRÓL et al., 2014). In addition to that, zeolite P is the most stable zeolite phase when synthesized at 100 °C during four days and, at higher temperatures, it tends to convert into analcime, a different zeolite mineral (KONGKACHUICHAY; LOHSOONTOM, 2006).

In addition to zeolites, aluminum-bearing phases, such as bayerite (Al(OH)<sub>3</sub>) and corundum (Al<sub>2</sub>O<sub>3</sub>), were also identified. Minor traces of bayerite were found in high aluminum content gels, mainly samples 1 and 6, and that indicates that the aluminum hydroxide employed in the synthesis was not fully reacted. Nonetheless, no other aluminum hydroxide polymorph (i.e., gibbsite or boehmite) were found. Moreover, corundum, a crystalline form of aluminum oxide, was identified in samples with low or no aluminum content (samples 1, 2, 3, 4, 7, 8, 11 and 12). The fact that aluminum oxide was found in

samples synthesized with purely sodium silicate and sodium hydroxide means that either one of these reagents was contaminated with aluminum.

Regarding the sodium-bearing minerals, two phases were identified: thermonatrite ( $\text{Na}_2\text{CO}_3 \cdot \text{H}_2\text{O}$ ) and sodium oxide ( $\text{Na}_2\text{O}$ ). The detection of thermonatrite in nearly all samples confirms that carbonation had occurred. Since the vessel's lid was closed during the 30-day synthesis, carbonation had likely occurred throughout the drying process, when the remaining alkali solution was exposed to the atmosphere.

Furthermore, since only samples 4, 8, 11 and 12 were not diagnosed with this phase, it might be implied that the degree of carbonation is directly proportional to the amount of aluminum available. Moreover, the fact that both thermonatrite and zeolite peaks were intensified in samples with high aluminum content bolster that assumption. Despite arising in combination, it is interesting to note that both aluminum and carbon compete for the available alkali, which means that there might be a hidden factor favoring the combination of zeolite P and thermonatrite.

It is also interesting to discuss why thermonatrite was formed, and not different sodium carbonate phases. In addition to thermonatrite, trona ( $\text{Na}_3\text{HCO}_3\text{CO}_3 \cdot 2\text{H}_2\text{O}$ ) and natron ( $\text{Na}_2\text{CO}_3 \cdot 10\text{H}_2\text{O}$ ) have been formed when alkali silica gel was synthesized with aggregate and glass powders as silicon sources (ALMEIDA, 2015). Trona and thermonatrite have also been detected as a sign of carbonation in the synthesis of MK and FA geopolymers (KRIVENKO; KOVALCHUK, 2007). In that study, the authors discuss that trona is more likely to be formed in a system with high water/solid ratio. In contrast, thermonatrite is favored in systems with low water/solid ratio and hydrothermal conditions. In this current study, the contact with the atmosphere was decisive for the occurrence of carbonation.

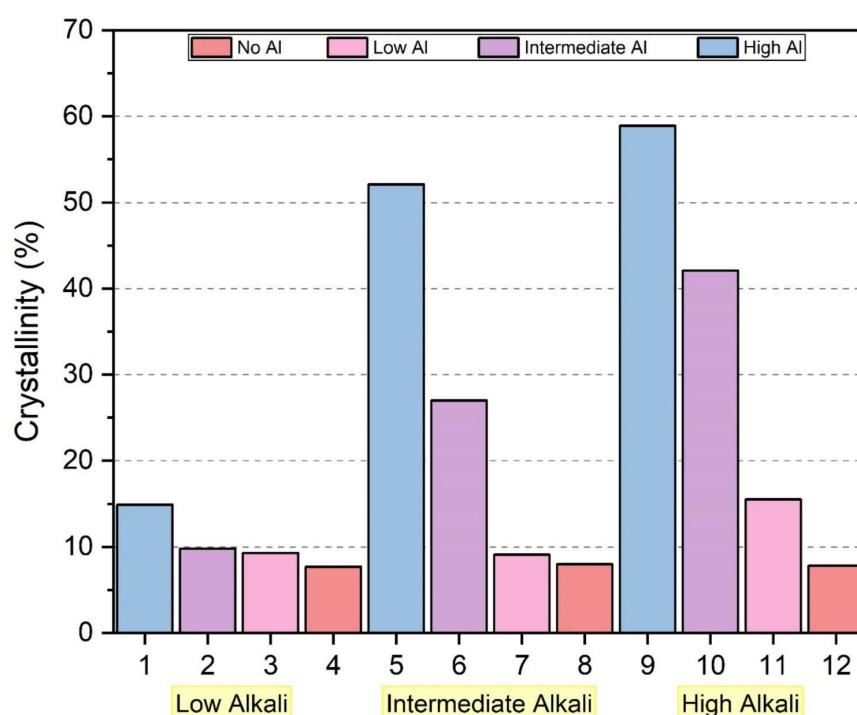
In consideration of the sodium oxide, its origin was unclear, only analyzing the XRD findings. Nonetheless, while scrutinizing the colored micrographs taken during the SEM/EDS analysis (see Figure 35, 35 and 36), it was found that a thin layer of a sodium-bearing phase was formed on the top surface of samples 3, 6 and 7. This leads to the assumption that the alkali dissolved in solution was precipitated as sodium oxide during the drying process.

Lastly, regarding the occurrence of silica polymorphs, it could be seen that the sodium silicate used in the synthesis featured an amorphous glassy structure with a couple of quartz peaks (see Figure 14). Nonetheless, with the addition of aluminum hydroxide, most of that nature disappeared. In samples with high aluminum content, the glassy silica structure

was absorbed and converted into the silica framework that composes zeolite minerals as well as the aluminosilicate gel.

However, in samples with limited availability of aluminum, quartz peaks remained, as in samples 2, 3, 4, 7, 8, 11 and 12, and are considered as a sign of unreacted sodium silicate, likewise, the bayerite peaks are a sign of unreacted aluminum hydroxide. It reveals that the silicate gel will only change its nature when a minimum amount of aluminum is available. In addition to quartz, different silica polymorphs were also found in the most crystalline samples as cristobalite (samples 5 and 9) and stishovite (sample 10).

Figure 26 – Crystallinity degree of synthetic gels.



Source: Own authorship

In addition to the phase identification, the crystallinity degree of the synthetic gels was also assessed with the assistance of Brucker DIFFRAC EVA software, as mentioned in section 3.3, and the results are shown in Figure 26. In this plot, it is seen that samples 5, 6, 9 and 10 showed the highest proportion of crystalline phases, whereas samples 2, 3, 4, 7, 8 and 12 displayed the lowest, achieving less than 10% of crystallinity degree. As can be seen, there is a tendency of increased crystallinity with a boost in the aluminum content. The same trend appears to occur with a raise in the alkali availability. These tendencies suggest that a combination in increase of both aluminum and alkali availability favors the formation of zeolite minerals and, as a result, significantly intensified the degree of crystallinity.

In summary, the XRD unveiled crucial points about the samples and how the synthesis procedure shaped the reaction products. First, the inclusion of aluminum,

especially followed by an increase in the alkali content, significantly boosted the crystallinity degree by favoring zeolite minerals as well as the formation of thermonatrite. Also, the detection of sodium carbonate phases in almost all samples indicates that sometime during the synthesis/drying procedure, the samples were in contact with the atmosphere and, consequently, carbonation occurred. Lastly, minor peaks of bayerite and quartz are a sign of unreacted reagents.

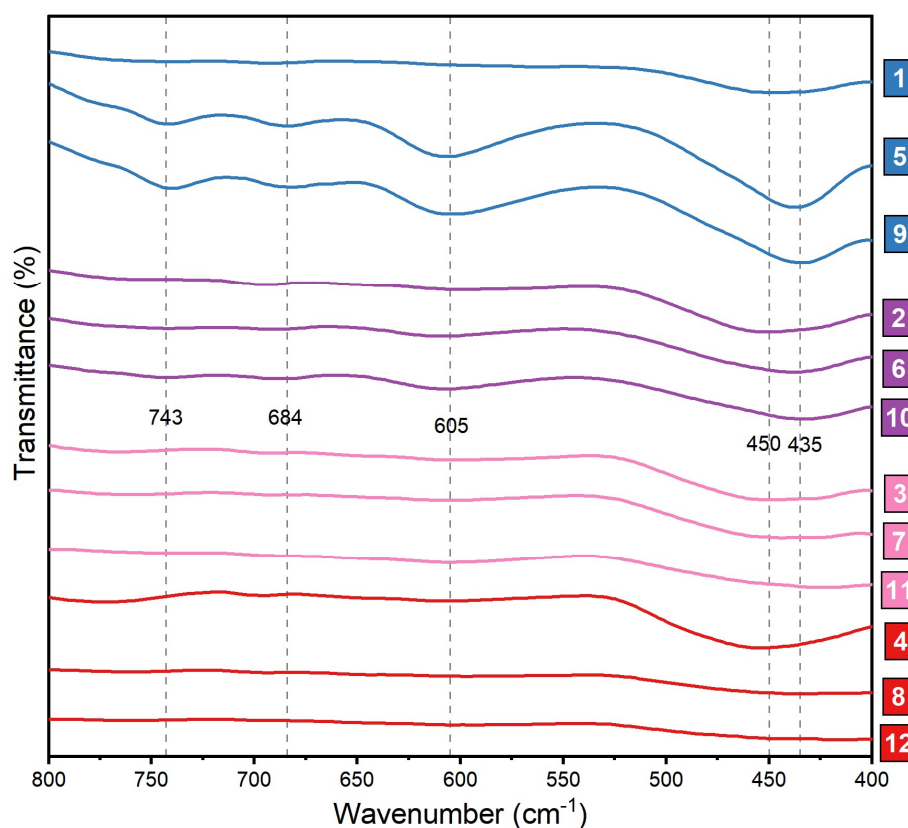
#### 4.4 Fourier-Transformed Infrared Spectroscopy (FTIR)

The infrared spectroscopy results of the synthesized gels are shown in Figure 27, 28 and 29, respectively, for the wavenumber ranges of 800-400  $\text{cm}^{-1}$ , 800-1500  $\text{cm}^{-1}$  and 4000-1500  $\text{cm}^{-1}$ . The color representation used in this section is the same utilized in the XRD result section (see section 4.3 X-Ray Diffraction), that is, blue, violet, pink and red respectively depicts samples with high (27% wt.  $\text{Al}_2\text{O}_3$ ), intermediate (18% wt.  $\text{Al}_2\text{O}_3$ ), low (9% wt.  $\text{Al}_2\text{O}_3$ ) and no-aluminum content (0% wt.  $\text{Al}_2\text{O}_3$ ). In addition to that, the samples are grouped by their aluminum content and sorted upwards in terms of its alkali proportion.

The FTIR analysis was employed as an additional characterization technique further to investigate the vibrational bonds in the synthetic gels. In this regard, broadbands at 1450  $\text{cm}^{-1}$  are observed in nearly all samples and are correlated to either the formation of  $\text{Na}_2\text{CO}_3$  or carbonation (KOMNITSAS; ZAHARAKI, 2007; YOUSUF et al., 1993). This finding corroborates the XRD result that the samples were in contact with the atmosphere and, as a result, carbonation occurred.

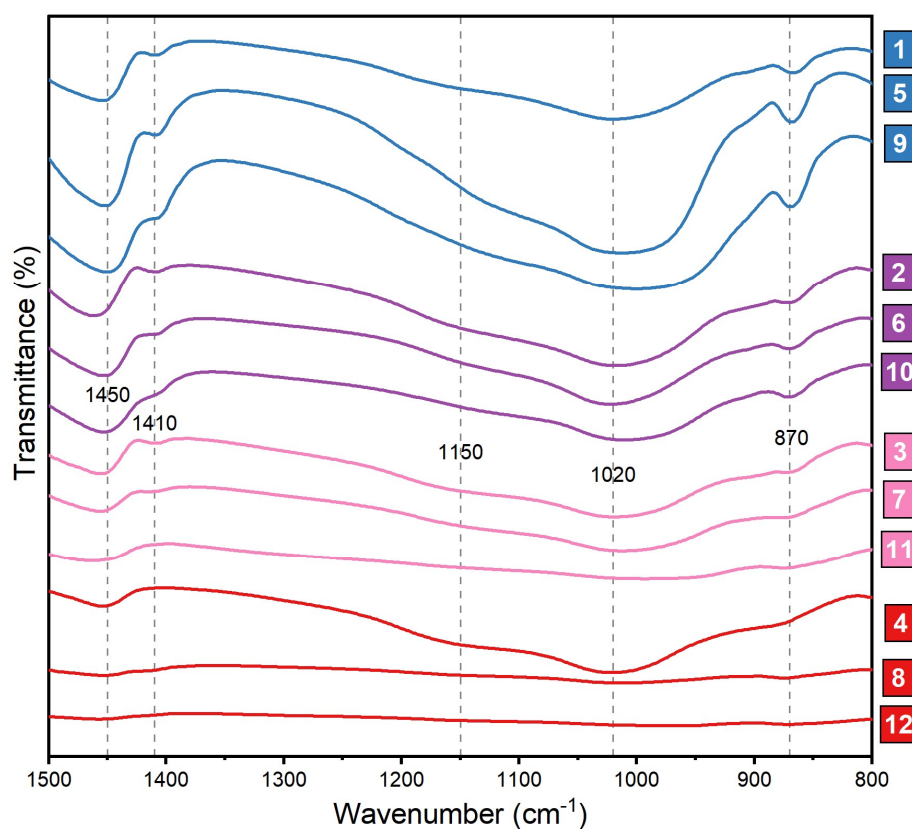
Moreover, broad bands resembling a shoulder are seen between 3600 and 3420  $\text{cm}^{-1}$  in every sample and are associated with the asymmetric stretching vibration of hydroxyl groups in chemically bonded water molecules (FIRDOUS; STEPHAN; DJOBO, 2018; PEREIRA; VASCONCELOS; VASCONCELOS, 2019; ZHENG et al., 2009). This finding was corroborated by the thermogravimetric analysis, which found that all samples lost around 7,73 to 13,45% of mass when heated from 25 to 100  $^{\circ}\text{C}$ , thus indicating the presence of absorbed water. This further confirms the hydrophilic nature of the synthetic gels.

Figure 27 – FTIR spectra of all synthetic gels in the range of 800-400  $\text{cm}^{-1}$ .

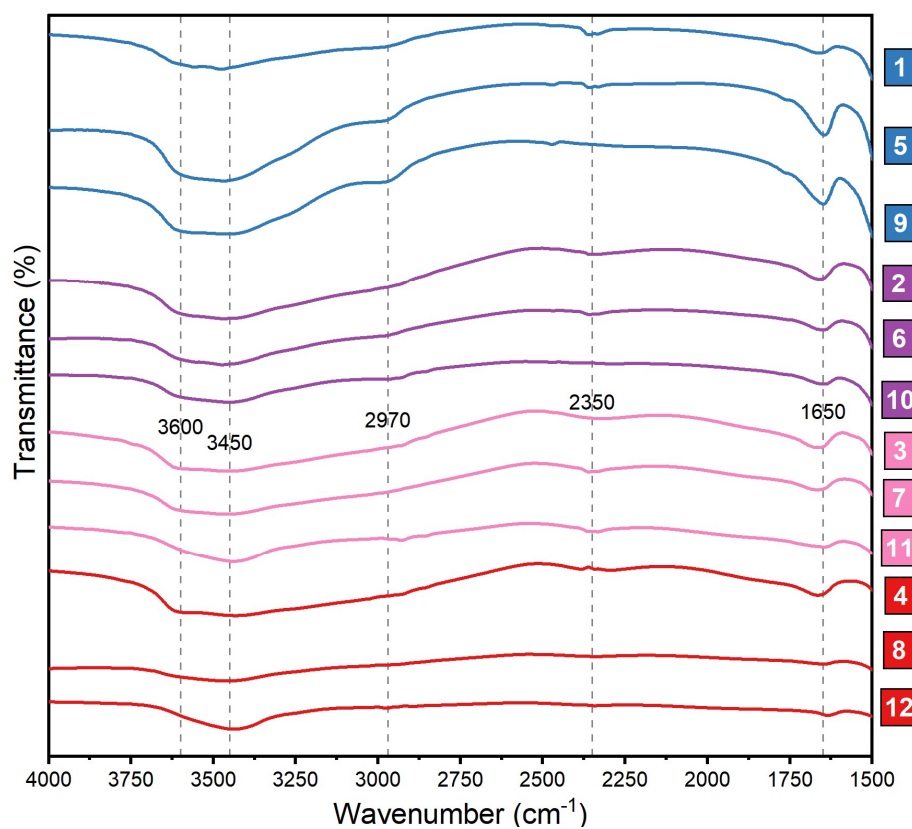


Source: Own authorship

Furthermore, major peaks are presented in the region of 1018 and 1150  $\text{cm}^{-1}$  and indicate the occurrence of respectively Si-O-Al and Si-O-Si bonds (GARCÍA-LODEIRO et al., 2008; PEREIRA; VASCONCELOS; VASCONCELOS, 2019; WALKLEY et al., 2016a), which highlight the occurrence of silicon and aluminum atoms in tetrahedral sites. Additionally, the 435  $\text{cm}^{-1}$  band is associated with the bending mode vibration of either Si-O or Al-O bonds (HUO et al., 2013). Also, the 680 and 745  $\text{cm}^{-1}$  are assigned to the symmetric stretching vibration of the internal tetrahedral (HUO et al., 2013). Considering the identified phases shown in the XRD result, the Si-O-Al bond is found in zeolite minerals as well as in the aluminosilicate gel framework. On the other hand, the Si-O-Si bond exists in silica polymorphs, such as quartz and cristobalite, alongside the alkali silica gel.

Figure 28 – FTIR spectra of all synthetic gels in the range of 1500-800  $\text{cm}^{-1}$ .

Source: Own authorship

Figure 29 – FTIR spectra of all synthetic gels in the range of 4000-1500  $\text{cm}^{-1}$ .

Source: Own authorship

Further evidence of aluminum in tetrahedral coordination is a band at  $870\text{ cm}^{-1}$  found in samples with high and intermediate aluminum content, depicted in blue and violet in Figure 28, which is associated with the asymmetric stretching of  $\text{AlO}_4^-$  in Si-O-Al bonds (WALKLEY et al., 2016b). It is noticeable that this band is even more pronounced in samples 5 and 9, which features the highest proportion of zeolite minerals in its structure. According to the XRD result, the zeolite minerals detected – zeolite P, zeolite P2 and gmelinite – all possess aluminum atoms in tetrahedral sites. Thus, this further confirms that the emergence of this band is related to the presence of such zeolite species.

Table 7 – FTIR result summary table.

Bands ( $\text{cm}^{-1}$ )	Samples												Associated bond
	1	2	3	4	5	6	7	8	9	10	11	12	
3600	✓	✓	✓	✓	✓	✓	✓	✓	✓	✓	✓	✓	Asymmetric stretching vibration of OH-groups in water molecules
3450	✓	✓	✓	✓	✓	✓	✓	✓	✓	✓	✓	✓	
2970	✓	✓	✓	✓	✓	✓	✓	✗	✓	✓	✗	✗	-
2350	✓	✓	✓	✗	✓	✓	✓	✗	✗	✗	✓	✗	Stretching vibration of O–H bonds
1650	✓	✓	✓	✓	✓	✓	✓	✗	✓	✓	✓	✗	Water molecules internal vibration
1454	✓	✓	✓	✓	✓	✓	✓	✓	✓	✓	✓	✓	Asymmetric stretching vibration of O–C–O
1410	✓	✓	✓	✗	✓	✓	✓	✗	✓	✓	✗	✗	-
1150	✓	✓	✓	✓	✓	✓	✓	✗	✓	✓	✗	✗	Si–O–Al bonds
1020	✓	✓	✓	✓	✓	✓	✓	✓	✓	✓	✓	✓	Si–O–Si bonds
997	✓	✓	✓	✓	✓	✓	✓	✗	✓	✓	✗	✗	Si–O–M <sup>+</sup> bond (M: Na or K)
870	✓	✓	✓	✓	✓	✓	✓	✗	✓	✓	✓	✗	Asymmetric stretching vibration of Si–O–Al bond
840	✗	✗	✗	✗	✗	✗	✗	✗	✗	✗	✗	✗	Silanol (Si–OH) groups
740	✗	✗	✗	✗	✓	✗	✗	✗	✓	✓	✗	✗	Asymmetric stretching vibration of T–O–T bonds (T: Si or Al)
684	✓	✗	✗	✗	✓	✗	✗	✗	✓	✓	✗	✗	
605	✓	✗	✗	✗	✓	✓	✗	✗	✓	✓	✗	✗	-
440	✓	✓	✓	✓	✓	✓	✓	✓	✓	✓	✓	✓	Bending vibration of T–O–T bonds

Source: Own authorship

In addition to that, silanol group vibrations found at  $840\text{ cm}^{-1}$  (FIRDOUS; STEPHAN; DJOBO, 2018; KUPWADE-PATIL; ALLOUCHE, 2012) were not detected in any of the spectra. It thus suggests that the silicate framework is well polymerized, being mainly composed of siloxane groups (Si–O–Si). Nonetheless, the band at  $997\text{ cm}^{-1}$  is



associated with the presence of  $\text{Si-O-M}^+$  (ALMEIDA, 2015) and is, therefore, a sign that sodium replaced hydrogen atoms in silanol groups at the ending of the silicate framework.

A summary of the identified bands, as well as its associated bound, are shown in Table 7. In conclusion, the FTIR analysis was helpful in both corroborating the XRD and Thermal Analysis results as well as providing additional insights about the gels framework arrangement. In this regard, the FTIR results confirmed the hydrophilic nature of the synthetic gels and that carbonation had occurred. It also strengthens the hypothesis of aluminum incorporation in tetrahedral sites in a well-polymerized silicate framework.

#### 4.5 Thermal Analysis (TGA/DTG/DSC)

The results of the heat flow and thermogravimetric analysis are shown in Figure 30 and 32. In these figures, each individual plot is depicted as a double-y graph, in which thermogravimetric data is shown in the blue left axis while the heat flow is portrayed in the red right axis. Additionally, Figure 32 shows the thermogravimetric result in a different format, where each colored bar refers to the amount of mass loss in a given temperature range (for example, red bar is associated with the mass loss at 25 to 100 °C while the blue bar depicts the amount of mass loss at 100 to 500 °C).

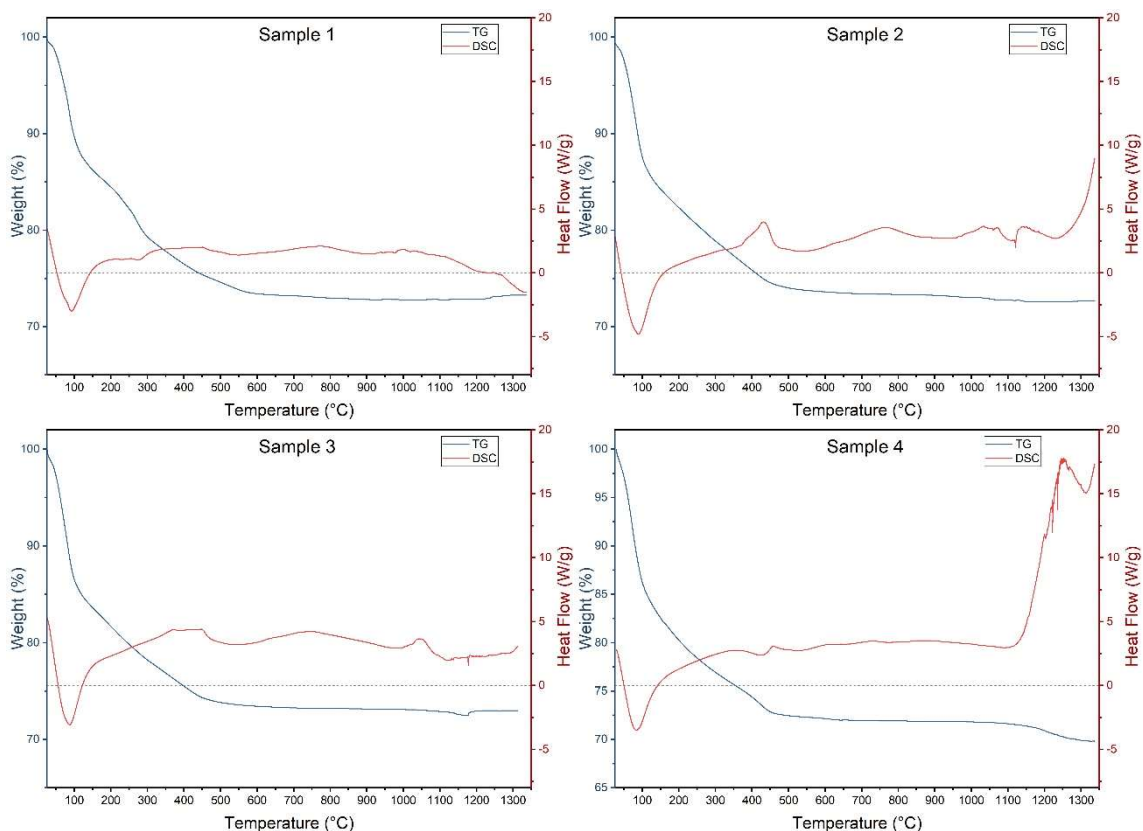
Considering the thermogravimetric analysis, the synthetic gels lose around 10% of its mass when heated from 25 to 100 °C. Samples 4 and 8 stand out as featuring the highest loss of mass, 13,75% and 13,93%, respectively. On the other hand, samples with the highest crystallinity degree (i.e., samples 5, 9 and 10) possess the lowest loss of mass in this temperature range, 8,54%, 7,85% and 7,74%, respectively. The loss of mass in this temperature variation is mainly accounted for the release of weakly-bonded water, which is associated with the ASR expansion. This indicates that the alkali silica gel present in samples with a low Al/Si ratio is significantly more hydrophilic than the aluminosilicate gel found in samples with high Al/Si. Therefore, it suggests that the incorporation of aluminum into the alkali silica gel reduces its water absorption capacity. Despite able to absorb water, zeolite crystals do not favor the loss of mass in this temperature range because the water molecules are trapped inside its nanometric cavities, thus requiring further energy to be released.

In the 100 to 500 °C temperature range, all synthetic gels lose on average 14% of its mass. Again, the most crystalline gels – samples 5, 9 and 10 – loses the lowest amount of mass, 11,12%, 10,32% and 12,21%. Again, there seems to exist a correlation between the

crystallinity degree and the loss of mass. This phenomenon becomes even more clear in the 500 to 750 °C temperature range. In this case, samples 1, 5, 6, 9 and 10 respectively loses 1,51%, 4,52%, 1,37%, 5,62% and 4,33% and the remaining samples lose on average 0,6%. This loss of mass is associated with the release of the imprisoned water inside the zeolite nanopores. After 750 °C, all samples stabilize and its mass loss is negligible.

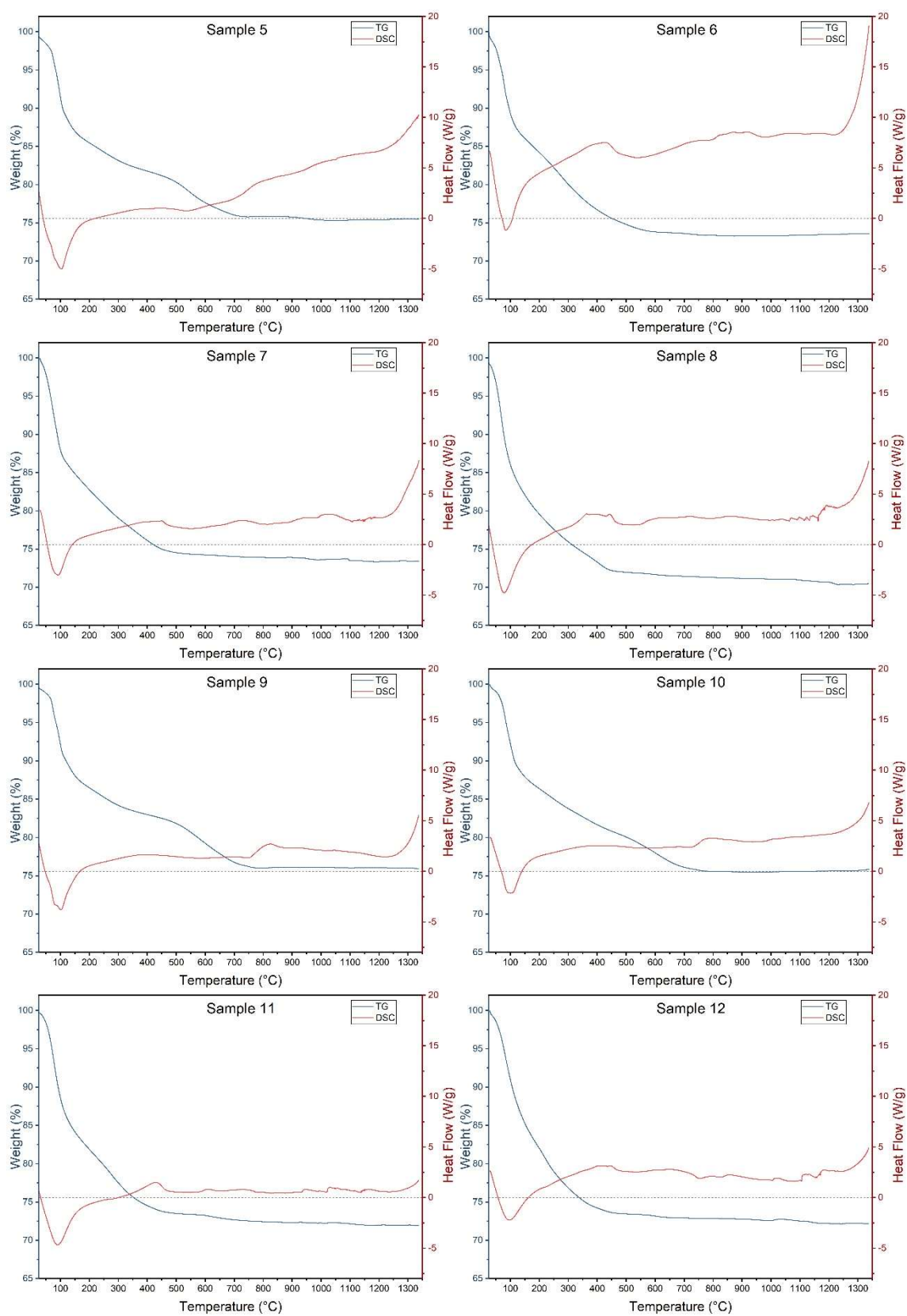
Moreover, it is interesting to note the correlation between the loss of mass and the crystallinity degree of the synthetic gels. Figure 33 shows a double-y graph, in which the loss of mass at 25 to 100 °C and 500 to 750 °C are shown in the red left and green right axis, respectively. From this plot, it can be seen a negative exponential relation between the degree of crystallinity and the loss of mass at 25 to 100 °C, that is, samples with the highest proportion of crystalline phases showed the lowest amount of mass loss. On the other hand, the loss of mass between 500 to 750 °C features a linear relationship with the crystallinity degree and corroborates the hypothesis of a higher loss of mass at this temperature range with the release of entrapped water from the zeolite nanopores.

Figure 30 – Individual thermogravimetric and heat flow plots of samples 1-4.



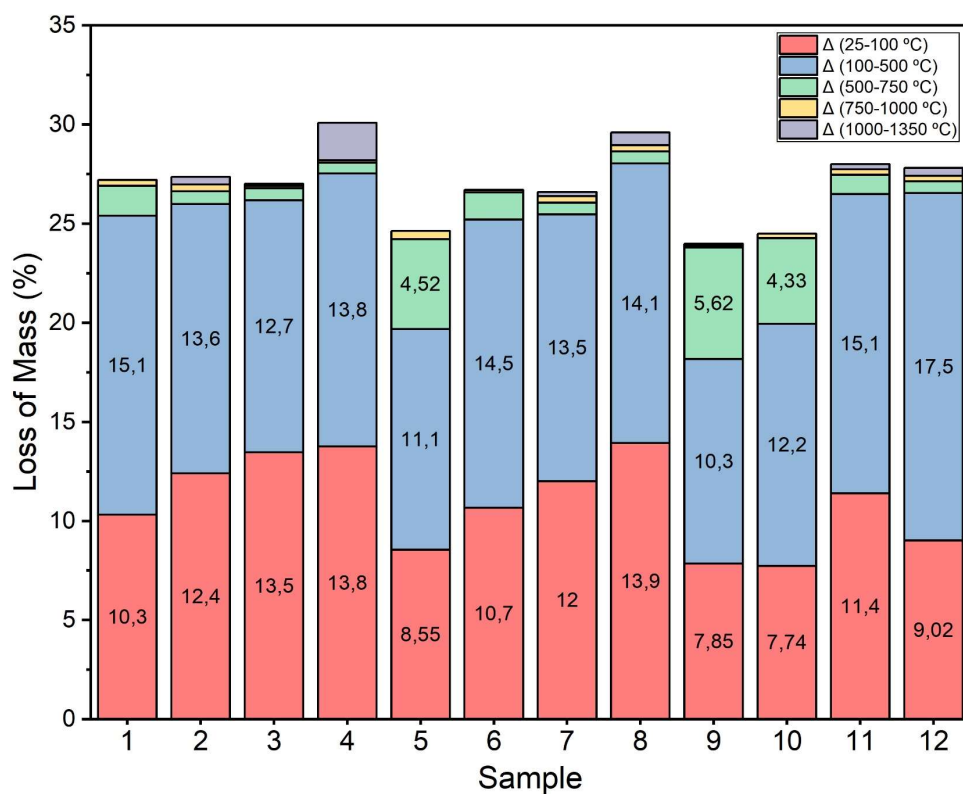
Source: Own authorship

Figure 31 – Individual thermogravimetric and heat flow plots of samples 5-12.



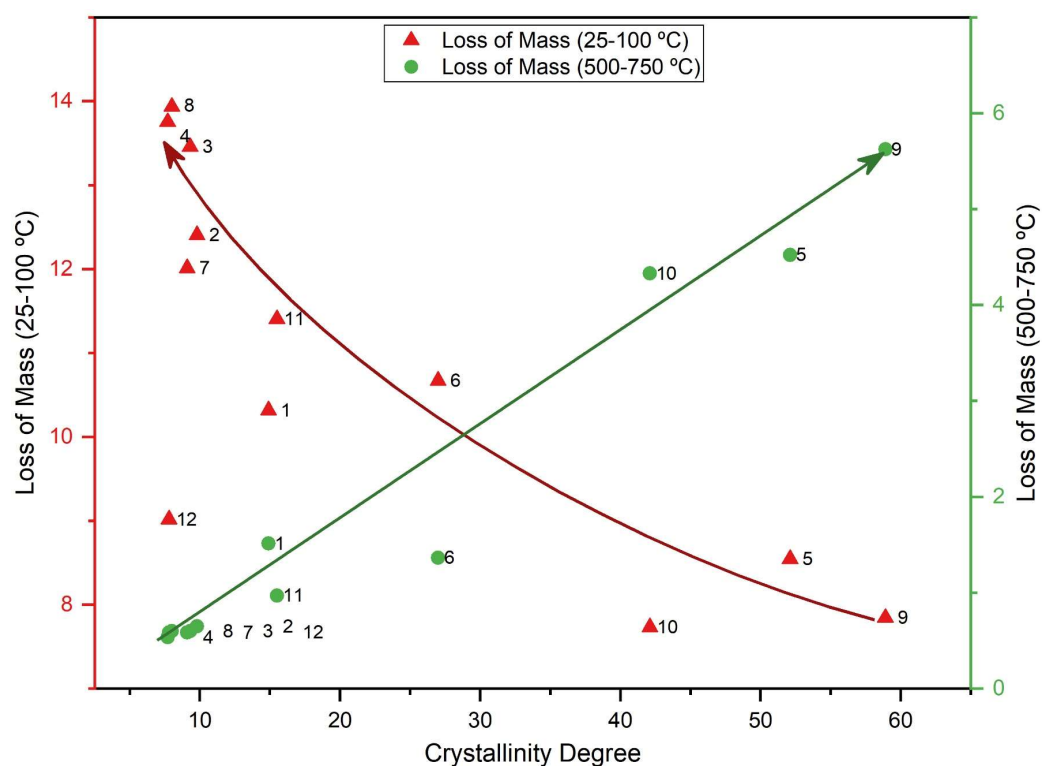
Source: Own authorship

Figure 32 – Thermogravimetric result depicted in terms of loss of mass for each temperature range.



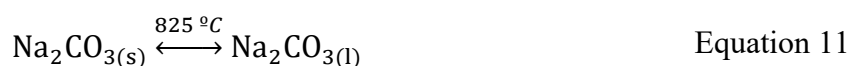
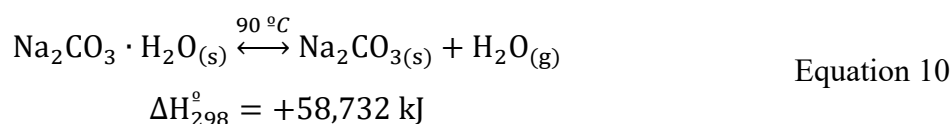
Source: Own authorship

Figure 33 – Correlation between the crystallinity degree and the loss of mass at 25-100 °C and 500-750 °C.



Source: Own authorship

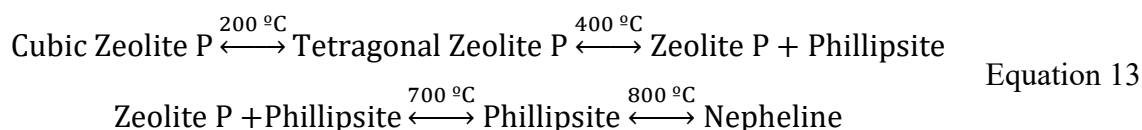
Regarding the thermal events that occurred throughout this experiment, a few observations are noted. First of all, thermonatrite releases its crystal water at around 90 °C in an endothermic process described in Equation 10 (HARTMAN et al., 2001; WATERFIELD; STAVELEY, 1967). Moreover, thermonatrite occurs at approximately 60 to 90 °C and above that, only anhydrous sodium carbonate forms (HARTMAN et al., 2001). This finding further indicates that the drying procedure adopted favored the formation of thermonatrite. Lastly, solid anhydrous sodium carbonation melts at 825 °C, as shown in Equation 11.



Considering the thermal behavior silica polymorphs detected by the XRD, that is,  $\alpha$ -quartz, cristobalite and stishovite, a few remarks are appropriate. First of all,  $\alpha$ -quartz is converted to  $\beta$ -quartz at 573 °C in a displacive transformation (BALDO; SANTOS, 2002). Later on,  $\beta$ -quartz is transformed into  $\beta$ -cristobalite at 870 °C and subsequently melts at 1760 °C (BALDO; SANTOS, 2002). This process is shown in Equation 12. Stishovite, on the other hand, does not undergo phase transformation in this temperature range.



Zeolite P, the most prominent zeolite mineral detected by the XRD result, also undergoes phase transformation in this temperature range. According to Huo et al. (2013), its cubic structure rearranges into a tetragonal phase at around 200 °C. Afterward, it gradually starts to convert into Na-phillipsite at 400-700 °C. Lastly, a very stable nepheline phase ( $\text{NaAlSiO}_4$ ) is formed at 800 °C (HUO et al., 2013). This process is shown in Equation 13.



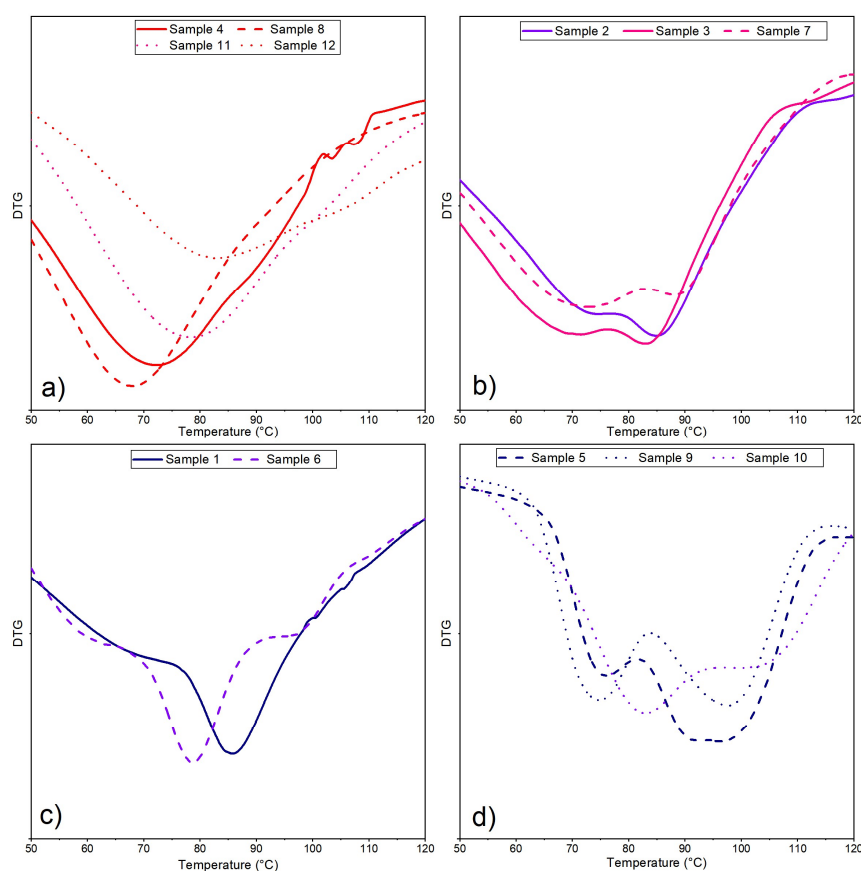
The DSC analysis revealed that all samples feature a major endothermic peak at 80-100 °C, which is associated with the loss of free water. Throughout the 200-1100 °C temperature range, all samples maintained a near-constant exothermic behavior, with ever more slightly mass loss. Few minor endothermic and exothermic peaks appeared in this process and are associated with the crystalline phase transformations described previously.

Figure 34 depicts different DTG patterns in the range of 50 to 120 °C. In the case of DTG analysis, each peak represents the maximum rate of mass loss which, in this

temperature range, is accounted for the dehydration of the samples. Figure 34-a shows that the temperature of maximum progressively increases sample 8 at 68 °C to sample 12 at 80 °C. In contrast, samples 2, 3 and 7 (see Figure 34-b) display a two-peak pattern, which implies that there more than one type of water being released. Samples 1 and 6 (see Figure 34-c) features single-peak increasing from 78 to 86 °C. Lastly, samples 5, 9 and 10 (see Figure 34-d) also feature a two-peak pattern behavior, but different from what was observed in samples 2, 3 and 7. Since these results were achieved by grouping together samples with similar crystallinity degree, it is thus concluded that the samples phase composition heavy governs its water absorption capabilities.

In summary, the thermal analysis was helpful and provided interesting insights about the gel's microstructure. First, it indicated the hydrophilic nature of the synthetic gels and further confirmed that the alkali silica gel is the most hydrophilic phase formed in this system. It also corroborated the existence of zeolite minerals by the mass loss between 500 and 700 °C, which was associated with the release of water imprisoned within nanometric pores.

Figure 34 – Different DTG pattern behavior on the range of 50-120 °C of samples: a) 4, 8, 11 and 12; b) 2, 3 and 7; c) 1 and 6; d) 5, 9 and 10.



Source: Own authorship

## 4.6 Scanning Electron Microscopy coupled with EDS (SEM/EDS)

### 4.6.1 Colored BSE analysis

Colored BSE micrographs of samples 1 to 4, 5 to 8 and 9 to 12 are shown in Figure 35, 34 and 35, respectively. These micrographs were taken at a magnification of 25x due to the wide view effect provided and are colored accordingly to the legend: regions in red, blue, and green depict matter rich in silicon, aluminum, and sodium, respectively. As a result, the alkali aluminosilicate gel is represented in blue-purplish tone, whereas alkali silica gel can be portrayed in yellow-reddish color. It should also be noted that each micrograph (except for samples 5 and 9) represents the cross-section of their corresponding sample. It means that in each picture, the top and bottom sections of each sample can be noticed as well as the transition zone between them.

Quickly glancing through these images, there are some noticeable key patterns. Primarily, several samples, namely 1, 2, 3, 6, 7, 10 and 11, display a distinctive case of phase segregation in which an alkaline aluminosilicate gel is found at the bottom of the sample while alkali silica remains at the top. This finding suggests that the formation of a dense aluminosilicate gel is kinetically favored, thus resulting in the maintenance of an alkali silica gel at the top. It also indicates that, if more aluminum was available, it would probably be incorporated by the alkali silica gel.

In contrast, the remaining samples possess a near homogeneous appearance at this magnification. Samples 4, 8 and 12 exhibit a uniform yellowish tone, depicting the expected alkali silica gel that it is composed. Despite the detection of corundum ( $\text{Al}_2\text{O}_3$ ) during the XRD analysis, there is no sign of blue regions in these micrographs. It suggests that corundum grains were formed during synthesis and did not cluster, remaining spread all around the sample, and as a result of the microscopic grain size it was not observable at this magnification.

Also displaying a near transition-less appearance, samples 5 and 9 feature an otherwise highly chaotic image. Due to its fragility, it was not possible to perform a cross-section cut without compromising the entire integrity of the fragment. For this reason, it was chosen to investigate the mid-section of both samples. As seen by the XRD result section, these samples are the most crystalline ones, possessing a significant amount of thermonatrite ( $\text{Na}_2\text{CO}_3 \cdot \text{H}_2\text{O}$ ) and zeolite minerals (zeolite P and zeolite P2) alongside a still apparent

amorphous content. From their respective micrographs, it can be concluded that all these phases are tangled with each other.

Cracks and fractures were observed in nearly all the samples. Minor cracks are dominant especially in the aluminosilicate gel regions (bottom section of samples 1, 2, 3, 6, 7, 10 and 11) and are a consequence of the water lost during the drying process. Since the alkali silica gel region does not feature as many minor cracks, it might be inferred that it did not lose as much free water as the aluminosilicate gel.

Furthermore, due to the widespread fractures within the gel, samples 6, 10 and 11 exhibited an elevated level of degradation. In samples 10 and 11, the evaporation was so intense that the sample became hollow, leaving an empty space in what was supposed to be the transition between the alkali silica and aluminosilicate gels. This phenomenon is macroscopically perceptible and can be seen in Figure 21.

An also noticeable phenomenon was the formation of a layer of a sodium-bearing phase at the top surface of samples 3, 7, and 11 and it is believed to be caused by the precipitation of sodium species from the liquid phase above during the drying procedure. According to the XRD result, thermonatrite peaks are minimal in these samples and pure sodium phase were not detected, except for minor peaks of sodium oxide in sample 11. Therefore, it is assumed that this phase is amorphous and thus is hidden in the background of the XRD result.

#### **4.6.2 EDS spot analysis**

In addition to the colored BSE analysis, a spot analysis consisting of measuring about 100-150 points scattered around the sample was carried out. The data gathered by the EDS detector was quantified in terms of C, O, Na, Al, and Si atomic concentrations and are shown in Appendix i – Eds spot analysis result. Most spots show on average 20% of carbon concentration. This higher concentration is credited to the higher voltage used – 20kV – which increases the beam's spatial resolution, thus increasing the chance of hitting the resin instead of the sample. To address this situation, a lower voltage – 15kV – was tested, but it caused a drastic reduction in signal, which resulted in longer measurement times, thus inhibiting its further use.

Due to the possibility of finding resins fragments inside the beam's area of influence, the absolute atomic value was disregarded, and instead, a ratio approach was adopted. That way, Al/Si and Na/Si ratios were calculated based on the data exposed in Appendix i – Eds



spot analysis result and its scatter plots are shown in Figure 35-e), 35-e) and 36-e). From these graphs, it can be seen that samples 4, 8 and 12 are depicted in a linear region with Al/Si ratio equals to zero and Na/Si ratio varying from 0,4 to 1,0. This result is very close to the A-S-G chemical composition argued by Hou, Struble and Kirkpatrick (2004), which varies between 0,1 to 1,2 sodium to silicon ratio. This further indicates that these samples are composed predominantly of alkali silica gel similar to those found in in-service concrete structure.

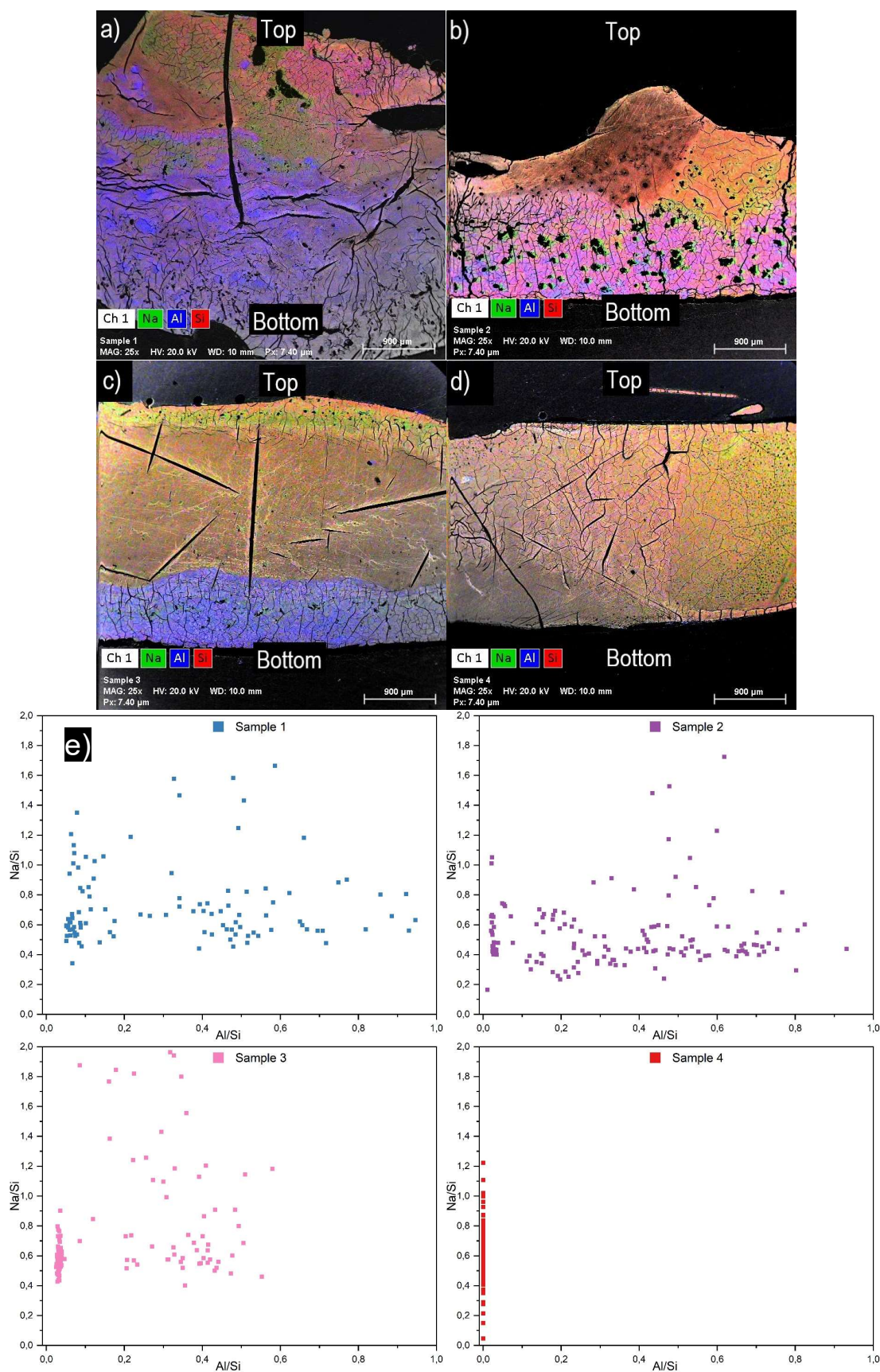
Samples 1, 2, 3 and 7, which featured a clear case of phase segregation in the previous section, displayed an interesting behavior in this analysis. The scatter plot of all these samples features a linear region, close to the A-S-G region but incorporating part of the available aluminum and a more widespread aluminosilicate region. The Al/Si ratio of the linear region varies between 0,02 to 0,07. This finding is a serious evidence that alkali silica gel is capable of absorbing aluminum when it is available.

Considering the synthetic gels with high alkali content (that is, samples 9, 10, 11 and 12, shown in Figure 37-e) the spot analysis revealed an interesting pattern. In this case, each sample is depicted as a linear region with near-constant Al/Si ratio and Na/Si ratio varying between 0,4 and 1,8.

Furthermore, Figure 387 and 38 respectively show the relative distribution of the Al/Si and Na/Si throughout each sample. Considering the case of Na/Si relative distribution, it can be seen the progression of the average ratio throughout the columns, as it was expected. In the case of Al/Si relative distributions, the same pattern is also found, as the Al/Si average value increases by progressing lines.

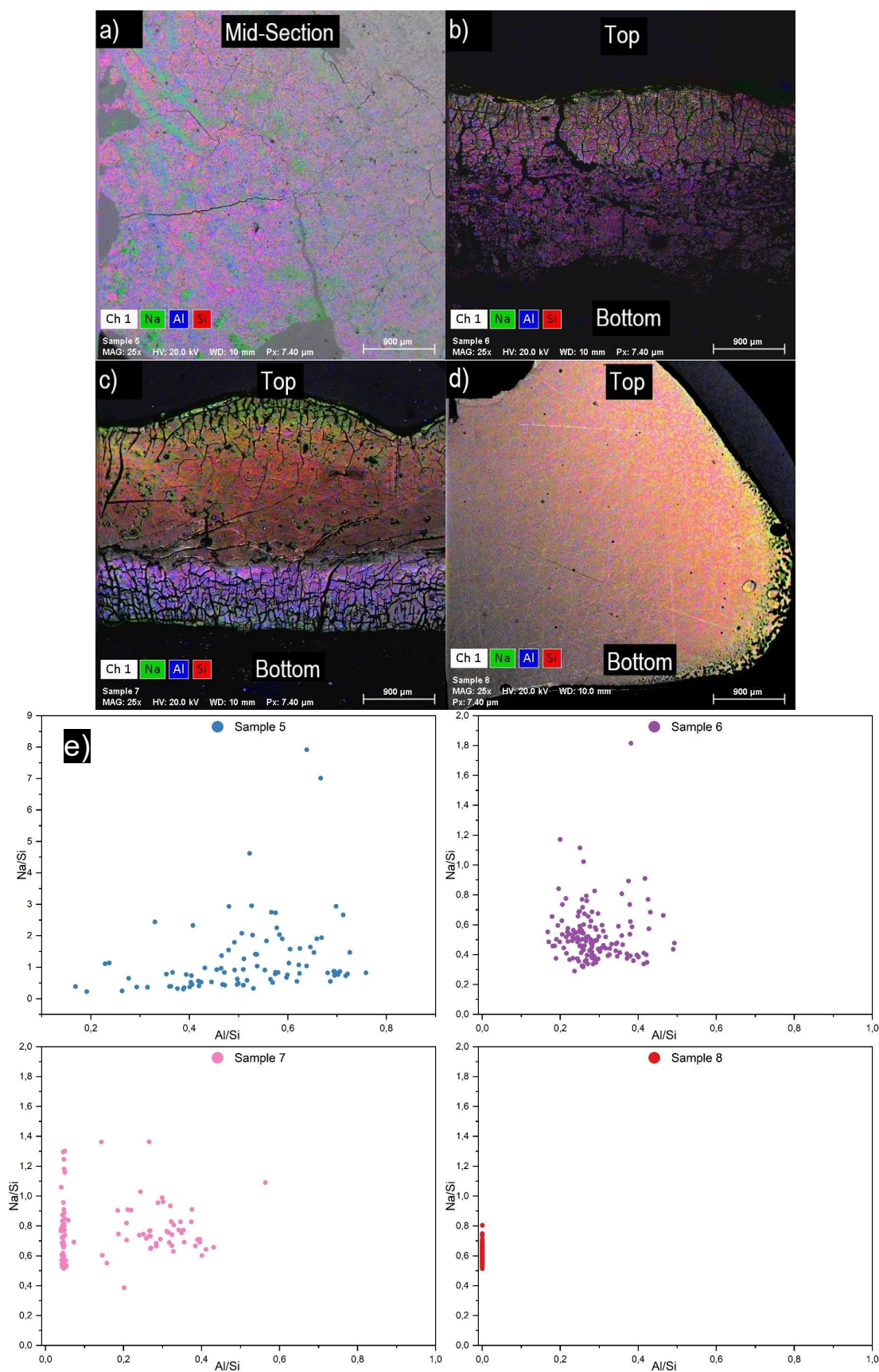
In conclusion, the scanning electron microscopy analysis was crucial for the conclusion of this work. Assisted by the EDS detector, it provided fruitful insights about the phase development of the synthetic samples. The colored BSE micrographs unveiled the layered structure present in samples 1, 2, 3 and 7 and confirmed the homogeneity of samples 4, 5, 8, 9 and 12. Additionally, the EDS spot analysis proved that the alkali silica gel can absorb the available aluminum.

Figure 35 – Colored BSE micrograph at a magnification of 25x of a) Sample 1, b) Sample 2, c) Sample 3 and d) Sample 4. The Al/Si x Na/Si scatter plot is shown in e).



Source: Own authorship

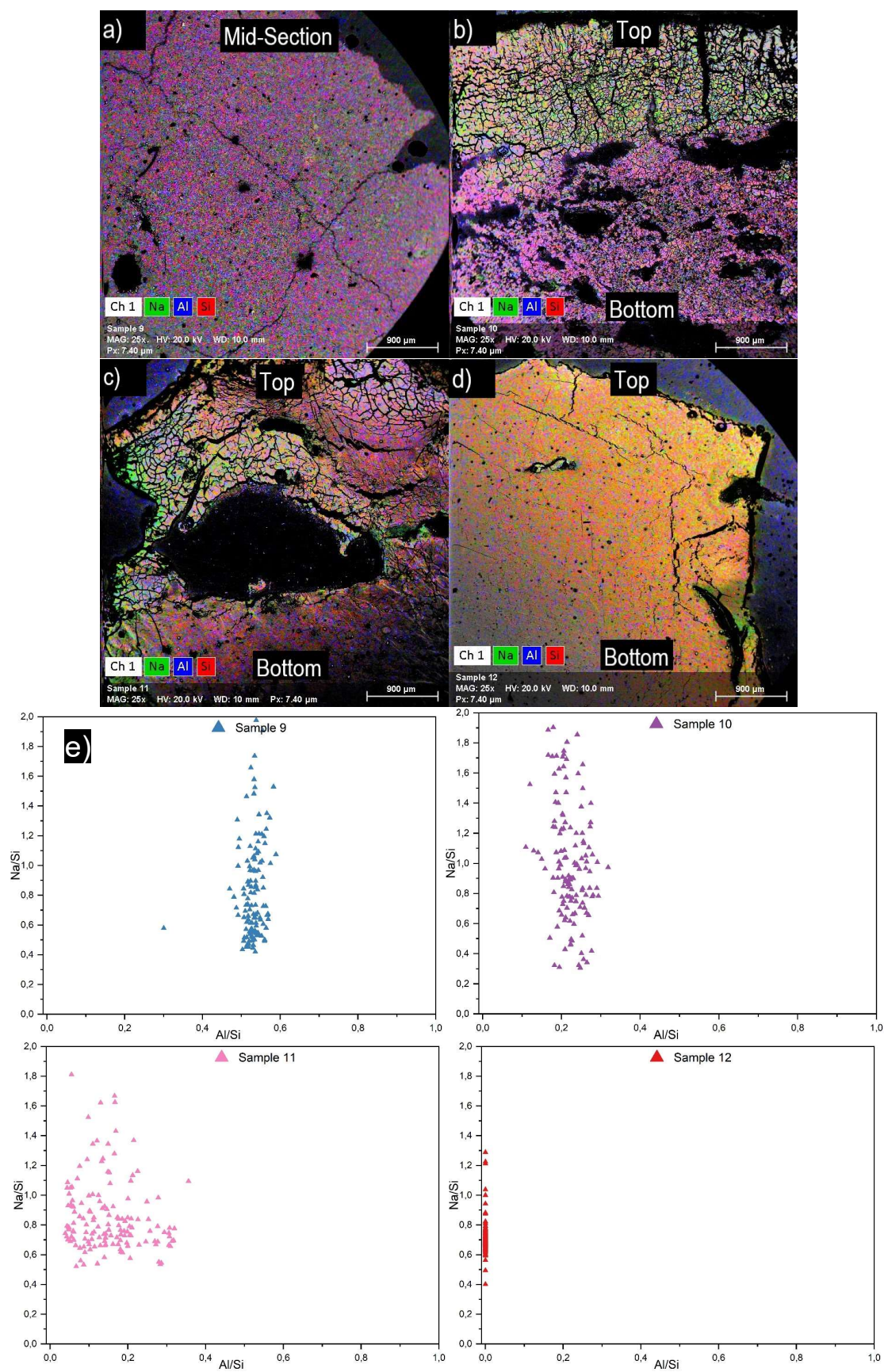
Figure 36 – Colored BSE micrograph at a magnification of 25x of a) Sample 5, b) Sample 6, c) Sample 7 and d) Sample 8. The Al/Si x Na/Si scatter plot is shown in e).



Source: Own authorship

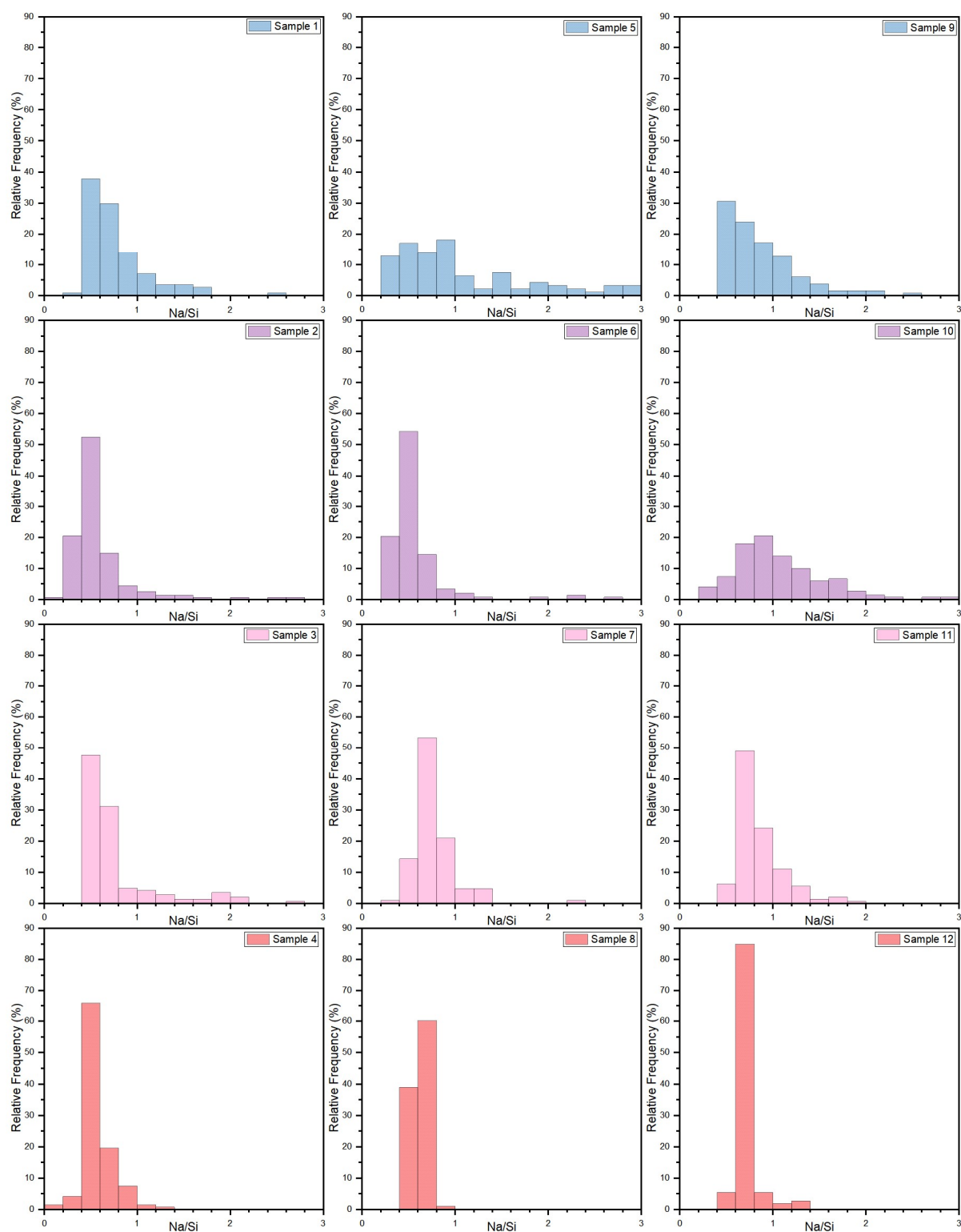


Figure 37 – Colored BSE micrograph at a magnification of 25x of a) Sample 9, b) Sample 10, c) Sample 11 and d) Sample 12. The Al/Si x Na/Si scatter plot is shown in e).



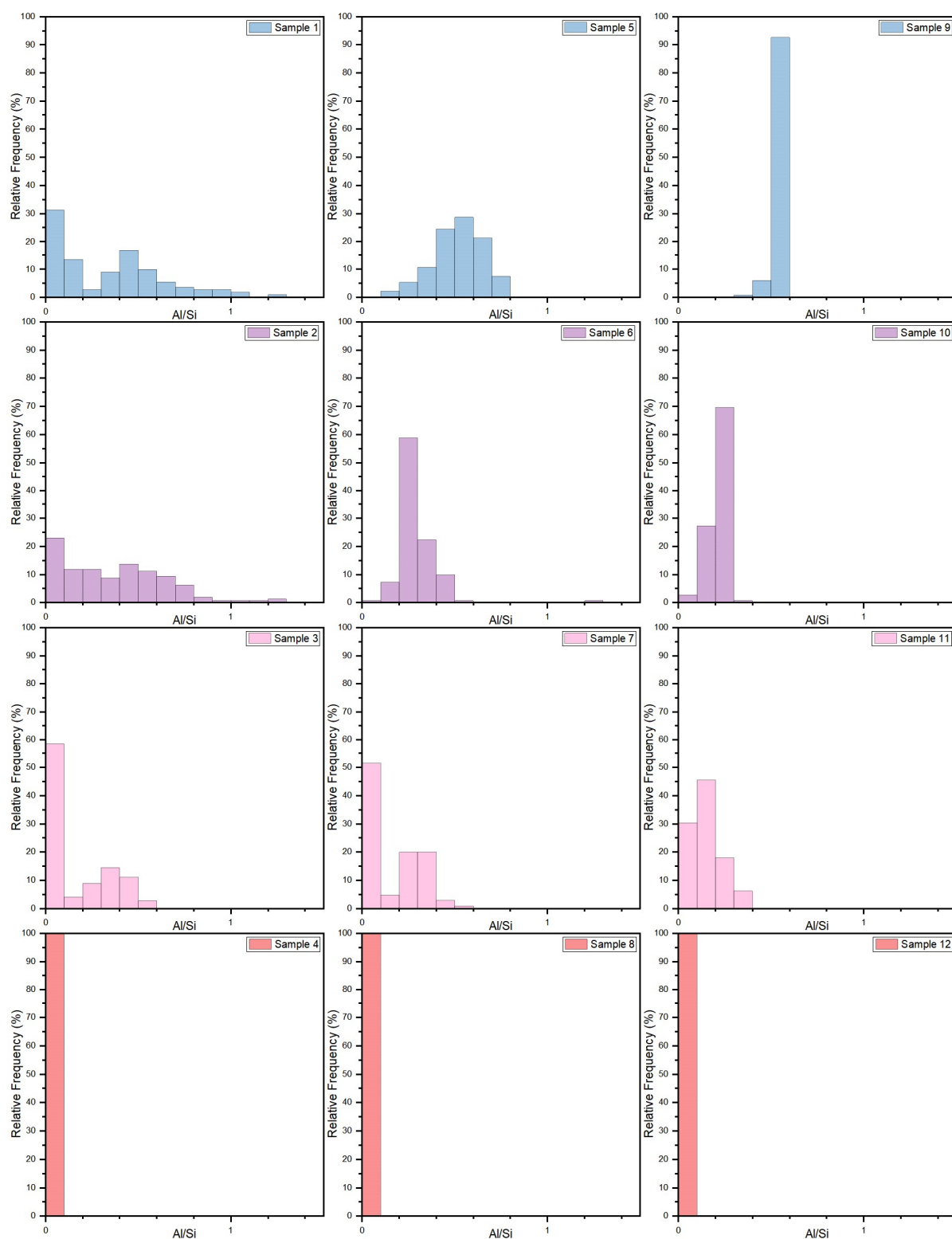
Source: Own authorship

Figure 38 – Relative frequency distribution of Na/Si of the synthetic gels.



Source: Own authorship

Figure 39 – Relative frequency distribution of Al/Si of the synthetic gels.



Source: Own authorship

## 5 CONCLUSION

Synthetic gels with bulk chemical composition between that of alkali silica and geopolymers gels were successfully synthesized using  $\text{Al}(\text{OH})_3$ ,  $\text{Na}_2\text{SiO}_3$ ,  $\text{NaOH}$  and distilled water. With the assistance of the various characterization techniques employed, a few conclusions might be stated.

- The XRF revealed that part of the alkali remained in solution, however an increase in the aluminum availability favored its absorption. It suggests that aluminum is being incorporated in tetrahedral sites, and thus requires the absorption of an alkali ion to charge balance the tetrahedral bond.
- The XRD unveiled the predominantly amorphous nature of the gels, yet a combination of increase in both aluminum and alkali availability promoted the formation of zeolite minerals.
- The FTIR and TG analysis exposed the hydrophilic character of the gels. It was found that the increase in aluminum content decreases the amount of weakly-bound water, which is correlated to the ASR expansion. It indicates that the incorporation of aluminum decreases the water absorption capacity of ordinary A-S-G.
- The FTIR observed that the gel's framework comprises Si and Al atoms in tetrahedral coordination. It was also detected the replacement of hydrogen ions ( $\text{H}^+$ ) by sodium ions ( $\text{Na}^+$ ) at the edges of the framework.
- In samples 1, 2, 3 and 7 (low alkali and low to high aluminum content), the SEM/EDS colored BSE micrographs unveiled a layered structure with a dense layer of aluminosilicate gel laying at the bottom and a layer of alkali silica gel at the top.
- Furthermore, in the same samples, the SEM/EDS dot analysis detected the incorporation of aluminum in the alkali silica gel in an Al/Si ratio of about 0,025 to 0,05. This result suggests that non-calcium A-S-G is capable of absorbing aluminum in its chemical composition.

These findings indicate that aluminum species released from supplementary cementitious materials are capable of being incorporated in the non-calcium variant of alkali silica gel. Additionally, the lower loss of mass between 25 to 100 °C, which is accounted for the release of weakly-bonded water, in samples containing aluminum indicates that the

incorporation of aluminum changes the water absorption capabilities in non-calcium alkali silica gel.

### **5.1 Implications for concrete science and technology**

This experimental work shows the importance of the use of a fundamental approach towards understanding and controlling complex phenomena such as the ASR. The incorporation of aluminum has a potentially positive effect in mitigating the ASR expansive phenomena, as, for instance, supplementary cementitious materials containing aluminum, such as metakaolin and fly ash, can provide the source of aluminum in order to help form less expansive types of aluminosilicate gels.

A possible technological approach to mitigate in-service concrete structures diagnosed with ASR is the injection of an aluminum alkali solution in the concrete crack opening. This would provide enough ions to alter the A-S-G chemical composition and its harmful behavior. Depending on the amount of alkalis given, two scenarios might occur:

- If the alkali concentration is around 10-11%, aluminosilicate gel should be formed;
- If the alkali concentration is around 12-14%, zeolite minerals will be favored.

Nonetheless, it must be emphasized that the concrete pore solution is replete with calcium species. As a result, further technological remarks cannot be made without a deeper understanding of the incorporation of aluminum in the  $\text{SiO}_2\text{-Al}_2\text{O}_3\text{-Na}_2\text{O-CaO}$  system.

### **5.2 Recommendation for future researches**

The decision to develop a research-based on the calcium-free  $\text{SiO}_2\text{-Al}_2\text{O}_3\text{-Na}_2\text{O}$  ternary diagram was chosen in order to simplify an already complex system. Although producing valuable insights about the incorporation of aluminum in pure alkali silica gel, that is not a representative circumstance of real-life concrete structures. In this case, calcium is prolific in the form of portlandite, C-S-H and dissolved in solution, and as a result, end up being absorbed by ordinary A-S-G in a  $\text{CaO/SiO}_2$  ratio of about 0,0 to 0,2 (HOU; STRUBLE; KIRKPATRICK, 2004). Plenty of research has been developed on the effects of calcium on ASR (see section 2.1.6 Calcium Effect), from the influence on silica dissolution to the



modification of A-S-G rheological properties, but very few have focused on the incorporation of aluminum in the gel structure.

In addition to that, in a long-lasting study, it would surely be interesting to assess different synthesis routes and conditions. Hydrothermal synthesis was selected because it would allow the gels synthesis at relatively low temperatures. However, this decision might have caused the crystallization of part of the aluminosilicate gel and the consequent formation of zeolite minerals. Thus, exploring different synthesis routes such as the sol-gel might be a necessary approach to prevent the formation of secondary reaction products. Furthermore, it is well known that temperature and reaction time plays a crucial role when synthesizing a given product. Therefore, experimenting with different synthesis conditions will probably be necessary.

Lastly, in terms of characterization techniques, XRD and SEM/EDS were essential for the conclusion of this study, especially with the upcoming implementation of Rietveld Refinement quantitative analysis. Nonetheless, these techniques offer almost no insight on the nanostructural ordering of amorphous gels, such as the case of A-S-G and N-A-S-H. For this reason, alternative techniques like  $^{29}\text{Si}$  and  $^{27}\text{Al}$  MAS NMR are often used when investigating these materials, especially considering its useful insights about the gel's polymerization state. Additionally, pair distribution function (PDF) and x-ray absorption fine structures (XASF) techniques have been recently used for the nanostructural refinement of A-S-G (MERAL; BENMORE; MONTEIRO, 2011; PRADO et al., 2019) and might contribute for the better understanding of the gels mentioned above.

## REFERENCES

- ABNT. **NBR 15577-5 - Agregados - Reatividade álcali-agregado Parte 5: Determinação da mitigação da expansão em barras de argamassa pelo método acelerado**, 2008a.
- ABNT. **NBR 15577-6 - Agregados - Reatividade álcali-agregado Parte 6: Determinação da expansão em prismas de concreto**, 2008b.
- ALMEIDA, T. DA S. **Síntese e caracterização de géis da reação álcali-sílica em condições aceleradas**. [s.l.] Universidade Federal da Paraíba, 2015.
- ANDRADE, T.; SILVA, J. J. R.; HASPARYK, N. P. **History of some AAR cases in the Recife region of Brazil**. Proceedings of the 13th International Conference on Alkali Aggregate Reaction (ICAAR). **Anais...**Trondheim: 2008
- AQUINO, W.; LANGE, D. A.; OLEK, J. The influence of metakaolin and silica fume on the chemistry of alkali - silica reaction products. **Cement and Concrete Composites**, v. 23, n. August, p. 485–493, 2001.
- ASTM C 150 - 07 Standard Specification for Portland Cement**. West Conshohocken, Pennsylvania American Society for Testing Materials, , 2007.
- ÁVILA, J. I. S. L.; FONTE, A. O. C. **Alkali-aggregate reaction in the pile caps of a bridge**. IBRACOM 44º Congresso Brasileiro do Concreto. **Anais...**Belo Horizonte: 2002
- BALDO, J. B.; SANTOS, W. N. DOS. Phase transitions and their effects on the thermal diffusivity behaviour of some SiO<sub>2</sub> polymorphs. **Cerâmica**, v. 48, n. 307, p. 172–177, 2002.
- BHAGATH SINGH, G. V. P.; SUBRAMANIAM, K. V. L. Quantitative XRD study of amorphous phase in alkali activated low calcium siliceous fly ash. **Construction and Building Materials**, v. 124, p. 139–147, 2016.
- BICKMORE, B. R. et al. The effect of Al(OH)<sub>4</sub>-on the dissolution rate of quartz. **Geochimica et Cosmochimica Acta**, v. 70, n. 2, p. 290–305, 2006.
- BLAND, W.; ROLLS, D. **Weathering: An Introduction to the Scientific Principles**. London: [s.n.].
- CALLISTER, W. D.; RETHWISCH, D. G. **Materials Science and Engineering: An Introduction**. Eighth Edi ed. United States: Wiley, 2009.
- CHAPPEX, T.; SCRIVENER, K. Alkali fixation of C-S-H in blended cement pastes and its relation to alkali silica reaction. **Cement and Concrete Research**, v. 42, n. 8, p. 1049–1054, 2012a.
- CHAPPEX, T.; SCRIVENER, K. L. The influence of aluminium on the dissolution of amorphous silica and its relation to alkali silica reaction. **Cement and Concrete Research**, v. 42, n. 12, p. 1645–1649, 2012b.

CHAPPEX, T.; SCRIVENER, K. L. The effect of aluminum in solution on the dissolution of amorphous silica and its relation to cementitious systems. **Journal of the American Ceramic Society**, v. 96, n. 2, p. 592–597, 2013.

DAVIDOVITS, J. **Synthesis of new high-temperature geo-polymers for reinforced plastics/composites**. SPE PACTEC. **Anais...**1979

DAVIDOVITS, J. Geopolymers - Inorganic polymeric new materials. **Journal of Thermal Analysis**, v. 37, n. 8, p. 1633–1656, 1991.

DAVIDOVITS, J. Properties of Geopolymer Cements. **First International Conference on Alkaline Cements and Concretes**, p. 131–149, 1994.

DENT GLASSER, L. S.; KATAOKA, N. The Chemistry of “Alkali-Aggregate” Reaction. **Cement and Concrete Research**, v. 11, n. c, p. 1–9, 1981.

DROLET, C.; DUCHESNE, J.; FOURNIER, B. Effect of alkali release by aggregates on alkali-silica reaction. **Construction and Building Materials**, v. 157, p. 263–276, 2017.

DUCHESNE, J.; BÉRUBÉ, M. A. The effectiveness of supplementary cementing materials in suppressing expansion due to ASR: Another look at the reaction mechanisms part 2: Pore solution chemistry. **Cement and Concrete Research**, v. 24, n. 2, p. 221–230, 1994.

DUXSON, P. et al. Understanding the relationship between geopolymer composition, microstructure and mechanical properties. **Colloids and Surfaces A: Physicochemical and Engineering Aspects**, v. 269, n. 1–3, p. 47–58, 2005.

DUXSON, P. The structure and thermal evolution of metakaolin geopolymers. n. February, p. 389, 2006.

DUXSON, P. et al. Geopolymer technology: The current state of the art. **Journal of Materials Science**, v. 42, n. 9, p. 2917–2933, 2007a.

DUXSON, P. et al. The role of inorganic polymer technology in the development of “green concrete”. **Cement and Concrete Research**, v. 37, n. 12, p. 1590–1597, 2007b.

DUXSON, P.; PROVIS, J. L. Designing precursors for geopolymer cements. **Journal of the American Ceramic Society**, v. 91, n. 12, p. 3864–3869, 2008.

DYER, T. **Concrete Durability**. [s.l.] CRC Press, 2014.

FAIRBAIRN, E. M. R. South and Central America. In: POOLE, A.; SIMS, I. (Eds.). . **Alkali-Aggregate Reaction in Concrete**. 1st. ed. London: CRC Press, 2017. p. 493–508.

FENG, X. et al. Studies on lithium salts to mitigate ASR-induced expansion in new concrete: A critical review. **Cement and Concrete Research**, v. 35, n. 9, p. 1789–1796, 2005.

FENG, X. et al. New observations on the mechanism of lithium nitrate against alkali silica reaction (ASR). **Cement and Concrete Research**, v. 40, n. 1, p. 94–101, 2010.

FERNÁNDEZ-JIMÉNEZ, A.; PALOMO, A. Chemical durability of geopolymers. In: **Geopolymers Structure, processing, properties and industrial applications**. [s.l.: s.n.].

FIRDOUS, R.; STEPHAN, D.; DJOBO, J. N. Y. Natural pozzolan based geopolymers: A review on mechanical, microstructural and durability characteristics. **Construction and Building Materials**, v. 190, p. 1251–1263, 2018.

FRÝBORT, A. et al. Variations in the composition and relations between alkali-silica gels and calcium silicate hydrates in highway concrete. **Materials Characterization**, v. 137, n. July 2017, p. 91–108, 2018.

GARCÍA-LODEIRO, I. et al. FTIR study of the sol-gel synthesis of cementitious gels: C-S-H and N-A-S-H. **Journal of Sol-Gel Science and Technology**, v. 45, n. 1, p. 63–72, 2008.

GARCIA-LODEIRO, I.; PALOMO, A.; FERNÁNDEZ-JIMÉNEZ, A. An overview of the chemistry of alkali-activated cement-based binders. In: **Handbook of Alkali-activated Cements, Mortars and Concrete**. Cambridge: Elsevier, 2015a. p. 19–47.

GARCIA-LODEIRO, I.; PALOMO, A.; FERNÁNDEZ-JIMÉNEZ, A. Crucial insights on the mix design of alkali-activated cement-based binders. In: PACHECO-TORGAL, F. et al. (Eds.). **Handbook of Alkali-activated Cements, Mortars and Concrete**. Cambridge: Elsevier, 2015b. p. 49–73.

GENG, G. et al. Atomistic structure of alkali-silica reaction products refined from X-ray diffraction and micro X-ray absorption data. **Cement and Concrete Research**, v. 129, n. December 2019, p. submitted, 2019.

GHOLIZADEH-VAYGHAN, A.; RAJABIPOUR, F. The influence of alkali-silica reaction (ASR) gel composition on its hydrophilic properties and free swelling in contact with water vapor. **Cement and Concrete Research**, v. 94, p. 49–58, 2017.

GHOLIZADEH VAYGHAN, A.; RAJABIPOUR, F.; ROSENBERGER, J. L. Composition-rheology relationships in alkali-silica reaction gels and the impact on the Gel's deleterious behavior. **Cement and Concrete Research**, v. 83, p. 45–56, 2016.

GUO, S.; DAI, Q.; SI, R. Effect of calcium and lithium on alkali-silica reaction kinetics and phase development. **Cement and Concrete Research**, v. 115, n. March 2018, p. 220–229, 2019.

HÅKANSSON, U.; FÄLTH, L.; HANSEN, S. Structure of a high-silica variety of zeolite Na-P. **Acta Crystallographica Section C Crystal Structure Communications**, v. 46, n. 8, p. 1363–1364, 1990.

HARTMAN, M. et al. Thermal dehydration of the sodium carbonate hydrates. **Chemical Engineering Communications**, v. 185, n. November 2014, p. 1–16, 2001.

HAY, R.; OSTERTAG, C. P. On utilization and mechanisms of waste aluminium in mitigating alkali-silica reaction (ASR) in concrete. **Journal of Cleaner Production**, v. 212, p. 864–879, 2019.

HELENE, P.; CARVALHO, M.; PACHECO, J. Engineering field tests for alkali-aggregate

reaction. **Structural Concrete**, v. 18, n. 2, p. 349–355, 2017.

HILDEBRANDO, E. A. et al. Synthesis and characterization of zeolite NaP using kaolin waste as a source of silicon and aluminum. **Materials Research**, v. 17, p. 174–179, 2014.

HONG, S. Y.; GLASSER, F. P. Alkali sorption by C-S-H and C-A-S-H gels: Part II. Role of alumina. **Cement and Concrete Research**, v. 32, n. 7, p. 1101–1111, 2002.

HOU, X. et al. Structural investigations of alkali silicate gels. **Journal of the American Ceramic Society**, v. 88, n. 4, p. 943–949, 2005.

HOU, X.; STRUBLE, L. J.; KIRKPATRICK, R. J. Formation of ASR gel and the roles of C-S-H and portlandite. **Cement and Concrete Research**, v. 34, n. 9, p. 1683–1696, 2004.

HUO, Z. et al. Thermal study of NaP zeolite with different morphologies. **Journal of Thermal Analysis and Calorimetry**, v. 111, n. 1, p. 365–369, 2013.

ILER, R. K. Effect of Adsorbed Alumina on the Solubility of Amorphous Silica in Water. **Journal of Colloid and Interface Science**, v. 43, n. 2, p. 399–408, 1973.

JUENGER, M. C. G.; OSTERTAG, C. P. Alkali-silica reactivity of large silica fume-derived particles. **Cement and Concrete Research**, v. 34, n. 8, p. 1389–1402, 2004.

KAWAMURA, M.; IWAHORI, K. ASR gel composition and expansive pressure in mortars under restraint. **Cement and Concrete Composites**, v. 26, n. 1, p. 47–56, 2004.

KHALE, D.; CHAUDHARY, R. Mechanism of geopolymerization and factors influencing its development: A review. **Journal of Materials Science**, v. 42, n. 3, p. 729–746, 2007.

KIM, T.; OLEK, J. Chemical sequence and kinetics of alkali-silica reaction part I. Experiments. **Journal of the American Ceramic Society**, v. 97, n. 7, p. 2195–2203, 2014.

KOMNITSAS, K.; ZAHARAKI, D. Geopolymerisation: A review and prospects for the minerals industry. **Minerals Engineering**, v. 20, n. 14, p. 1261–1277, 2007.

KONGKACHUICHAY, P.; LOHSOONTOM, P. Phase diagram of zeolite synthesized from perlite and rice husk ash. **ScienceAsia**, v. 32, n. 1, p. 13–16, 2006.

KRIVENKO, P. V.; KOVALCHUK, G. Y. Directed synthesis of alkaline aluminosilicate minerals in a geocement matrix. **Journal of Materials Science**, v. 42, n. 9, p. 2944–2952, 2007.

KRÓL, M. et al. Low-temperature synthesis of zeolite from perlite waste - Part I: Review of methods and phase compositions of resulting products. **Materials Science- Poland**, v. 32, n. 3, p. 503–513, 2014.

KUPWADE-PATIL, K.; ALLOUCHE, E. N. Impact of Alkali Silica Reaction on Fly Ash-Based Geopolymer Concrete. **Journal of Materials in Civil Engineering**, v. 25, n. 1, p. 131–139, 2012.

KURDOWSKI, W. **Cement and Concrete Chemistry**. London: Springer, 2014.

LEEMANN, A. et al. Alkali-Silica reaction: The Influence of calcium on silica dissolution and the formation of reaction products. **Journal of the American Ceramic Society**, v. 94, n. 4, p. 1243–1249, 2011.

LEEMANN, A. et al. Mitigation of ASR by the use of  $\text{LiNO}_3$  - Characterization of the reaction products. **Cement and Concrete Research**, v. 59, p. 73–86, 2014.

LEEMANN, A. et al. ASR prevention - Effect of aluminum and lithium ions on the reaction products. **Cement and Concrete Research**, v. 76, p. 192–201, 2015.

MARAGHECHI, H. Development and assessment of alkali activated recycled glass-based concretes for civil infrastructure. n. August, p. 229, 2014.

MCCOY, W. J.; CALDWELL, A. G. New approach to inhibiting alkali-aggregate expansion. **Journal of the American Concrete Institute**, v. 22, n. 9, p. 693–706, 1951.

MEHTA, P. K.; MONTEIRO, P. J. M. **Concrete: Microstructure, Properties, and Material**. Third Edit ed. New York: McGraw-Hill, 2006.

MERAL, C.; BENMORE, C. J.; MONTEIRO, P. J. M. The study of disorder and nanocrystallinity in C-S-H, supplementary cementitious materials and geopolymers using pair distribution function analysis. **Cement and Concrete Research**, v. 41, n. 7, p. 696–710, 2011.

NOGUCHI, N. et al. Influence of portlandite on Pyrex glass dissolution and the formation of alkali-silica chemical reaction products. **Journal of the American Ceramic Society**, v. 101, n. 10, p. 4549–4559, 2018.

PEREIRA, M. A.; VASCONCELOS, D. C. L.; VASCONCELOS, W. L. Synthetic Aluminosilicates for Geopolymer Production. **Materials Research**, v. 22, n. 2, 2019.

POOLE, A.; SIMS, I. **Alkali-Aggregate Reaction in Concrete**. London: CRC Press, 2017.

POUHET, R.; CYR, M. Alkali-silica reaction in metakaolin-based geopolymer mortar. **Materials and Structures/Materiaux et Constructions**, v. 48, n. 3, p. 571–583, 2014.

PRADO, R. J. et al. Structural characterization of alkali-silica reaction gel: An x-ray absorption fine structure study. **Cement and Concrete Research**, v. 123, n. May, 2019.

PROVIS, J. L. Activating solution chemistry for geopolymers. In: PROVIS, J. L.; VAN DEVENTER, J. S. J. (Eds.). **Geopolymers Structure, processing, properties and industrial applications**. Melbourne: CRC Press, 2009. p. 50–71.

PROVIS, J. L. Alkali-activated materials. **Cement and Concrete Research**, v. 114, n. 1, p. 40–48, 2017.

PROVIS, J. L.; LUKEY, G. C.; VAN DEVENTER, J. S. J. Do geopolymers actually contain nanocrystalline zeolites? a reexamination of existing results. **Chemistry of Materials**, v. 17, n. 12, p. 3075–3085, 2005.

PROVIS, J. L.; VAN DEVENTER, J. S. J. **Geopolymers Structure, processing,**

**properties and industrial applications.** Cambridge: CRC Press, 2009.

PROVIS, J. L.; YONG, S. L.; DUXSON, P. Nanostructure/microstructure of metakaolin geopolymers. In: **Geopolymers Structure, processing, properties and industrial applications.** Cam: CRC Press, 2009. p. 72–88.

RAJABIPOUR, F. et al. Alkali-silica reaction: Current understanding of the reaction mechanisms and the knowledge gaps. **Cement and Concrete Research**, v. 76, p. 130–146, 2015.

RHODES, C. J. Zeolites: Physical aspects and environmental applications. **Annual Reports on the Progress of Chemistry - Section C**, v. 103, p. 287–325, 2007.

RICHARDSON, I. G. The calcium silicate hydrates. **Cement and Concrete Research**, v. 38, n. 2, p. 137–158, 2008.

RIVARD, P. et al. Monitoring of an hydraulic structure affected by ASR: A case study. **Cement and Concrete Research**, v. 40, n. 4, p. 676–680, 2010.

SAHA, A. K. et al. The ASR mechanism of reactive aggregates in concrete and its mitigation by fly ash: A critical review. **Construction and Building Materials**, v. 171, p. 743–758, 2018.

SHAFATIAN, S. M. H. et al. How does fly ash mitigate alkali-silica reaction (ASR) in accelerated mortar bar test (ASTM C1567)? **Cement and Concrete Composites**, v. 37, n. 1, p. 143–153, 2013.

SHI, Z. et al. Synthesis, characterization, and water uptake property of alkali-silica reaction products. **Cement and Concrete Research**, v. 121, n. March, p. 58–71, 2019.

SHI, Z.; LOTHENBACH, B. The combined effect of potassium, sodium and calcium on the formation of alkali-silica reaction products. **Cement and Concrete Research**, v. 127, n. September 2019, p. 105914, 2020.

STANTON, T. E. **Expansion of concrete through reaction between cement and aggregate.** Proceeding American Society of Civil Engineering. **Anais...**1940

STRUBLE; DIAMOND, S. Swelling properties of synthetic alkali silica gels. **Journal of the American ceramic society**, v. 64, n. 11, p. 652–655, 1981.

SZELES, T. et al. Mitigation of Alkali–Silica Reaction by Hydrated Alumina. **Transportation Research Record: Journal of the Transportation Research Board**, v. 2629, n. 2629, p. 15–23, 2017.

TAYLOR, H. F. W. **Cement Chemistry.** London: Academic Press, 1990.

THOMAS, M. The effect of supplementary cementing materials on alkali-silica reaction: A review. **Cement and Concrete Research**, v. 41, n. 12, p. 1224–1231, 2011.

TIECHER, F. et al. Relationship between degree of deformation in quartz and silica dissolution for the development of alkali-silica reaction in concrete. **Materials**, v. 10, n. 9, 2017.

TREMBLAY, C. et al. Experimental investigation of the mechanisms by which  $\text{LiNO}_3$  is effective against ASR. **Cement and Concrete Research**, v. 40, n. 4, p. 583–597, 2010.

URHAN, S. Alkali silica and pozzolanic reactions in concrete. Part 1: Observations on expanded perlite aggregate concretes Interpretation of published results and an hypothesis concerning the mechanism. **Cement and Concrete Research**, v. 17, n. c, p. 141–152, 1987.

VAN DEVENTER, J. S. J. et al. Reaction mechanisms in the geopolymeric conversion of inorganic waste to useful products. **Journal of Hazardous Materials**, v. 139, n. 3, p. 506–513, 2007.

WALKLEY, B. et al. Phase evolution of  $\text{Na}_2\text{O}-\text{Al}_2\text{O}_3-\text{SiO}_2-\text{H}_2\text{O}$  gels in synthetic aluminosilicate binders. **Dalton Transactions**, v. 45, n. 13, p. 5521–5535, 2016a.

WALKLEY, B. et al. Phase evolution of C-(N)-A-S-H/N-A-S-H gel blends investigated via alkali-activation of synthetic calcium aluminosilicate precursors. **Cement and Concrete Research**, v. 89, p. 120–135, 2016b.

WATERFIELD, C. G.; STAVELEY, L. A. K. Thermodynamic investigation of disorder in the hydrates of disodium hydrogen phosphate. **Transactions of the Faraday Society**, v. 63, p. 2349–2356, 1967.

WEST, A. R. **Solid state chemistry and its applications**. [s.l: s.n.].

YANG, L. **Materials Characterisation: Introduction to Microscopic and Spectroscopic Methods**. [s.l: s.n.].

YOUSUF, M. et al. An FTIR and XPS investigations of the effects of carbonation on the solidification/stabilization of cement based systems-Portland type V with zinc. **Cement and Concrete Research**, v. 23, n. 4, p. 773–784, 1993.

ZHENG, G. et al. Preparation of geopolymer precursors by sol-gel method and their characterization. **Journal of Materials Science**, v. 44, n. 15, p. 3991–3996, 2009.



# APPENDIX I – EDS SPOT ANALYSIS RESULT

Sample 1					
Spot	C	O	Na	Al	Si
1	20,12	49,58	9,01	7,67	13,62
2	20,29	49,26	7,87	10,60	11,97
3	22,24	46,98	10,64	5,69	14,45
4	20,87	46,98	8,46	8,22	15,47
5	23,36	49,72	9,71	5,47	11,75
6	20,39	49,28	10,62	5,02	14,70
7	18,80	53,64	8,86	6,87	11,83
8	19,99	49,42	9,03	10,34	11,21
9	20,70	48,99	10,61	3,83	15,86
10	13,95	54,41	14,40	5,68	11,55
11	24,27	48,30	9,45	5,26	12,73
12	20,07	50,48	9,08	6,74	13,64
13	20,12	47,90	7,21	11,93	12,84
14	20,37	49,23	7,26	10,42	12,73
15	20,45	49,71	7,30	10,96	11,58
16	19,40	50,34	8,02	8,81	13,43
17	21,29	47,01	7,83	9,90	13,97
18	25,32	43,98	9,26	9,89	11,55
19	21,12	47,56	7,98	9,35	13,99
20	19,98	49,08	7,68	9,54	13,72
21	20,45	48,07	10,57	8,95	11,96
22	21,04	47,67	10,96	7,32	13,02
23	18,96	52,25	7,87	8,24	12,68
24	21,93	46,27	10,73	9,17	11,90
25	22,09	45,01	10,98	8,42	13,51
26	21,09	49,89	14,15	5,00	9,88
27	22,02	44,74	17,37	4,04	11,84
28	21,99	46,37	8,35	8,52	14,77
29	21,85	47,05	8,00	7,87	15,23
30	19,62	48,80	6,87	10,32	14,39
31	19,03	49,92	10,38	5,66	15,01
32	20,78	47,19	10,97	4,42	16,63
33	19,49	48,94	10,47	6,71	14,38
34	19,56	50,48	9,66	6,27	14,02
35	19,45	51,27	6,65	11,82	10,81
36	24,09	50,04	9,50	4,17	12,20
37	17,89	52,54	8,78	11,62	9,17
38	23,82	46,80	9,93	4,57	14,88
39	20,25	48,02	12,04	2,59	17,11
40	21,90	46,22	9,36	7,36	15,16
41	18,61	47,94	9,29	7,78	16,38
42	19,93	48,58	7,58	8,13	15,78
43	20,85	48,13	7,27	7,69	16,06
44	24,28	43,91	7,65	6,80	17,36
45	18,79	50,68	8,34	6,61	15,57
46	18,00	50,67	8,79	7,48	15,06
47	20,02	48,32	8,38	7,60	15,67
48	20,62	48,80	9,82	6,18	14,58
49	18,47	51,31	8,46	6,88	14,89
50	20,02	47,55	8,24	7,75	16,44

Sample 1					
Spot	C	O	Na	Al	Si
51	21,60	46,92	9,19	6,95	15,35
52	17,54	53,64	7,07	11,26	10,49
53	23,07	48,46	7,24	7,48	13,76
54	18,10	48,30	18,24	3,79	11,57
55	19,02	50,50	10,73	6,70	13,05
56	19,86	49,41	8,66	6,37	15,70
57	21,46	47,62	10,21	5,95	14,75
58	24,50	40,14	21,10	1,68	12,58
59	20,56	47,05	16,00	2,91	13,47
60	24,07	43,31	18,12	1,06	13,43
61	21,28	46,22	21,18	3,16	8,17
62	20,32	46,97	16,75	5,90	10,07
63	18,40	48,51	17,10	5,18	10,81
64	14,26	53,82	13,32	4,52	14,07
65	18,85	48,34	13,65	7,62	11,54
66	17,77	50,65	10,98	1,16	19,44
67	17,53	50,89	11,60	1,17	18,82
68	16,82	51,71	11,31	1,02	19,14
69	17,45	50,99	11,20	1,08	19,27
70	16,63	51,68	11,44	1,62	18,63
71	17,59	51,28	11,44	1,10	18,59
72	18,31	51,35	10,54	2,95	16,86
73	16,18	51,99	11,51	0,99	19,34
74	16,14	52,44	11,28	1,07	19,07
75	17,48	50,88	11,39	0,99	19,26
76	16,01	51,99	10,65	1,24	20,11
77	17,86	50,61	11,15	1,35	19,04
78	17,82	50,65	10,50	1,06	19,98
79	20,71	47,16	17,07	0,90	14,16
80	18,64	46,65	16,33	1,03	17,34
81	19,42	46,68	15,18	2,03	16,69
82	20,80	45,11	11,84	1,42	20,83
83	27,45	42,69	12,83	1,45	15,57
84	21,17	46,69	14,07	1,45	16,62
85	19,76	46,98	16,69	1,11	15,46
86	19,44	47,54	15,84	2,19	14,99
87	19,93	46,33	17,36	1,07	15,31
88	21,91	43,57	16,77	1,15	16,60
89	20,50	46,35	15,78	1,31	16,06
90	20,67	47,52	15,56	1,50	14,75
91	23,70	44,46	13,22	1,85	16,76
92	26,84	41,41	13,80	1,75	16,21
93	23,70	42,91	12,92	2,09	18,39
94	20,78	47,42	11,34	1,89	18,57
95	24,30	43,14	12,35	2,65	17,56
96	23,73	43,79	9,67	2,74	20,07
97	22,24	46,30	10,12	2,99	18,35
98	27,14	41,65	7,58	1,47	22,16
99	20,52	49,40	10,49	1,59	18,01
100	24,52	42,87	10,83	1,59	20,19

Sample 1					
Spot	C	O	Na	Al	Si
101	26,55	40,71	9,64	1,92	21,17
102	25,71	41,81	10,67	1,51	20,29
103	20,86	47,06	9,90	3,27	18,91
104	20,04	51,04	11,18	1,10	16,64
105	22,99	45,69	9,97	1,04	20,31
106	20,41	48,34	11,77	1,04	18,43
107	21,58	48,50	11,58	1,41	16,93
108	23,73	43,90	10,95	1,45	19,96
109	24,40	44,10	11,87	1,22	18,40
110	24,50	43,19	11,43	1,69	19,19
111	24,93	41,79	10,20	1,79	21,29
112	26,50	33,35	2,36	36,40	1,38
113	33,23	30,44	0,86	34,83	0,65
114	43,39	38,21	8,78	1,06	8,56

Sample 2					
Spot	C	O	Na	Al	Si
1	29,43	36,91	6,54	10,94	16,17
2	30,98	38,27	6,16	9,89	14,70
3	28,79	39,79	8,21	6,87	16,35
4	26,04	47,24	7,75	5,78	13,19
5	35,60	36,51	9,28	3,23	15,39
6	23,84	47,53	10,78	4,98	12,87
7	32,99	36,63	7,37	9,93	13,08
8	27,04	42,02	8,86	7,08	15,00
9	25,75	42,16	5,05	14,78	12,26
10	27,82	38,94	8,47	7,36	17,41
11	26,80	45,75	11,20	3,58	12,67
12	28,39	40,43	12,67	4,58	13,92
13	27,46	39,51	9,02	7,03	16,97
14	18,81	51,20	9,69	2,71	17,60
15	19,13	51,92	10,14	2,84	15,97
16	26,15	43,93	7,93	4,15	17,84
17	25,45	43,52	7,56	6,29	17,18
18	23,15	46,18	8,73	6,37	15,58
19	23,62	49,55	9,86	2,29	14,68
20	20,71	54,28	9,23	2,46	13,32
21	19,66	54,52	9,31	2,83	13,68
22	39,89	40,64	7,01	1,65	10,81
23	22,45	52,29	9,12	2,46	13,67
24	20,54	53,19	9,99	2,05	14,22
25	23,28	49,45	9,26	3,41	14,60
26	20,02	53,96	8,43	3,26	14,33
27	22,70	47,23	9,76	3,33	16,99
28	22,29	49,83	9,66	2,20	16,02
29	20,39	50,13	9,10	4,07	16,32
30	25,60	41,53	7,56	7,75	17,55
31	25,52	42,76	6,52	10,07	15,15
32	24,38	44,52	7,16	7,74	16,20
33	25,95	41,68	8,32	5,73	18,32

Sample 2					
Spot	C	O	Na	Al	Si
34	29,04	36,35	8,75	3,47	22,39
35	24,57	44,49	6,18	10,64	14,13
36	23,63	45,22	6,52	10,27	14,36
37	25,72	42,12	10,18	8,06	13,91
38	27,31	39,29	16,98	4,97	11,46
39	25,01	42,59	6,98	10,74	14,68
40	26,21	41,55	7,73	7,16	17,35
41	25,75	42,48	7,82	8,37	15,59
42	27,75	39,68	13,23	6,70	12,64
43	29,03	37,29	17,11	5,35	11,21
44	33,16	37,71	9,56	7,99	11,58
45	33,19	38,13	7,72	7,85	13,11
46	30,18	37,96	7,26	8,57	16,03
47	30,67	39,38	10,64	6,82	12,49
48	29,44	38,49	6,76	9,67	15,63
49	27,91	43,50	5,81	4,30	18,48
50	20,30	54,66	10,18	0,79	14,07
51	20,05	54,10	9,82	1,06	14,97
52	17,99	55,26	11,10	0,73	14,92
53	19,61	54,74	10,56	0,77	14,32
54	31,88	41,77	4,32	3,63	18,41
55	30,60	40,13	6,20	2,51	20,55
56	31,96	40,66	3,84	10,47	13,06
57	35,71	33,24	6,12	6,32	18,61
58	32,90	34,91	6,14	4,54	21,51
59	31,08	38,41	5,92	3,73	20,86
60	25,69	44,51	6,82	2,99	20,00
61	25,84	47,62	4,73	3,50	18,30
62	25,57	47,27	4,64	4,04	18,48
63	24,12	46,76	7,59	2,79	18,74
64	27,06	45,22	5,93	5,47	16,32
65	28,32	43,96	6,71	2,11	18,91
66	27,71	45,32	6,99	2,12	17,86
67	27,59	43,45	6,83	2,67	19,47
68	28,68	43,26	5,09	4,51	18,47
69	29,36	38,00	7,09	10,18	15,37
70	31,19	37,30	5,84	12,87	12,80
71	30,41	38,29	7,43	10,65	13,21
72	27,37	39,93	12,47	6,68	13,55
73	28,11	40,59	7,03	8,29	15,97
74	27,37	38,96	6,74	9,78	17,16
75	25,70	41,78	6,73	9,93	15,86
76	26,40	41,16	6,50	9,51	16,43
77	26,13	40,80	6,74	10,51	15,82
78	28,15	40,10	7,84	5,80	18,10
79	27,21	38,53	8,32	5,54	20,40
80	25,00	43,47	4,81	14,95	11,76
81	27,41	40,10	12,40	10,57	9,52
82	26,25	43,14	5,78	8,88	15,95
83	24,70	43,25	5,94	12,59	13,52

Sample 2					
Spot	C	O	Na	Al	Si
84	27,73	38,65	11,80	7,03	14,80
85	27,06	43,28	18,53	4,36	6,78
86	28,23	41,00	6,55	8,61	15,61
87	27,15	40,01	6,78	8,85	17,21
88	25,22	42,27	7,37	8,24	16,90
89	23,74	44,44	7,44	6,69	17,69
90	22,93	45,66	7,98	4,76	18,67
91	32,81	36,43	5,99	6,59	18,17
92	34,73	34,98	4,27	8,24	17,78
93	31,57	36,56	5,61	8,03	18,23
94	30,34	37,23	7,02	5,75	19,67
95	26,48	42,31	6,47	5,60	19,14
96	19,77	49,78	6,93	7,14	16,38
97	31,26	36,87	6,86	6,23	18,78
98	26,47	41,63	7,67	5,01	19,22
99	23,60	45,88	6,94	6,95	16,62
100	23,16	46,11	8,77	5,20	16,75
101	18,30	49,84	6,84	8,03	16,99
102	27,50	42,16	6,92	5,54	17,88
103	31,00	36,05	6,72	6,45	19,78
104	23,60	46,03	8,40	4,16	17,81
105	24,68	43,33	7,64	6,92	17,43
106	32,39	35,73	7,03	4,85	20,01
107	22,52	46,74	8,87	4,87	17,00
108	34,17	32,90	9,56	7,04	16,33
109	31,77	37,03	7,61	8,19	15,40
110	30,22	40,63	16,01	5,69	7,46
111	36,33	31,15	10,28	9,65	12,59
112	34,12	33,93	7,05	9,99	14,92
113	29,07	40,69	18,23	4,49	7,51
114	26,78	42,32	7,95	7,76	15,20
115	24,94	43,17	6,49	10,05	15,35
116	25,33	41,12	6,58	11,29	15,67
117	25,41	43,29	8,30	8,87	14,12
118	25,35	42,67	9,32	7,02	15,63
119	25,77	42,32	6,10	10,16	15,65
120	27,13	41,74	13,52	6,60	11,01
121	26,08	40,38	11,01	8,37	14,17
122	30,29	36,40	14,76	5,98	12,58
123	23,54	45,33	6,66	10,09	14,38
124	23,90	45,31	7,50	9,60	13,69
125	25,30	42,75	6,93	8,42	16,60
126	23,89	44,37	6,84	10,21	14,70
127	24,65	42,34	8,19	11,22	13,61
128	26,89	37,45	18,40	6,60	10,67
129	25,85	43,06	5,89	10,44	14,76
130	30,91	30,04	5,48	0,37	33,20
131	34,89	42,06	8,97	0,36	13,73
132	23,66	45,39	9,07	0,58	21,30
133	24,49	43,78	8,84	0,76	22,13

Sample 2					
Spot	C	O	Na	Al	Si
134	23,14	44,97	9,38	0,58	21,93
135	21,44	46,77	9,72	0,54	21,53
136	21,21	46,53	10,30	0,59	21,38
137	20,32	48,27	9,63	0,56	21,22
138	21,37	47,12	9,39	0,55	21,57
139	21,67	46,29	9,35	0,53	22,15
140	21,45	46,72	9,44	0,56	21,82
141	22,57	46,80	9,44	0,50	20,69
142	21,37	46,77	9,80	0,56	21,49
143	22,04	47,06	9,18	0,64	21,09
144	23,00	46,41	9,66	0,76	20,17
145	21,54	47,18	9,37	0,57	21,34
146	24,09	45,36	9,01	0,71	20,83
147	22,52	45,74	9,17	0,56	22,02
148	25,51	43,54	8,70	0,72	21,53
149	23,03	45,86	9,08	0,53	21,49
150	23,11	45,21	8,93	0,59	22,17
151	24,92	41,29	13,22	0,42	20,15
152	26,63	40,71	12,28	0,44	19,93
153	27,13	39,80	11,72	0,43	20,92
154	26,77	41,55	9,78	1,54	20,37
155	26,61	39,80	12,18	0,58	20,83
156	24,91	43,37	12,39	0,44	18,90
157	25,68	41,19	13,02	0,45	19,65
158	26,07	40,14	13,34	0,46	19,99
159	27,13	37,82	17,77	0,38	16,89
160	27,34	37,73	17,38	0,37	17,18
161	23,82	44,31	10,92	0,49	20,47
162	26,41	40,85	11,44	0,48	20,82

Sample 3					
Spot	C	O	Na	Al	Si
1	19,15	53,09	10,62	0,52	16,62
2	21,51	50,12	9,36	0,59	18,41
3	19,29	51,70	8,61	0,66	19,74
4	20,43	51,53	9,09	0,59	18,36
5	19,46	52,17	8,84	0,63	18,90
6	22,91	48,00	9,74	0,64	18,70
7	19,89	52,98	9,38	0,55	17,20
8	19,22	51,18	9,56	0,58	19,46
9	21,92	49,42	11,22	0,50	16,93
10	20,27	50,77	9,11	0,58	19,26
11	23,20	47,03	8,74	0,59	20,44
12	20,17	51,55	9,99	0,61	17,68
13	26,16	48,65	9,37	0,50	15,32
14	18,99	53,09	9,99	0,56	17,37
15	18,52	54,19	10,49	0,58	16,22
16	19,76	52,91	9,68	0,56	17,09
17	20,21	52,84	8,84	0,56	17,55
18	19,15	53,56	9,30	0,67	17,32

Sample 3					
Spot	C	O	Na	Al	Si
19	21,24	51,91	9,65	0,66	16,54
20	23,79	50,55	8,94	0,59	16,14
21	18,31	54,36	9,04	0,60	17,69
22	18,04	53,61	10,02	0,60	17,72
23	16,94	54,21	9,74	0,69	18,42
24	18,67	54,41	9,99	0,58	16,36
25	13,42	60,50	10,48	0,52	15,09
26	14,03	58,25	10,73	0,60	16,39
27	20,35	50,41	7,78	6,52	14,94
28	21,28	49,88	10,07	6,20	12,58
29	21,44	49,57	6,64	7,95	14,40
30	22,26	49,10	8,57	3,42	16,64
31	20,93	49,67	9,33	3,68	16,40
32	20,35	51,12	7,04	6,90	14,59
33	24,84	47,32	11,92	5,84	10,08
34	22,10	48,76	9,70	5,34	14,10
35	24,73	47,74	8,88	5,47	13,18
36	20,28	50,82	6,62	5,84	16,44
37	24,51	46,72	10,96	5,13	12,68
38	22,71	49,05	7,31	6,31	14,63
39	27,52	47,13	7,87	5,12	12,37
40	22,27	48,10	8,23	5,54	15,86
41	22,78	49,26	8,10	6,41	13,45
42	21,17	47,80	18,44	3,10	9,49
43	21,55	48,75	11,28	6,01	12,41
44	21,05	49,01	10,25	4,20	15,50
45	21,79	46,83	17,07	2,00	12,32
46	24,21	47,28	11,06	5,27	12,17
47	22,33	48,62	10,21	5,03	13,81
48	21,05	48,28	14,03	3,84	12,79
49	20,69	48,60	13,75	4,77	12,18
50	20,39	49,97	13,97	3,88	11,80
51	22,38	46,30	14,43	4,90	11,98
52	21,06	49,34	12,77	5,68	11,15
53	22,16	47,66	16,11	3,72	10,35
54	23,05	44,62	12,22	3,40	16,71
55	23,78	47,92	14,25	2,56	11,49
56	23,17	47,65	13,57	3,35	12,25
57	18,86	52,59	10,13	0,56	17,86
58	18,67	53,16	10,86	0,55	16,75
59	18,54	53,17	9,93	0,56	17,80
60	18,88	52,21	10,43	0,56	17,92
61	20,12	52,08	9,83	0,54	17,43
62	18,21	53,42	10,53	0,65	17,19
63	19,32	52,39	10,09	0,51	17,69
64	16,91	55,14	11,34	0,54	16,07
65	17,23	54,00	10,70	0,68	17,40
66	34,79	46,56	7,78	1,10	9,20
67	18,12	53,24	10,56	0,63	17,45
68	18,98	50,96	22,07	0,00	7,99

Sample 3					
Spot	C	O	Na	Al	Si
69	18,50	54,17	10,48	0,54	16,31
70	18,15	53,24	11,09	0,52	16,99
71	19,01	53,26	10,23	0,54	16,96
72	19,56	52,14	10,33	0,56	17,41
73	17,79	52,89	11,04	0,56	17,72
74	18,07	53,18	10,44	0,56	17,75
75	21,55	51,18	11,30	0,56	15,40
76	22,74	51,33	11,13	0,44	14,36
77	21,24	48,83	10,36	0,50	19,06
78	20,42	49,83	10,29	0,58	18,89
79	20,69	49,56	10,38	0,56	18,81
80	23,71	49,51	12,47	0,49	13,82
81	20,46	51,66	9,44	0,56	17,88
82	20,99	50,53	10,15	0,59	17,74
83	24,02	48,76	9,19	0,57	17,47
84	21,70	49,97	10,63	0,57	17,13
85	21,08	49,00	9,75	0,61	19,55
86	21,11	48,25	10,86	0,56	19,22
87	22,85	48,16	10,05	0,56	18,38
88	15,49	55,04	11,21	0,56	17,70
89	25,85	46,53	12,06	0,44	15,12
90	22,12	48,02	10,73	0,59	18,54
91	21,64	49,31	8,68	0,61	19,75
92	21,53	48,36	11,19	0,50	18,43
93	20,05	51,59	9,79	0,54	18,04
94	19,43	52,19	9,53	0,57	18,28
95	25,09	47,54	11,35	0,47	15,55
96	7,91	64,70	9,80	0,64	16,95
97	22,57	49,47	10,26	0,48	17,22
98	20,81	51,09	9,88	0,58	17,65
99	24,03	46,46	11,11	0,70	17,70
100	21,61	49,39	10,46	0,59	17,94
101	25,52	47,81	9,95	0,57	16,14
102	24,27	48,17	9,32	0,45	17,78
103	26,63	44,80	9,14	0,51	18,92
104	19,96	51,20	9,53	0,63	18,69
105	21,95	49,04	8,84	4,81	15,37
106	22,68	48,64	8,74	4,73	15,21
107	20,23	50,60	9,16	4,94	15,07
108	20,22	50,98	8,79	3,79	16,22
109	18,82	51,11	11,10	0,51	18,46
110	21,37	49,02	11,07	0,57	17,98
111	22,31	48,48	10,75	0,50	17,96
112	20,60	49,91	10,09	0,51	18,89
113	21,51	49,25	11,08	0,56	17,60
114	20,16	49,49	10,80	0,86	18,69
115	20,92	48,22	11,63	3,44	15,79
116	16,60	55,83	10,79	1,33	15,45
117	20,65	51,08	10,95	0,54	16,78
118	19,93	50,63	11,04	0,57	17,83

Sample 3					
Spot	C	O	Na	Al	Si
119	20,39	51,05	12,16	0,52	15,87
120	23,15	42,60	31,69	0,00	2,56
121	24,20	46,94	17,26	2,13	9,48
122	23,76	45,43	18,80	1,82	10,19
123	22,43	46,41	19,74	0,90	10,53
124	22,42	47,30	17,15	3,30	9,53
125	23,79	45,18	18,72	1,70	10,60
126	22,18	45,96	20,37	1,58	9,91
127	22,25	47,59	18,05	2,92	9,19
128	22,81	46,34	19,71	1,67	9,46
129	23,01	46,71	18,74	2,53	9,03
130	22,18	47,87	8,37	6,60	14,97
131	22,61	46,50	9,10	6,26	15,53
132	22,63	47,36	10,29	5,64	14,07
133	22,32	48,23	8,33	5,99	15,14
134	20,77	49,76	8,50	6,20	14,76
135	21,85	47,17	9,76	5,91	15,31
136	21,46	48,69	15,67	3,23	10,96
137	21,44	47,19	9,21	5,68	16,48
138	37,34	37,21	12,73	2,59	10,13
139	20,40	48,76	9,93	3,58	17,33
140	22,07	48,72	8,22	6,14	14,85
141	21,13	48,35	9,55	7,04	13,93
142	23,31	47,05	9,81	4,87	14,96
143	22,23	47,36	9,20	5,49	15,72
144	22,62	48,14	8,25	5,91	15,07
145	20,69	50,79	12,30	3,82	12,40

Sample 4					
Spot	C	O	Na	Al	Si
1	30,51	42,62	8,4	0,00	18,47
2	24,46	43,8	9,34	0,00	22,4
3	19,73	49,87	8,96	0,00	21,44
4	25,13	45,31	8,81	0,00	20,75
5	21,82	47,96	10,77	0,00	19,45
6	18,35	50,36	9,06	0,00	22,23
7	20,02	50,79	11,03	0,00	18,16
8	16,29	51,78	9,64	0,00	22,29
9	18,34	49,96	9,45	0,00	22,26
10	27,53	46,39	12,14	0,00	13,94
11	18,12	50,67	11,23	0,00	19,97
12	20,22	48,19	14,74	0,00	16,85
13	19,25	48,38	11,29	0,00	21,08
14	16,34	51,87	11,45	0,00	20,34
15	18,56	48,99	9,76	0,00	22,69
16	18,34	49,83	10,03	0,00	21,81
17	20,76	47,68	9,79	0,00	21,77
18	34,47	41,22	8,19	0,00	16,11
19	51,07	33,33	6,55	0,00	9,05
20	40,23	36,2	8,75	0,00	14,82

Sample 4					
Spot	C	O	Na	Al	Si
21	19,34	50,35	8,9	0,00	21,41
22	18,04	51,35	9,99	0,00	20,62
23	26,66	47,64	9,46	0,00	16,24
24	17,33	51,29	10,3	0,00	21,09
25	21,12	49,73	8,75	0,00	20,4
26	21,07	46,06	9,73	0,00	23,14
27	19,83	48,44	9,54	0,00	22,19
28	19,54	48,58	9,55	0,00	22,34
29	17,96	48,6	10,69	0,00	22,75
30	17,54	49,68	10,02	0,00	22,77
31	22,69	46,83	8,02	0,00	22,46
32	19,65	47,81	8,87	0,00	23,68
33	23,14	46,69	9,9	0,00	20,26
34	18,97	49,35	10,61	0,00	21,07
35	20,64	49,37	12,99	0,00	17,01
36	22,11	46,6	10,35	0,00	20,93
37	28,96	43,95	9,69	0,00	17,41
38	45,91	35,44	7,93	0,00	10,73
39	58,23	30,49	4,1	0,00	7,18
40	20,46	48,62	11,26	0,00	19,66
41	19,15	49,7	9,67	0,00	21,48
42	19,31	49,73	9,6	0,00	21,36
43	22,32	45,62	9,33	0,00	22,73
44	20,23	48,01	8,24	0,00	23,52
45	28,49	45,72	8,38	0,00	17,41
46	23,25	46,05	8,86	0,00	21,84
47	21,8	48,46	9,84	0,00	19,9
48	33,59	43,85	8,35	0,00	14,21
49	53,69	32,72	5,06	0,00	8,52
50	49,5	13,46	1,69	0,00	35,35
51	55,8	30,6	6,14	0,00	7,46
52	52,9	31,91	6,77	0,00	8,41
53	53,47	32,04	7,31	0,00	7,17
54	56,07	30,87	5,14	0,00	7,92
55	18,44	49,83	9,59	0,00	22,14
56	19,29	48,36	10,06	0,00	22,28
57	29,61	43,42	9,21	0,00	17,76
58	31,57	43,19	12,15	0,00	13,1
59	21,01	47,11	10,35	0,00	21,54
60	22,69	46,34	10,32	0,00	20,65
61	19,33	48,64	10,84	0,00	21,18
62	26,21	45,73	11,54	0,00	16,51
63	24,64	46,39	11,22	0,00	17,75
64	27,83	45,24	11,23	0,00	15,7
65	24,24	46,17	11,78	0,00	17,8
66	29,04	44,63	10,97	0,00	15,35
67	21,88	47,66	10,52	0,00	19,95
68	32,18	44,35	10,2	0,00	13,26
69	44,39	37,87	9,76	0,00	7,98
70	23,69	47,46	9,01	0,00	19,84

Sample 4					
Spot	C	O	Na	Al	Si
71	20,33	48,13	10,94	0,00	20,6
72	18	49,05	10,64	0,00	22,3
73	16,98	50,01	10,62	0,00	22,39
74	17,4	49,89	10,7	0,00	22,01
75	23,14	47,19	11,64	0,00	18,03
76	17,3	49,74	10,97	0,00	22
77	18,48	48,93	11,07	0,00	21,52
78	25,92	45,87	12,8	0,00	15,41
79	26,87	45,8	12,02	0,00	15,31
80	29,34	44,48	11,59	0,00	14,59
81	27,47	44,41	13,08	0,00	15,04
82	21,03	48,74	12,08	0,00	18,15
83	30,32	43,19	11,92	0,00	14,56
84	17,88	49,35	11,16	0,00	21,61
85	18,22	49,21	10,78	0,00	21,8
86	21,37	47,66	10,51	0,00	20,46
87	20	48,36	10,81	0,00	20,82
88	17,37	49,42	10,81	0,00	22,4
89	21,32	47,92	10,11	0,00	20,64
90	17,74	49,14	10,58	0,00	22,53
91	27,96	44,22	11,03	0,00	16,8
92	25,96	46,31	12,11	0,00	15,62
93	27,19	46,69	12,81	0,00	13,32
94	28,63	45,14	13,1	0,00	13,14
95	25,57	46,14	11,15	0,00	17,14
96	22,55	47,16	10,54	0,00	19,75
97	22,25	47,37	11,94	0,00	18,44
98	26,03	45,68	12	0,00	16,29
99	22,06	46,27	11,07	0,00	20,6
100	19,85	47,9	11,21	0,00	21,03
101	25,01	46,03	10,51	0,00	18,44
102	22,1	46,58	10,5	0,00	20,82
103	26,3	46,05	10,49	0,00	17,16
104	29,77	44,78	13,37	0,00	12,07
105	28,05	45	10,61	0,00	16,33
106	25,08	47,72	11,07	0,00	16,13
107	23,68	48,96	10,9	0,00	16,45
108	22,07	49,16	11,47	0,00	17,3
109	24,23	49,87	8,87	0,00	17,02
110	46,2	38,38	6,63	0,00	8,78
111	18,37	51,19	9,93	0,00	20,51
112	18,79	50,61	10,38	0,00	20,22
113	18,74	51,06	9,65	0,00	20,55
114	20,01	48,41	10,96	0,00	20,62
115	18,12	48,86	11,31	0,00	21,72
116	20,5	46,09	10,1	0,00	23,3
117	17,12	50,64	11,07	0,00	21,17
118	18,7	47,83	11,53	0,00	21,94
119	18,8	48,51	10,94	0,00	21,75
120	17,88	51,89	10,57	0,00	19,66

Sample 4					
Spot	C	O	Na	Al	Si
120	17,88	51,89	10,57	0,00	19,66
121	20,24	50,42	10,1	0,00	19,24
122	22,04	49,67	10,14	0,00	18,15
123	19,6	49,92	10,3	0,00	20,18
124	20,31	51,02	9,98	0,00	18,69
125	28,19	44,32	12,52	0,00	14,98
126	18,22	49,12	10,74	0,00	21,92
127	20,97	47,28	10,22	0,00	21,53
128	20,18	47,98	10,75	0,00	21,09
129	19,52	49,51	10,1	0,00	20,88
130	18,89	49,49	10,67	0,00	20,95
131	17,46	49,99	10,53	0,00	22,02
132	19,24	48,83	11,58	0,00	20,35
133	25,23	44,54	11,01	0,00	19,22
134	19,22	48,85	11,02	0,00	20,9
135	22,65	46,71	11,53	0,00	19,11
136	19,04	48,88	11,07	0,00	21,02
137	19,79	48,02	11	0,00	21,19
138	23,82	44,62	9,34	0,00	22,22
139	27,97	42,95	8,88	0,00	20,2
140	23,49	47,02	9,86	0,00	19,64
141	25,62	45,82	9,99	0,00	18,58
142	21,62	49,92	9,8	0,00	18,66
143	44,4	32,06	3,08	0,00	20,45
144	28,68	40,05	7,02	0,00	24,26
145	53,14	30,65	7,12	0,00	9,08
146	61,14	26,98	4,59	0,00	7,28
147	33,56	42,57	7,87	0,00	16
148	38,59	32,17	6,36	0,00	22,88
149	36,41	33,96	5,25	0,00	24,37

Sample 5					
Spot	C	O	Na	Al	Si
1	22,00	45,59	8,73	7,05	16,63
2	19,23	46,91	11,29	8,24	14,34
3	23,63	44,37	15,85	6,09	10,07
4	18,60	50,23	12,92	6,86	11,39
5	29,18	47,07	11,17	4,97	7,61
6	61,77	26,94	6,17	1,69	3,44
7	33,51	40,23	9,14	6,25	10,87
8	32,65	42,69	13,88	3,97	6,81
9	44,97	35,53	9,32	3,56	6,63
10	31,92	42,58	8,76	4,82	11,92
11	22,87	47,56	7,49	8,44	13,65
12	22,94	44,77	10,87	4,64	16,77
13	25,20	44,62	11,72	5,78	12,69
14	22,26	47,19	12,41	5,47	12,67
15	69,79	22,31	5,25	0,86	1,79
16	72,70	21,34	3,93	0,70	1,33
17	29,26	42,87	7,90	7,21	12,77

Sample 5					
Spot	C	O	Na	Al	Si
18	33,67	42,48	8,47	4,34	11,03
19	23,84	45,19	9,21	8,14	13,63
20	27,37	42,37	14,61	4,97	10,68
21	27,52	42,11	15,18	5,96	9,23
22	20,07	50,17	10,01	8,18	11,59
23	24,36	42,84	26,50	2,52	3,78
24	26,59	43,73	8,06	6,21	15,40
25	21,31	46,91	9,04	6,71	16,03
26	78,62	17,62	2,44	0,33	1,00
27	47,20	34,77	11,44	2,41	4,19
28	26,15	41,76	16,42	5,08	10,59
29	24,31	44,37	11,87	5,21	14,24
30	22,17	47,26	13,94	5,62	11,00
31	22,38	50,24	10,03	4,53	12,82
32	24,25	46,35	11,81	6,15	11,44
33	26,14	43,96	8,76	7,02	14,11
34	26,26	43,96	7,01	7,25	15,51
35	23,49	44,19	12,31	6,75	13,25
36	64,96	22,71	9,28	1,05	2,01
37	65,26	26,26	4,63	1,43	2,43
38	23,88	42,30	9,11	7,61	17,10
39	49,98	28,86	10,16	3,83	7,17
40	50,77	31,13	4,48	4,94	8,68
41	20,62	47,41	7,09	6,58	18,30
42	24,74	45,82	6,50	7,74	15,20
43	20,84	49,76	9,25	8,44	11,70
44	29,28	40,76	6,54	5,61	17,81
45	21,74	45,35	6,23	7,29	19,40
46	25,81	42,98	7,57	6,82	16,81
47	28,37	39,78	19,86	3,47	8,52
48	32,10	38,55	15,77	5,44	8,14
49	21,73	44,88	6,03	7,65	19,72
50	22,91	43,80	8,14	8,38	16,77
51	24,67	41,59	16,03	3,30	14,41
52	21,71	47,94	9,96	8,26	12,13
53	20,70	47,07	10,97	8,71	12,55
54	21,90	45,29	8,07	10,07	14,67
55	44,36	35,79	10,61	3,67	5,57
56	25,12	48,24	7,90	7,83	10,91
57	22,62	45,47	11,55	6,52	13,84
58	23,89	40,97	21,39	5,72	8,03
59	20,42	45,22	5,60	6,00	22,78
60	70,14	22,81	2,81	1,63	2,62
61	22,67	48,83	9,28	7,91	11,32
62	64,06	27,49	5,35	1,27	1,82
63	20,84	43,96	6,16	10,06	18,98
64	24,02	42,76	7,37	7,64	18,21
65	30,68	40,86	10,81	5,82	11,83
66	22,65	48,26	9,61	7,48	11,99
67	21,95	43,18	8,06	8,90	17,91

Sample 5					
Spot	C	O	Na	Al	Si
68	20,85	45,23	7,69	8,41	17,82
69	20,21	45,66	6,81	7,66	19,67
70	20,78	45,08	5,42	4,62	24,10
71	23,90	41,79	19,54	5,11	9,67
72	20,90	46,23	7,27	8,65	16,96
73	27,39	40,13	26,92	2,17	3,40
74	41,31	35,71	11,38	4,46	7,14
75	41,45	33,68	14,43	3,51	6,93
76	46,30	32,79	11,31	3,43	6,16
77	39,90	37,91	8,19	4,99	9,02
78	39,23	37,35	8,08	5,63	9,70
79	44,57	32,42	14,66	3,02	5,33
80	25,01	45,31	6,60	6,14	16,94
81	23,96	44,34	14,59	7,20	9,92
82	28,30	46,60	8,06	6,38	10,65
83	23,53	50,37	8,10	7,42	10,57
84	20,84	51,50	8,40	7,90	11,37
85	19,05	48,75	10,27	9,46	12,47
86	23,41	44,79	15,22	3,18	13,40
87	24,00	43,05	8,21	3,57	21,17
88	40,09	40,98	7,35	4,51	7,07
89	21,37	49,97	9,70	7,76	11,20
90	20,85	45,24	7,56	5,97	20,37
91	30,08	42,46	7,63	6,76	13,07
92	28,22	42,62	11,60	5,57	11,99
93	23,36	45,56	6,54	7,02	17,52
94	38,72	37,61	13,92	3,57	6,18

Sample 6					
Spot	C	O	Na	Al	Si
1	21,21	48,08	9,19	3,81	17,71
2	21,64	46,08	9,01	3,56	19,71
3	27,04	41,61	11,13	4,01	16,22
4	26,09	40,91	7,72	4,77	20,52
5	23,32	44,61	9,17	4,13	18,78
6	23,18	45,89	8,32	3,91	18,71
7	22,86	49,02	13,89	2,37	11,86
8	28,45	48,78	8,13	2,22	12,41
9	20,39	48,42	8,39	4,60	18,20
10	26,12	46,96	8,46	3,71	14,76
11	50,69	35,96	5,98	1,52	5,85
12	20,99	48,45	8,31	4,90	17,35
13	21,46	46,16	8,13	5,23	19,02
14	21,40	45,75	8,34	5,73	18,79
15	21,26	48,08	8,92	4,64	17,09
16	22,71	43,61	8,94	5,44	19,30
17	22,13	46,50	8,76	4,93	17,68
18	21,49	47,31	9,46	4,12	17,62
19	22,73	44,77	9,43	4,48	18,60
20	22,52	45,00	8,16	5,85	18,47

Sample 6					
Spot	C	O	Na	Al	Si
21	25,78	43,95	8,45	4,59	17,23
22	22,62	45,52	9,59	4,59	17,68
23	21,33	47,60	9,65	4,81	16,61
24	21,49	47,18	9,89	4,64	16,80
25	26,31	45,26	9,12	3,87	15,44
26	21,37	45,28	8,51	6,58	18,26
27	21,36	46,28	9,02	3,66	19,68
28	49,72	37,34	5,06	2,32	5,56
29	21,95	45,40	7,15	7,55	17,94
30	20,71	45,67	7,23	7,55	18,84
31	46,10	38,51	4,31	2,92	8,16
32	23,38	40,72	7,40	5,80	22,70
33	22,87	43,00	6,48	5,29	22,36
34	19,14	47,54	7,61	6,96	18,76
35	21,38	46,97	7,71	5,55	18,39
36	25,09	41,92	6,76	5,39	20,83
37	21,97	44,52	6,75	5,50	21,27
38	22,71	45,53	6,99	5,17	19,60
39	30,04	42,43	10,32	3,64	13,58
40	22,18	46,33	7,19	5,34	18,96
41	21,10	45,71	7,33	5,79	20,06
42	23,48	43,72	7,29	5,06	20,46
43	22,28	46,51	9,70	5,92	15,59
44	20,27	46,09	7,52	5,50	20,62
45	21,48	46,32	6,82	5,73	19,64
46	23,80	45,38	7,69	5,70	17,42
47	19,93	48,10	9,54	5,31	17,11
48	26,62	46,90	8,49	3,24	14,75
49	40,47	41,26	6,82	3,02	8,44
50	21,61	46,73	6,10	7,49	18,08
51	24,15	43,77	8,90	5,26	17,92
52	26,14	42,49	7,27	5,27	18,84
53	39,13	35,57	7,93	4,08	13,28
54	28,99	43,23	8,01	3,28	16,50
55	24,83	43,46	7,54	5,12	19,04
56	35,48	34,43	22,80	2,08	5,21
57	34,04	34,99	23,61	1,74	5,61
58	45,69	37,22	8,06	1,81	7,23
59	25,11	43,81	6,11	7,42	17,55
60	24,54	43,42	6,73	5,39	19,92
61	45,55	29,74	15,17	2,90	6,65
62	33,35	38,42	9,85	4,04	14,34
63	25,50	43,44	6,47	5,44	19,16
64	48,37	34,09	6,90	2,90	7,73
65	25,12	43,85	8,07	5,86	17,09
66	23,11	46,31	9,33	3,88	17,38
67	52,81	30,66	5,87	2,13	8,53
68	21,47	47,98	8,43	4,95	17,18
69	21,36	46,81	6,55	7,06	18,21
70	20,05	50,30	8,69	3,05	17,91

Sample 6					
Spot	C	O	Na	Al	Si
71	21,98	45,42	7,82	3,94	20,84
72	47,15	36,31	5,35	3,37	7,82
73	25,83	42,63	6,86	7,04	17,63
74	23,18	44,57	10,36	3,15	18,75
75	21,85	44,08	8,95	6,45	18,68
76	21,48	47,16	7,24	4,73	19,39
77	47,75	38,36	4,24	2,18	7,46
78	23,17	44,99	9,99	4,14	17,71
79	23,72	45,72	6,92	7,77	15,87
80	23,44	44,80	9,68	4,44	17,63
81	21,48	44,66	7,54	6,03	20,30
82	21,49	46,94	7,32	5,96	18,28
83	27,28	44,30	8,46	5,54	14,42
84	21,97	46,48	7,22	5,93	18,39
85	19,45	48,06	7,31	7,38	17,81
86	19,99	46,63	7,69	4,70	21,00
87	19,55	47,69	7,68	6,54	18,55
88	21,32	45,85	9,20	6,49	17,14
89	20,17	47,57	7,70	5,39	19,17
90	22,22	46,66	6,90	6,87	17,34
91	20,68	45,01	7,36	7,30	19,65
92	20,36	47,26	7,54	5,54	19,30
93	21,30	46,19	7,28	6,49	18,74
94	20,13	47,81	9,13	4,58	18,35
95	19,95	46,28	8,36	5,14	20,28
96	24,84	46,10	8,06	4,72	16,28
97	22,28	46,72	7,98	4,72	18,30
98	32,10	41,22	6,46	6,67	13,54
99	22,29	45,54	9,20	4,69	18,27
100	23,45	45,93	11,97	4,17	14,48
101	21,52	48,59	8,17	4,75	16,97
102	21,63	44,27	12,92	3,61	17,56
103	23,46	40,30	33,08	0,00	3,15
104	24,21	44,91	12,04	3,33	15,52
105	21,88	44,59	9,46	5,24	18,84
106	28,52	45,60	8,81	3,65	13,43
107	37,28	33,98	11,06	3,72	13,95
108	26,22	47,50	9,99	3,32	12,97
109	23,90	43,91	8,62	4,71	18,86
110	24,28	44,50	8,11	5,07	18,04
111	25,38	44,51	9,89	4,41	15,82
112	21,07	48,16	9,94	4,30	16,53
113	21,26	46,67	11,64	4,18	16,25
114	23,61	46,36	8,84	3,99	17,19
115	27,31	41,86	7,75	4,10	18,98
116	23,76	43,41	11,34	4,24	17,25
117	20,72	48,61	9,43	4,23	17,02
118	22,94	45,12	10,63	3,46	17,84
119	20,48	48,61	8,95	4,63	17,33
120	23,86	43,90	8,75	5,12	18,36



Sample 6					
Spot	C	O	Na	Al	Si
121	25,36	43,62	8,10	5,43	17,49
122	25,25	46,52	8,68	3,33	16,22
123	21,25	48,06	9,39	4,11	17,18
124	23,52	47,41	8,33	4,77	15,97
125	23,99	45,26	8,79	4,12	17,84
126	22,46	46,76	8,22	4,69	17,86
127	23,27	45,49	8,62	5,06	17,55
128	22,60	46,54	8,66	4,36	17,83
129	22,67	46,34	9,20	3,48	18,32
130	21,42	47,14	9,69	4,43	17,33
131	25,11	44,27	7,82	4,70	18,10
132	23,64	46,33	10,29	3,35	16,40
133	27,32	43,33	10,21	3,98	15,17
134	22,18	46,83	7,82	5,31	17,87
135	21,75	47,74	9,52	3,76	17,23
136	25,67	43,10	9,15	4,34	17,74
137	24,85	42,51	13,48	3,14	16,02
138	54,35	21,78	13,56	2,85	7,47
139	70,83	17,61	4,22	4,14	3,20
140	53,98	23,07	15,09	2,27	5,60
141	40,90	31,03	16,84	3,93	7,30
142	43,48	30,01	18,37	2,52	5,61
143	34,65	37,07	8,61	5,09	14,58
144	41,40	38,35	6,93	3,05	10,27
145	36,04	36,64	7,12	5,03	15,16
146	36,89	44,72	6,40	3,29	8,70
147	45,32	33,05	6,74	4,72	10,17
148	31,19	38,44	8,58	5,24	16,55
149	38,04	38,00	5,77	4,64	13,55
150	53,97	28,33	4,35	2,93	10,42
151	44,30	28,09	9,68	5,35	12,58
152	39,46	34,81	5,69	5,52	14,52
153	32,85	36,42	8,80	6,56	15,36

Sample 7					
Spot	C	O	Na	Al	Si
1	19,28	51,55	9,19	6,02	13,96
2	16,91	53,47	8,90	5,93	14,79
3	16,82	53,15	11,58	4,50	13,96
4	14,34	58,65	9,12	4,69	13,20
5	19,67	50,16	10,49	4,35	15,33
6	13,98	56,91	9,83	4,09	15,19
7	15,53	57,13	10,02	3,62	13,70
8	17,58	54,76	9,33	5,14	13,19
9	19,60	44,51	8,73	4,56	22,59
10	15,50	54,62	11,90	4,91	13,07
11	15,96	53,99	9,77	5,63	14,66
12	16,95	54,61	10,61	3,46	14,38
13	17,36	54,16	10,42	4,60	13,47
14	15,39	53,77	12,67	6,55	11,62

Sample 7					
Spot	C	O	Na	Al	Si
15	13,45	57,34	10,98	4,96	13,27
16	14,84	55,50	11,19	3,89	14,58
17	15,42	56,19	10,81	4,52	13,06
18	17,64	53,57	9,82	4,20	14,77
19	17,47	53,46	9,87	4,09	15,11
20	16,27	54,89	12,47	2,56	13,81
21	14,54	55,60	12,07	3,06	14,73
22	15,97	54,69	12,50	3,03	13,81
23	18,83	52,48	10,49	3,86	14,34
24	17,50	54,45	9,95	4,12	13,98
25	14,65	55,75	11,05	3,72	14,82
26	16,42	54,64	11,17	2,80	14,97
27	16,63	54,48	10,54	4,40	13,95
28	13,12	60,23	10,06	3,51	13,08
29	35,49	41,87	9,71	2,25	10,68
30	18,83	53,46	8,94	2,55	16,22
31	30,30	40,58	10,05	2,42	16,65
32	16,56	53,88	9,51	4,95	15,10
33	21,04	50,54	10,47	3,09	14,86
34	14,26	56,32	10,68	3,85	14,89
35	19,92	52,15	10,29	4,18	13,46
36	19,34	49,86	16,75	1,76	12,30
37	19,69	50,39	9,37	5,99	14,56
38	15,92	53,92	10,36	4,77	15,02
39	15,89	53,74	10,18	4,94	15,25
40	15,74	55,11	9,85	5,47	13,83
41	15,78	54,22	10,90	4,99	14,11
42	28,86	47,24	9,90	3,39	10,60
43	19,20	52,11	12,21	3,69	12,79
44	22,06	50,26	11,77	3,69	12,23
45	19,87	51,44	12,40	3,75	12,54
46	22,33	47,52	15,63	3,05	11,47
47	18,63	52,37	10,41	4,55	14,03
48	17,47	51,68	10,21	5,85	14,78
49	17,93	52,94	13,19	3,12	12,82
50	14,94	55,77	11,07	4,51	13,72
51	17,55	53,77	10,28	4,76	13,64
52	13,09	56,52	11,17	0,77	18,45
53	19,18	51,08	12,63	0,65	16,46
54	19,71	53,66	10,95	0,68	14,99
55	17,61	52,36	12,85	0,65	16,52
56	16,55	55,38	9,85	0,78	17,44
57	12,54	56,85	10,34	1,02	19,25
58	14,97	55,09	10,27	0,82	18,84
59	15,35	54,52	10,16	0,89	19,09
60	15,72	55,09	9,98	0,77	18,45
61	17,31	54,41	9,44	0,79	18,05
62	14,05	55,69	11,18	0,80	18,28
63	15,37	53,29	12,45	0,77	18,13
64	20,26	51,23	11,67	0,69	16,15

Sample 7					
Spot	C	O	Na	Al	Si
65	17,78	53,20	10,27	0,74	18,02
66	15,68	55,20	10,47	0,80	17,85
67	17,63	53,86	10,01	0,91	17,59
68	16,63	53,96	9,70	0,88	18,83
69	16,48	55,18	9,56	0,79	18,00
70	19,82	52,10	9,38	0,94	17,77
71	14,84	55,20	10,39	0,85	18,71
72	16,08	53,60	13,82	0,69	15,80
73	16,61	54,00	11,70	0,77	16,91
74	15,58	54,65	12,67	0,72	16,39
75	14,62	55,47	11,70	0,78	17,43
76	14,42	54,85	11,44	0,82	18,47
77	16,24	55,43	10,34	0,80	17,19
78	15,54	55,23	10,63	0,81	17,79
79	22,67	52,02	10,73	0,67	13,90
80	16,00	53,75	13,11	0,71	16,43
81	21,25	48,63	15,19	0,58	14,35
82	15,02	56,56	11,09	0,79	16,54
83	19,29	52,23	14,95	0,64	12,90
84	18,46	53,08	13,60	0,65	14,22
85	21,10	48,47	21,08	0,39	8,96
86	23,59	51,28	13,91	0,53	10,69
87	21,53	51,67	14,56	0,55	11,68
88	19,10	51,98	15,32	0,62	12,97
89	17,71	55,42	12,31	0,67	13,88
90	17,23	54,60	12,60	0,73	14,84
91	18,51	53,09	11,61	0,73	16,06
92	14,04	55,65	14,09	0,73	15,49
93	12,67	57,53	11,57	0,79	17,44
94	13,30	56,55	13,12	0,72	16,30
95	13,31	55,74	13,74	0,72	16,48
96	13,02	56,49	13,32	0,77	16,40
97	14,20	55,44	11,71	0,82	17,82
98	15,80	55,27	11,91	0,74	16,29
99	16,85	51,16	17,70	0,62	13,67
100	12,26	57,75	12,70	0,77	16,52
101	12,94	57,63	13,01	0,90	15,52
102	12,50	58,01	12,18	0,82	16,49
103	12,70	56,29	13,42	0,77	16,82
104	14,46	54,92	13,26	0,79	16,58
105	13,55	56,61	11,70	1,23	16,91

Sample 8					
Spot	C	O	Na	Al	Si
1	17,85	53,41	11,76	0,00	16,98
2	19,23	51,71	11,08	0,00	17,99
3	18,60	52,79	11,53	0,00	17,08
4	16,17	52,96	11,62	0,00	19,25
5	16,50	52,31	12,38	0,00	18,80
6	17,55	52,10	12,30	0,00	18,04

Sample 8					
Spot	C	O	Na	Al	Si
7	16,84	52,07	12,51	0,00	18,58
8	16,25	52,33	12,09	0,00	19,32
9	18,42	51,36	11,68	0,00	18,53
10	18,11	51,92	11,85	0,00	18,12
11	19,53	51,25	11,62	0,00	17,60
12	20,61	50,55	11,87	0,00	16,97
13	18,25	52,20	11,45	0,00	18,10
14	16,92	52,18	12,35	0,00	18,55
15	16,08	52,64	10,83	0,00	20,45
16	16,60	52,26	12,16	0,00	18,97
17	19,82	50,99	11,63	0,00	17,56
18	21,05	48,98	11,11	0,00	18,86
19	20,08	51,49	10,69	0,00	17,74
20	24,57	47,27	11,48	0,00	16,68
21	25,25	47,99	11,12	0,00	15,64
22	16,36	53,23	11,79	0,00	18,62
23	16,14	53,04	11,51	0,00	19,31
24	15,80	53,40	11,03	0,00	19,76
25	16,74	53,19	12,04	0,00	18,04
26	19,14	51,62	11,89	0,00	17,35
27	15,73	53,03	12,51	0,00	18,73
28	16,38	52,80	12,31	0,00	18,51
29	16,81	52,79	12,11	0,00	18,29
30	16,94	52,71	11,23	0,00	19,13
31	16,18	52,71	12,34	0,00	18,77
32	18,17	52,43	11,39	0,00	18,02
33	15,20	53,54	12,65	0,00	18,61
34	15,17	53,52	12,34	0,00	18,98
35	15,58	52,84	12,45	0,00	19,12
36	15,74	53,29	11,72	0,00	19,25
37	15,27	53,35	12,47	0,00	18,91
38	15,81	53,26	11,94	0,00	18,99
39	15,81	53,26	11,94	0,00	18,99
40	17,75	52,43	12,64	0,00	17,18
41	32,33	42,58	9,70	0,00	15,39
42	18,28	50,66	10,77	0,00	20,29
43	18,18	50,69	10,72	0,00	20,41
44	18,74	49,46	11,42	0,00	20,37
45	18,72	49,80	11,61	0,00	19,87
46	18,58	49,72	11,41	0,00	20,28
47	20,97	49,33	11,15	0,00	18,55
48	17,53	50,98	11,23	0,00	20,26
49	20,08	49,80	10,58	0,00	19,54
50	19,40	48,94	11,47	0,00	20,18
51	26,97	46,88	9,46	0,00	16,69
52	20,09	50,26	10,48	0,00	19,17
53	26,63	47,06	10,52	0,00	15,80
54	24,58	47,55	10,25	0,00	17,61
55	19,19	49,72	11,20	0,00	19,89
56	18,90	50,43	10,74	0,00	19,93

Sample 8					
Spot	C	O	Na	Al	Si
57	19,01	50,33	10,41	0,00	20,24
58	18,01	50,68	11,27	0,00	20,04
59	19,62	48,94	11,24	0,00	20,21
60	21,92	49,30	10,74	0,00	18,04
61	50,39	25,30	9,50	0,00	14,80
62	18,51	50,84	11,72	0,00	18,93
63	18,98	50,78	11,43	0,00	18,80
64	20,27	49,74	11,48	0,00	18,52
65	18,91	50,36	12,58	0,00	18,15
66	18,37	51,11	11,55	0,00	18,97
67	19,67	49,57	12,28	0,00	18,48
68	17,95	51,10	11,90	0,00	19,05
69	17,76	50,75	11,83	0,00	19,65
70	17,77	50,69	11,64	0,00	19,90
71	17,64	50,90	12,38	0,00	19,08
72	29,75	46,27	9,30	0,00	14,68
73	19,59	49,99	10,99	0,00	19,43
74	20,19	50,83	10,34	0,00	18,64
75	24,30	49,48	10,58	0,00	15,64
76	20,08	50,93	10,79	0,00	18,20
77	24,98	48,45	9,86	0,00	16,70
78	31,37	45,58	9,50	0,00	13,55
79	18,21	50,35	11,54	0,00	19,90
80	19,07	50,05	11,06	0,00	19,82
81	20,83	48,95	10,84	0,00	19,38
82	19,14	50,08	11,49	0,00	19,29
83	25,48	47,33	10,70	0,00	16,49
84	23,91	47,93	10,65	0,00	17,51
85	25,57	47,46	10,55	0,00	16,42
86	28,87	47,35	9,14	0,00	14,64
87	32,45	44,62	9,06	0,00	13,87
88	19,26	49,99	10,87	0,00	19,89
89	19,41	49,71	10,97	0,00	19,92
90	19,21	50,40	11,66	0,00	18,74
91	58,34	33,54	3,62	0,00	4,50
92	19,25	50,25	11,57	0,00	18,94
93	17,93	50,98	10,80	0,00	20,29
94	18,30	51,18	11,02	0,00	19,51
95	19,63	50,08	11,13	0,00	19,16
96	18,68	50,19	11,33	0,00	19,79
97	17,92	50,57	11,53	0,00	19,98
98	18,20	50,64	11,07	0,00	20,09
99	17,58	49,51	12,39	0,00	20,52
100	21,48	50,06	10,25	0,00	18,22
101	20,34	49,57	11,37	0,00	18,72
102	26,36	47,04	10,46	0,00	16,14
103	19,77	49,33	11,46	0,00	19,45
104	23,95	48,67	10,56	0,00	16,82
105	21,15	49,88	10,66	0,00	18,31
106	18,59	50,36	12,47	0,00	18,57

Sample 8					
Spot	C	O	Na	Al	Si
107	42,14	41,45	7,03	0,00	9,38
108	19,67	49,57	12,28	0,00	18,48

Sample 9					
Spot	C	O	Na	Al	Si
1	74,82	15,89	2,09	2,49	4,70
2	77,44	20,21	0,82	0,50	1,04
3	77,96	16,41	1,53	1,41	2,69
4	76,86	14,98	1,92	2,12	4,12
5	30,76	41,61	10,71	5,88	11,04
6	31,65	39,87	8,28	6,86	13,34
7	35,83	40,52	9,39	5,05	9,21
8	50,03	32,98	4,19	4,30	8,50
9	43,87	36,74	5,99	4,42	8,99
10	47,21	34,86	5,14	4,40	8,40
11	61,47	28,07	3,33	2,55	4,58
12	59,16	28,40	3,67	3,10	5,66
13	52,23	33,47	3,87	3,76	6,67
14	73,08	19,19	2,33	1,96	3,45
15	52,57	29,70	6,26	4,10	7,37
16	69,44	22,83	2,31	1,96	3,46
17	54,68	30,83	4,34	3,68	6,48
18	77,57	17,21	1,33	1,32	2,57
19	73,64	19,57	1,86	1,70	3,23
20	74,71	17,19	1,97	2,20	3,93
21	76,59	16,97	1,73	1,62	3,10
22	76,21	17,73	1,55	1,58	2,93
23	74,92	18,53	1,90	1,69	2,97
24	73,14	22,02	2,14	0,97	1,72
25	43,16	38,43	6,62	4,06	7,73
26	28,80	46,14	13,30	4,09	7,66
27	24,90	46,33	20,06	2,94	5,76
28	36,83	39,88	7,56	5,15	10,57
29	40,83	37,52	8,37	4,59	8,68
30	25,31	49,85	11,55	4,69	8,60
31	56,49	32,70	4,48	2,23	4,10
32	47,45	35,20	7,02	3,51	6,81
33	28,07	46,58	0,94	22,80	1,62
34	43,05	35,13	7,61	4,78	9,43
35	42,26	37,82	5,80	5,01	9,12
36	40,43	38,09	8,86	4,42	8,19
37	71,12	18,26	2,69	2,74	5,19
38	63,93	24,90	3,32	2,73	5,11
39	76,88	17,40	1,41	1,50	2,81
40	79,06	16,58	1,41	1,03	1,92
41	51,33	32,58	6,45	3,18	6,47
42	51,30	33,34	4,40	3,78	7,17
43	71,84	19,06	2,44	2,32	4,34
44	52,91	31,23	4,53	3,96	7,37
45	46,81	35,56	4,06	4,60	8,97

Sample 9					
Spot	C	O	Na	Al	Si
46	38,73	39,36	8,11	4,70	9,10
47	31,73	42,60	11,02	5,16	9,50
48	57,80	31,27	4,36	2,34	4,23
49	59,89	30,12	4,91	1,87	3,21
50	56,43	33,29	6,36	1,35	2,56
51	72,24	22,80	2,87	0,73	1,37
52	45,45	35,60	5,28	4,78	8,88
53	70,44	23,48	2,67	1,20	2,20
54	47,01	34,75	7,21	3,78	7,25
55	26,82	46,53	13,52	4,56	8,56
56	55,73	30,31	3,54	3,71	6,72
57	68,91	20,16	2,90	2,77	5,26
58	63,99	28,08	3,62	1,57	2,74
59	73,87	15,82	2,69	2,61	5,00
60	75,35	19,10	1,82	1,27	2,46
61	69,62	18,67	2,52	3,21	5,99
62	44,52	36,85	5,69	4,49	8,45
63	43,34	36,66	6,07	4,75	9,18
64	33,28	40,49	12,90	4,63	8,70
65	53,54	31,12	4,12	3,86	7,36
66	72,79	19,36	4,41	1,20	2,23
67	33,79	43,03	10,07	4,70	8,42
68	41,03	37,37	8,03	4,84	8,72
69	38,48	39,54	5,87	5,52	10,58
70	39,19	39,31	7,29	4,84	9,37
71	49,86	33,69	5,91	3,54	7,00
72	52,76	32,07	4,82	3,73	6,63
73	46,66	34,95	6,01	4,19	8,18
74	57,43	30,22	5,19	2,50	4,66
75	39,79	40,35	5,57	5,11	9,19
76	71,46	23,64	2,27	0,95	1,68
77	43,17	35,15	5,52	5,44	10,72
78	70,70	21,88	2,91	1,65	2,87
79	48,47	32,01	5,89	4,58	9,04
80	43,34	39,03	7,48	3,65	6,51
81	42,26	37,08	7,65	4,43	8,57
82	74,97	18,66	1,71	1,61	3,05
83	76,71	18,63	1,47	1,09	2,09
84	79,21	18,87	0,70	0,39	0,83
85	74,23	21,23	1,62	1,02	1,90
86	42,86	38,11	6,92	4,13	7,97
87	28,74	44,95	13,12	4,60	8,60
88	67,70	21,85	2,51	2,85	5,09
89	63,23	28,15	5,01	1,26	2,35
90	53,11	32,97	5,62	3,08	5,23
91	71,19	24,70	2,27	0,66	1,19
92	47,79	31,87	5,21	5,22	9,91
93	45,40	36,37	5,59	4,44	8,20
94	65,13	23,13	4,35	2,54	4,85
95	75,52	20,48	1,87	0,70	1,43

Sample 9					
Spot	C	O	Na	Al	Si
96	47,24	35,00	6,16	4,03	7,56
97	43,18	36,97	7,31	4,38	8,16
98	46,24	32,51	4,90	5,55	10,80
99	64,92	26,93	3,59	1,59	2,96
100	46,00	35,74	5,63	2,92	9,72
101	70,94	23,99	2,24	0,94	1,90
102	63,88	23,12	5,25	2,70	5,05
103	54,00	29,61	4,84	3,94	7,61
104	45,65	34,01	6,18	4,95	9,22
105	70,92	18,18	2,45	2,83	5,63
106	43,43	36,39	5,27	5,21	9,70
107	46,43	35,98	7,20	3,61	6,78
108	46,66	34,31	7,32	4,09	7,62
109	50,06	34,05	4,20	4,05	7,64
110	47,00	35,12	4,70	4,62	8,57
111	42,59	36,37	5,61	5,28	10,14
112	54,77	30,49	3,79	3,86	7,10
113	54,79	29,23	3,91	4,17	7,90
114	37,30	37,86	10,89	4,97	8,99
115	59,06	26,89	4,18	3,44	6,43
116	55,17	30,63	4,60	3,31	6,29
117	72,61	21,63	2,03	1,31	2,42
118	70,55	22,30	3,73	1,18	2,25
119	69,12	20,74	4,13	2,08	3,93
120	72,83	17,68	2,21	2,52	4,75
121	76,37	18,10	1,74	1,28	2,51
122	61,82	25,84	3,23	3,21	5,91
123	54,51	29,24	5,86	3,63	6,76
124	51,46	30,35	4,99	4,47	8,73
125	45,55	35,37	5,66	4,66	8,75
126	42,21	35,15	8,72	4,90	9,01
127	38,47	38,74	8,85	4,78	9,15
128	51,92	32,36	7,73	2,71	5,28
129	50,64	34,19	6,46	2,99	5,72
130	37,15	37,87	10,72	4,70	9,55
131	39,75	37,94	7,79	4,99	9,52
132	40,90	36,02	5,64	5,97	11,48
133	43,78	35,41	4,94	5,42	10,45
134	47,83	33,09	4,38	5,02	9,68

Sample 10					
Spot	C	O	Na	Al	Si
1	19,92	51,15	13,66	1,99	13,28
2	25,60	46,83	17,04	1,50	9,03
3	20,30	49,94	16,15	2,12	11,48
4	21,89	49,96	10,67	3,80	13,67
5	22,70	51,08	14,93	2,29	9,01
6	37,03	42,81	15,84	0,73	3,58
7	18,52	50,80	15,95	2,27	12,46
8	15,78	54,54	11,43	3,79	14,46

Sample 10					
Spot	C	O	Na	Al	Si
9	28,10	45,87	12,01	2,45	11,56
10	25,30	47,94	12,46	3,04	11,27
11	16,30	54,67	13,77	2,53	12,73
12	23,32	47,07	18,28	1,72	9,60
13	22,04	51,93	12,36	2,15	11,52
14	23,46	48,51	13,71	2,89	11,42
15	16,33	53,40	12,52	3,21	14,54
16	24,47	46,51	14,50	1,43	13,09
17	23,90	47,32	12,77	3,06	12,94
18	23,99	44,90	10,79	4,24	16,08
19	23,05	45,67	11,99	3,29	16,00
20	25,91	45,68	11,26	3,46	13,70
21	24,42	44,56	12,81	3,10	15,11
22	23,23	47,01	11,70	4,06	14,00
23	26,40	46,21	11,68	3,36	12,35
24	24,27	46,64	11,09	3,94	14,06
25	25,01	43,41	13,77	3,51	14,30
26	25,45	44,21	17,85	2,13	10,35
27	23,73	44,39	16,34	2,69	12,84
28	27,52	43,47	15,79	2,68	10,54
29	24,62	48,18	13,44	2,95	10,81
30	30,04	44,33	14,93	1,88	8,83
31	24,94	44,94	12,04	3,66	14,42
32	23,44	44,39	15,27	3,22	13,67
33	27,78	42,16	11,69	3,33	15,05
34	21,09	49,94	14,04	1,84	13,09
35	23,66	49,09	11,73	2,62	12,91
36	26,09	42,07	15,09	2,88	13,87
37	30,16	39,51	10,49	3,45	16,38
38	23,03	49,42	13,06	2,96	11,53
39	21,24	48,59	14,85	2,94	12,37
40	22,18	48,46	17,56	2,08	9,72
41	25,35	43,88	13,71	3,29	13,78
42	22,93	47,17	11,27	4,23	14,40
43	29,59	40,63	12,84	2,71	14,22
44	26,19	43,74	13,79	2,64	13,64
45	25,31	44,39	13,77	3,43	13,10
46	34,91	34,32	12,50	2,80	15,48
47	26,65	41,87	11,97	3,57	15,94
48	26,06	40,78	16,24	1,94	14,98
49	32,98	34,96	14,56	2,39	15,10
50	34,74	38,05	10,68	2,77	13,76
51	26,39	39,99	11,81	4,14	17,67
52	23,96	44,52	13,38	3,15	14,98
53	37,98	33,23	16,53	1,89	10,37
54	28,08	40,92	15,92	2,29	12,80
55	29,77	37,73	12,26	3,42	16,81
56	25,72	37,51	14,31	4,04	18,42
57	27,51	44,25	11,20	3,64	13,39
58	27,40	41,91	11,94	3,60	15,15

Sample 10					
Spot	C	O	Na	Al	Si
59	26,33	42,35	12,61	3,45	15,26
60	22,83	48,53	13,67	3,05	11,93
61	25,15	42,64	18,57	1,46	12,18
62	25,86	41,80	11,98	4,12	16,24
63	35,35	38,97	13,13	1,95	10,59
64	27,88	37,98	12,09	3,68	18,37
65	26,89	44,17	12,98	3,02	12,94
66	27,83	43,02	12,96	3,38	12,81
67	29,61	41,87	14,97	2,28	11,26
68	28,58	45,45	11,03	3,61	11,33
69	26,94	42,54	8,67	4,04	17,81
70	27,07	40,59	19,11	2,09	11,15
71	26,02	39,96	12,33	4,30	17,39
72	28,85	40,00	13,17	3,36	14,62
73	27,66	40,74	13,40	3,33	14,87
74	26,13	46,82	13,51	2,91	10,62
75	26,65	44,11	16,87	2,01	10,36
76	25,56	45,50	16,27	2,47	10,19
77	25,22	42,96	16,64	2,57	12,61
78	28,98	41,64	12,88	3,72	12,78
79	30,06	43,52	19,66	1,20	5,56
80	23,95	48,69	20,45	1,43	5,48
81	32,64	40,38	14,14	2,57	10,27
82	31,13	44,57	8,72	3,20	12,38
83	25,92	48,09	13,60	2,67	9,72
84	26,66	41,58	13,79	3,73	14,25
85	27,96	47,96	10,90	2,87	10,30
86	21,08	46,25	23,41	1,31	7,95
87	28,13	41,75	17,00	2,29	10,83
88	29,97	43,49	20,54	0,97	5,03
89	43,89	40,64	10,00	0,76	4,70
90	28,35	42,26	17,61	2,28	9,49
91	27,19	36,36	25,20	1,56	9,68
92	30,08	39,53	17,53	2,19	10,67
93	27,94	41,49	20,15	1,82	8,60
94	29,30	39,55	14,08	3,43	13,64
95	27,82	40,99	14,39	2,89	13,90
96	31,45	41,96	14,58	2,10	9,91
97	24,49	40,43	11,92	3,99	19,16
98	26,38	38,31	12,88	3,65	18,77
99	24,77	41,02	13,19	3,89	17,13
100	24,96	42,41	11,98	3,64	17,00
101	22,53	40,76	15,77	3,75	17,19
102	23,42	39,10	18,77	3,07	15,65
103	28,03	41,09	13,07	3,31	14,50
104	24,48	41,99	14,17	3,48	15,88
105	23,54	42,95	11,42	4,68	17,41
106	28,94	37,87	18,38	2,32	12,49
107	23,00	42,64	12,95	4,10	17,32
108	28,70	39,72	18,81	1,82	10,94

Sample 10					
Spot	C	O	Na	Al	Si
109	18,68	38,74	17,96	4,48	20,14
110	31,21	37,77	12,67	3,29	15,06
111	30,38	40,31	14,82	2,47	12,03
112	26,73	42,51	12,87	3,20	14,69
113	25,70	40,39	18,33	2,51	13,08
114	25,21	40,03	14,63	3,49	16,64
115	28,88	36,98	20,22	2,09	11,82
116	27,20	42,10	15,44	2,78	12,48
117	26,38	40,88	13,55	3,41	15,77
118	22,56	40,98	11,91	4,62	19,94
119	16,78	44,76	16,69	3,30	18,46
120	29,08	40,09	19,80	1,95	9,09
121	20,70	42,16	34,82	0,00	2,33
122	20,52	41,75	34,46	0,00	3,28
123	21,11	40,54	35,47	0,00	2,88
124	23,83	43,93	29,34	0,36	2,54
125	25,66	41,60	30,60	0,32	1,81
126	26,38	40,66	14,74	2,95	15,27
127	22,50	39,49	35,90	0,00	2,11
128	27,28	39,61	19,58	2,31	11,21
129	23,21	43,11	11,03	3,61	19,04
130	25,98	39,31	9,09	4,43	21,18
131	27,23	38,07	10,17	4,95	19,57
132	26,97	40,03	11,54	3,99	17,47
133	26,33	41,64	10,75	3,86	17,42
134	23,45	41,08	10,69	3,61	21,17
135	25,38	44,42	26,84	0,50	2,86
136	26,94	42,91	25,62	0,52	4,01
137	25,21	43,14	12,41	3,39	15,85
138	24,43	40,53	9,61	4,65	20,78
139	34,78	32,46	14,83	2,96	14,97
140	28,75	38,17	19,40	2,31	11,37
141	23,87	44,10	16,19	2,64	13,20
142	25,99	38,89	10,12	4,59	20,41
143	21,76	43,54	7,17	5,40	22,12
144	22,77	42,87	8,38	5,21	20,78
145	24,85	41,52	8,30	5,49	19,84
146	22,03	45,68	6,66	4,18	21,45
147	24,98	42,51	6,92	5,36	20,23
148	25,86	44,00	6,75	4,77	18,62
149	28,35	37,60	6,71	5,43	21,91
150	29,69	40,77	8,07	3,91	17,55
151	21,23	43,83	7,49	4,23	23,21

Sample 11					
Spot	C	O	Na	Al	Si
1	25,91	42,76	14,91	2,82	13,59
2	29,88	40,54	10,69	1,55	17,34
3	34,08	36,77	9,85	2,36	16,93
4	31,11	33,73	12,98	2,77	19,41

Sample 11					
Spot	C	O	Na	Al	Si
5	23,63	45,38	12,19	2,88	15,91
6	19,86	52,05	11,88	1,38	14,82
7	17,47	52,85	12,86	1,70	15,13
8	23,68	48,27	14,68	1,60	11,78
9	26,18	42,29	12,40	1,57	17,56
10	27,26	43,15	11,34	1,12	17,13
11	27,76	40,29	10,92	1,53	19,51
12	20,64	48,04	11,46	2,76	17,09
13	20,44	47,91	14,02	2,46	15,18
14	21,13	47,66	12,50	1,82	16,89
15	26,25	42,32	10,22	2,30	18,91
16	20,00	49,81	11,88	2,29	16,02
17	20,30	50,50	12,48	0,77	15,94
18	20,25	49,67	11,35	2,30	16,43
19	28,48	40,26	14,73	0,84	15,69
20	26,69	42,66	11,79	2,35	16,50
21	23,01	44,49	12,20	1,62	18,69
22	20,86	48,00	11,38	1,84	17,92
23	27,32	43,86	10,58	2,26	15,98
24	20,12	48,15	11,90	1,41	18,42
25	22,52	46,18	10,30	1,67	19,33
26	23,90	45,80	11,90	3,20	15,21
27	20,89	46,75	11,51	4,12	16,73
28	24,38	44,97	11,37	2,95	16,33
29	19,86	51,10	10,00	4,07	14,96
30	21,78	46,04	11,69	3,05	17,44
31	22,04	47,32	9,91	3,54	17,19
32	21,69	45,38	9,70	5,13	18,10
33	21,53	46,63	9,48	4,97	17,39
34	21,40	46,80	12,03	1,80	17,97
35	23,49	45,89	11,91	1,81	16,91
36	21,79	45,32	11,30	3,32	18,27
37	30,50	43,40	12,41	1,35	12,34
38	55,36	32,94	6,44	0,76	4,50
39	45,98	38,28	6,24	1,61	7,89
40	49,15	36,97	7,60	0,62	5,65
41	24,49	46,06	11,16	2,94	15,34
42	32,10	39,73	14,82	0,94	12,40
43	41,17	34,07	13,15	1,01	10,60
44	31,98	40,49	12,27	1,81	13,45
45	24,61	47,06	12,23	0,67	15,43
46	17,01	52,24	12,22	1,06	17,48
47	19,71	50,00	12,00	0,90	17,39
48	20,90	48,85	12,14	0,79	17,31
49	28,38	44,12	12,80	0,83	13,87
50	35,59	41,86	11,26	0,56	10,73
51	35,37	39,12	12,79	0,53	12,19
52	23,07	46,75	12,54	1,01	16,64
53	27,80	44,78	10,66	1,88	14,88
54	25,03	45,05	15,25	0,96	13,71

Sample 11					
Spot	C	O	Na	Al	Si
55	23,39	47,27	12,56	1,68	15,10
56	21,13	47,27	14,51	1,93	15,15
57	18,71	49,85	15,00	0,89	15,55
58	18,84	48,15	15,41	1,31	16,29
59	24,44	45,83	12,10	1,49	16,14
60	22,08	47,89	13,12	1,33	15,58
61	22,76	47,63	10,95	1,91	16,74
62	29,47	43,73	11,36	0,70	14,75
63	25,96	42,40	13,30	2,72	15,63
64	35,40	38,65	9,59	1,87	14,49
65	21,52	43,99	14,30	3,36	16,85
66	20,24	48,63	15,04	2,15	13,94
67	18,99	50,23	11,68	2,80	16,31
68	19,53	49,98	13,65	2,07	14,76
69	18,55	50,79	11,94	2,99	15,73
70	26,89	47,61	10,72	2,18	12,61
71	31,45	42,80	10,58	2,62	12,56
72	20,18	50,19	13,21	1,54	14,88
73	19,94	50,76	11,83	2,62	14,86
74	25,16	48,98	15,25	1,22	9,40
75	20,71	50,74	10,80	3,02	14,73
76	21,84	52,29	10,00	2,63	13,24
77	20,03	51,73	10,92	2,34	14,98
78	21,21	51,86	11,08	2,06	13,79
79	23,41	50,40	13,71	1,77	10,71
80	23,86	47,92	8,50	4,31	15,41
81	22,37	50,98	13,33	1,76	11,56
82	19,85	50,60	12,09	2,82	14,64
83	18,83	52,42	10,41	3,02	15,31
84	20,43	50,61	12,02	2,65	14,30
85	25,92	43,53	14,53	1,45	14,57
86	19,72	52,47	9,85	2,99	14,97
87	34,33	46,03	7,97	2,15	9,52
88	20,95	51,97	9,54	3,72	13,82
89	26,13	47,79	11,65	3,79	10,65
90	23,51	50,51	9,54	3,73	12,70
91	25,59	49,37	9,58	3,35	12,11
92	22,64	51,02	9,08	4,12	13,13
93	25,54	50,01	8,71	3,70	12,05
94	26,13	49,13	9,24	3,64	11,85
95	25,98	49,55	10,64	3,01	10,82
96	24,32	49,84	9,04	3,64	13,15
97	24,37	50,00	9,32	3,82	12,50
98	25,03	50,69	8,39	3,83	12,06
99	26,04	48,39	9,47	3,90	12,20
100	24,95	49,82	8,51	3,91	12,81
101	26,59	46,79	9,36	3,21	14,04
102	22,23	48,70	10,18	2,89	16,00
103	21,60	51,59	8,95	4,22	13,64
104	25,45	48,24	10,55	3,18	12,58

Sample 11					
Spot	C	O	Na	Al	Si
105	21,05	50,06	15,87	1,40	11,62
106	19,69	51,37	9,88	2,99	16,07
107	22,69	50,24	13,09	2,45	11,54
108	21,38	50,15	16,58	1,70	10,20
109	21,55	50,44	14,84	2,33	10,84
110	22,30	49,90	14,46	1,56	11,78
111	22,17	49,50	16,46	1,06	10,80
112	20,10	51,52	12,31	3,20	12,86
113	22,78	51,30	10,81	2,26	12,85
114	22,33	49,53	12,08	2,11	13,95
115	21,81	52,22	12,64	2,45	10,88
116	22,53	50,53	12,09	2,48	12,38
117	26,02	49,00	11,03	1,78	12,18
118	26,74	45,58	13,03	1,62	13,03
119	20,33	52,66	10,17	3,44	13,40
120	24,89	48,44	10,24	2,53	13,91
121	19,36	50,85	11,22	3,19	15,37
122	21,15	50,77	11,58	1,81	14,70
123	25,37	47,67	10,78	2,12	14,06
124	24,03	49,13	13,48	1,73	11,64
125	20,25	51,82	15,06	1,67	11,20
126	20,95	48,85	12,26	0,93	17,01
127	19,30	51,71	13,19	0,93	14,86
128	21,72	50,96	16,09	1,60	9,65
129	17,31	52,01	12,55	0,74	17,39
130	19,17	49,65	13,01	0,68	17,49
131	25,20	36,61	12,54	1,61	24,04
132	20,05	34,51	18,34	2,75	24,36
133	19,89	50,02	12,57	0,98	16,54
134	23,45	46,74	13,22	1,17	15,42
135	21,62	48,85	14,77	0,78	13,99
136	22,45	47,75	13,90	0,85	15,05
137	19,72	48,66	12,44	2,33	16,85
138	18,08	49,78	15,76	0,76	15,61
139	16,70	50,50	16,72	0,69	15,39
140	18,77	50,84	14,30	0,71	15,38
141	19,36	50,52	13,06	0,97	16,08
142	19,74	50,27	12,86	0,77	16,36
143	20,13	48,20	12,19	1,74	17,74
144	21,32	51,55	17,14	0,52	9,46
145	19,15	53,10	12,44	1,41	13,90

Sample 12					
Spot	C	O	Na	Al	Si
1	26,90	44,06	11,84	0,00	17,20
2	33,89	42,43	9,86	0,00	13,81
3	32,64	42,78	10,09	0,00	14,49
4	28,84	43,68	10,91	0,00	16,57
5	27,33	45,41	11,14	0,00	16,12
6	24,23	47,97	11,41	0,00	16,39

Sample 12					
Spot	C	O	Na	Al	Si
7	36,48	39,52	8,65	0,00	15,35
8	70,17	23,48	2,86	0,00	3,48
9	29,05	43,38	11,29	0,00	16,29
10	29,07	43,86	10,82	0,00	16,25
11	31,24	41,66	11,61	0,00	15,49
12	31,31	43,07	10,16	0,00	15,47
13	26,35	45,13	11,14	0,00	17,38
14	33,21	42,12	10,29	0,00	14,38
15	22,42	47,53	12,98	0,00	17,07
16	26,16	45,02	11,58	0,00	17,23
17	31,08	42,13	10,08	0,00	16,70
18	28,06	44,17	10,88	0,00	16,89
19	34,55	41,74	9,80	0,00	13,90
20	23,52	46,72	11,93	0,00	17,84
21	27,66	44,56	11,31	0,00	16,48
22	23,37	46,79	11,99	0,00	17,84
23	33,02	42,63	10,38	0,00	13,97
24	29,76	42,58	12,10	0,00	15,56
25	35,25	40,47	9,80	0,00	14,48
26	59,48	33,00	4,14	0,00	3,38
27	60,78	27,25	4,91	0,00	7,06
28	57,61	31,03	5,02	0,00	6,34
29	25,97	44,89	11,88	0,00	17,26
30	55,47	33,45	4,81	0,00	6,26
31	61,86	27,86	4,55	0,00	5,73
32	26,64	45,13	11,32	0,00	16,91
33	22,55	47,38	12,66	0,00	17,41
34	21,75	48,39	12,82	0,00	17,04
35	22,74	47,99	10,97	0,00	18,30
36	22,50	47,68	11,90	0,00	17,92
37	22,68	47,53	12,01	0,00	17,78
38	22,96	46,71	12,63	0,00	17,70
39	20,90	48,84	12,31	0,00	17,95
40	38,12	38,98	9,42	0,00	13,48
41	32,76	42,04	10,58	0,00	14,62
42	31,22	42,67	10,95	0,00	15,16
43	29,88	42,76	10,55	0,00	16,81
44	28,70	44,05	11,36	0,00	15,89
45	34,86	39,95	9,95	0,00	15,24
46	49,21	36,85	6,10	0,00	7,85
47	50,35	35,46	7,09	0,00	7,09
48	53,46	34,50	5,38	0,00	6,65
49	30,03	49,68	5,81	0,00	14,48
50	33,56	40,94	10,56	0,00	14,94
51	30,08	42,21	11,21	0,00	16,50
52	34,62	42,01	9,45	0,00	13,92
53	28,67	43,76	10,67	0,00	16,90
54	29,54	43,26	10,88	0,00	16,32
55	26,68	44,52	11,59	0,00	17,21
56	26,09	45,21	10,93	0,00	17,77

Sample 12					
Spot	C	O	Na	Al	Si
57	25,99	45,26	11,95	0,00	16,80
58	32,60	41,11	10,11	0,00	16,19
59	32,35	40,34	11,07	0,00	16,24
60	32,86	40,81	10,32	0,00	16,01
61	35,02	40,82	10,19	0,00	13,96
62	32,13	41,81	11,04	0,00	15,02
63	34,10	42,55	10,02	0,00	13,33
64	51,80	35,90	6,74	0,00	5,56
65	29,79	49,40	10,60	0,00	10,21
66	52,82	34,80	6,01	0,00	6,37
67	59,70	31,74	4,82	0,00	3,74
68	53,34	35,56	4,80	0,00	6,30
69	28,70	42,22	12,11	0,00	16,97
70	40,65	35,33	9,94	0,00	14,09
71	29,24	41,36	11,91	0,00	17,48
72	30,96	42,03	10,84	0,00	16,17
73	31,68	42,78	10,01	0,00	15,54
74	29,17	41,81	10,81	0,00	18,22
75	27,72	43,09	11,39	0,00	17,81
76	29,21	41,24	11,49	0,00	18,06
77	26,58	43,65	12,51	0,00	17,26
78	39,71	38,91	8,55	0,00	12,83
79	26,44	45,45	11,37	0,00	16,74
80	50,15	36,14	6,42	0,00	7,28
81	59,57	30,90	4,45	0,00	5,08
82	54,50	31,36	6,05	0,00	8,09
83	27,18	44,12	11,53	0,00	17,17
84	33,87	40,96	9,68	0,00	15,48
85	37,43	39,21	9,22	0,00	14,14
86	30,58	42,52	11,46	0,00	15,44
87	26,25	46,80	10,77	0,00	16,18
88	27,05	44,62	10,79	0,00	17,54
89	32,00	41,51	10,61	0,00	15,89
90	25,18	45,03	11,22	0,00	18,57
91	27,64	43,96	11,65	0,00	16,75
92	24,55	45,73	11,54	0,00	18,18
93	26,45	45,34	12,31	0,00	15,90
94	28,90	43,31	11,33	0,00	16,47
95	28,32	40,11	10,44	0,00	21,12
96	28,00	43,15	10,79	0,00	18,06
97	28,32	44,28	11,47	0,00	15,93
98	32,05	42,28	10,55	0,00	15,11
99	30,13	42,21	11,96	0,00	15,70
100	32,35	40,49	11,07	0,00	16,10
101	33,77	40,48	10,80	0,00	14,95
102	37,99	38,23	9,67	0,00	14,11
103	39,01	37,17	9,57	0,00	14,25
104	26,55	44,26	11,62	0,00	17,57
105	35,84	39,05	10,25	0,00	14,86
106	39,19	38,72	9,54	0,00	12,55